REPUBLIQUE DU CAMEROUN
Paix – Travail – Patrie
****
UNIVERSITE DE YAOUNDE I
FACULTE DES SCIENCES
DEPARTEMENT DE PHYSIQUE
****
CENTRE DE RECHERCHE ET DE FORMATION DOCTORALE EN SCIENCES, TECHNOLOGIE ET GEOSCIENCES

REPUBLIC OF CAMEROUN
Peace – Work – Fatherland
****
UNIVERSITY OF YAOUNDE I
FACULTY OF SCIENCE
DEPARTMENT OF PHYSICS
****
POSTGRADUATE SCHOOL OF SCIENCE, TECHNOLOGY AND GEOSCIENCES

NATURAL RADIATION EXPOSURE TO THE PUBLIC IN DOUALA CITY, CAMEROON

Submitted and defended in Fulfillment of the Requirements for the Degree of Doctor of Philosophy/PhD in Physics

Par : **TAKOUKAM SOH SERGE DIDIER**
DEA in Physics

Sous la direction de
OUMAROU BOUBA
MC

Année Académique :

UNIVERSITE DE YAOUNDE I
THE UNIVERSITY OF YAOUNDE I

FACULTE DES SCIENCES
FACULTY OF SCIENCE

DEPARTEMENT DE PHYSIQUE
DEPARTMENT OF PHYSICS

ATTESTATION DE CORRECTION DE LA THESE DE DOCTORAT/PhD

Nous, Professeur **BEN-BOLIE Germain Hubert** et Professeur **NDJAKA Jean-Marie Bienvenu**, respectivement Examinateur et Président du jury de la Thèse de Doctorat/Ph.D de Monsieur **TAKOUKAM SOH Serge Didier**, Matricule **12W1980,** préparée sous la direction des Professeurs **SAÏDOU** et **OUMAROU Bouba,** intitulée : **«NATURAL RADIATION EXPOSURE TO THE PUBLIC IN DOUALA CITY, CAMEROON»**, soutenue le **Mardi 28 Juillet 2020**, en vue de l'obtention du grade de Docteur/Ph.D en Physique, Spécialité **Physique Nucléaire, Atomique, Moléculaire, et Biophysique** option **Physique Nucléaire, Dosimétrie et Radioprotection,** attestons que toutes les corrections demandées par le jury de soutenance ont été effectuées.

En foi de quoi, la présente attestation lui est délivrée pour servir et valoir ce que de droit.

Fait à Yaoundé, le 29 JUIL 2020

Examinateur

BEN-BOLIE Germain Hubert
Professeur

Le Président du jury

NDJAKA Jean-Marie Bienvenu
Professeur

Le Chef de Département de Physique

UNIVERSITE DE YAOUNDE I
FACULTE DES SCIENCES
Le Chef de Département
DEPARTEMENT DE PHYSIQUE

Ndjaka Jean-Marie Bienvenu
Professeur

Dedication

This thesis is dedicated to God Almighty.

✠ Particular thanks goes to My Mother **MAHOUE Marie** and **Family SOH** for their love, patience and support.

Acknowledgements

At the end of the PhD study, I am deeply grateful for the opportunity to have learned from and worked with so many brilliant teachers, collaborators and students. I am happy to express my sincere gratitude to all those from who near or far have accompanied me during these doctoral years and have directly or indirectly contributed to the completion of this document. Nevertheless, I will do my best to condense my thoughts about this.

My gratitude goes to **Professor SAÏDOU**, for the supervision of this thesis. He was able to define a research topic, which was in one hand, very pertinent according to the objectives which were set up, and in the other hand very enriching as far as the multidisciplinary aspect of the fields is concerned. His involvement during the thesis, was a perfect compromise between a careful follow-up of my work, and a certain freedom granted in the scientific process. This has led to the genesis of ideas and the development of my quest for this research. I am also honored for the trust he placed in me, by supporting my work. He permits the work to be presented during several meetings, working groups and congress. I would also like to thank him, for his involvement in my professional integration efforts. Last but not least, I want to emphasize on his human qualities that have been real assets for the achievement of this thesis in the best conditions.

I would also like to thank my Co-director, **Professor OUMAROU Bouba** (deceased in August 2018) for his constant support, availability and constructive suggestions, which were determinant for the accomplishment of the work presented in this thesis.

I am also grateful to the Institute of Geological and Mining Research (**IRGM**) for financial and technical support during this thesis.

I am specially thankful to the **University of Hirosaky** (Japan) for providing the various facilities (financial and equipment), which have helped in my research.

For the quality of his teaching, I also thank **Professor OWONO OWONO Luc Calvin**, Register of the University of Yaounde I, head of the Department of Physics at ENS and Coordinator of the physics and applications research unit at the postgraduate school for Science, Technology and Geosciences, UY1.

I express my gratitude to **Professor NDJAKA Jean-Marie Bienvenu**, head of the Department of Physics and head of the Laboratory of Materials science for his administrative support. I am very grateful for the quality of his teaching and for his constructive comments.

I would like to thank **Professor KOFANE Timoléon Crépin** head of the Laboratory of Mechanics, Materials and Structures for his vision in the evolution of science.

Special thanks goes to **Professor BEN – BOLIE Germain Hubert** head of the Laboratory of Nuclear Physics for his kindness, availability and his encouragement.

I would like to thank **Professor ELE ABIAMA Patrice** Permanent Secretary of National Committee for Technologies Development (**CNDT**) for his teaching. I highly appreciate his vision in the evolution of Science.

I would like to thank all the Professors of the laboratory of Nuclear Physics, **Professor BOYOMO Marthe** and **Doctor ABDOURAHIMI** for their lectures.

I also thank **Professor FEWO Serge Ibraïd** and **Professor VONDOU Debertin** for their encouragement and their moral support.

I would like to deeply thanks the honorable **Members of the Jury**, who agreed to put aside their multitude occupations so as to evaluate this work. I express to them all my greatest respect.

I specially express my acknowledgement to the staff of the Department of **Physics**, Faculty of Science, University of Yaounde I for their lectures during my higher education. My sincere thanks go to the Postgraduate School of Science, Technology and Geosciences.

I would like to thank **Doctor SIAKA Yvette** of IRGM for his encouragement and all researchers of IRGM, namely **Doctor DJEPANG Serge, Doctor KOUNTCHOU Michaux, NDJANA NKOULOU II Joseph, YOUNUI, MANGA, NGUEMHE**

Fils, NDUCOL Nasser, OUMAR and **AHMADOU** for their warmth and sympathy within the laboratory and for their contribution to the evolution of research.

For his moral support and encouragement during my PhD studies I am grateful to my Academic elder **BINENG Guillaume Samuel** with whom I worked.

I Thank **ATANGANA BINGANA Serge** my Academic elder for his encouragement during my Thesis.

My sincere thanks go to the editors and referees of **Radioprotection, Isotopes in Environmental and Health Studies, Radiation Protection Dosimetry** and **AIP Conference Proceedings** for their detailed review, constructive criticism and excellent advice during the preparation of my different publications.

My sincere appreciation to Trauma Centre Cameroon (for Refugies) for its warm welcome and its support during my thesis. This goes especially to the Head of the Center Mister **PETER KUM Che**, the **Dr MALICK SY**, all the **NURSES**, Madam **KENE**, Madam **FOTIO**, Mister **MANFO joel**, Madam **TCHOUPOU Solange** , Madam **KAPTUE Nathalie, ONANA Moisa** for their moral support.

I am grateful to all my colleagues **TAMIAN Kevin, NGA ONGODO, EBODE Fabien, OMON Yves, FOKOU Martin, GUEMBOU Sébastien** and **MBETKWE Laetitia** for their trust, support and encouragement.

I would like to show my gratitude and my love to my family for their support and love through the duration of my PhD life. One of the most important motivations to achieve my PhD has been to make you proud.

I would like to thank Mother **FOZE MODJOM Marthe** epse **Mbou** for his moral support.

I am grateful to all my friends **NGOMSEU, NOUMBI, ONGKABION Doucette, FOKAM Syliane, NTANKEU, KUNGO, TALEGHANG Elise, TCHOUNKE Romaric, NGEUPI Christian** and all teachers in **College excellence plus** Yaounde.

The authors are highly thankful for the helpful local people, house owners, for making it possible to carry out the measurement campaigns.

Lastly, I offer my appreciations to all those who supported me in various respects during the completion of my PhD Thesis.

Contents

List of Figures

List of Tables

List of Abbreviations

DDREF: **D**ose and **D**ose **R**ate **E**ffectiveness **F**actor
EERC : **E**quilibrium **E**quivalent **R**adon **C**oncentration
EETC : **E**quilibrium **E**quivalent **T**horon **C**oncentration
EPA : **E**nvironmental **P**rotection **A**gency
E-PERM : **E**lectret-**P**assive **E**nvironmental **R**adon **M**onitor
GPS : **G**lobal **P**ositioning **S**ystem
IAEA : **I**nternational **A**tomic **E**nergy **A**gency
ICRP : **I**nternational **C**ommission on **R**adiological **P**rotection
ICRU : **I**nternational **C**ommission on **R**adiation **U**nits and **M**easurements
ISO : **I**nternational **O**rganization for **S**tandardization
JCGM : **J**oint **C**ommittee for **G**uides in **M**etrology
kerma : **K**inetic **E**nergy **R**eleased in **M**atter
LC : **D**ecision **T**hreshold
LD : **D**etection **L**imit
MDA : **M**inimum **D**etectable **A**ctivity
NaI(TL) : **T**hallium- **a**ctivated **S**odium **I**odide
NIRS : **N**ational **I**nstitute of **R**adiological **S**ciences
OECD : **O**rganization of **E**conomic **C**ooperation and **D**evelopment
RADUET : **P**assive **I**ntegrated **R**adon-**T**horon **D**iscriminative **D**etectors
TEL : **L**inear **E**nergy **T**ransfer
UNSCEAR : **U**nited **N**ations **S**cientific **C**ommittee on **E**ffects of **A**tomic **R**adiation
WHO : **W**orld **H**ealth **O**rganization

Abstract

The purpose of this study was to evaluate the level of natural radioactivity exposure to the public in Douala city. A car-borne survey was carried out in Douala, the largest city in Cameroon to make a detailed distribution map of the absorbed dose rate in the city, to locate the high natural radiation areas prior to indoor radon, thoron, and thoron progeny measurements. Gamma-ray dose rates were measured using 3-in $\times$ 3-in NaI(Tl) detector. Activity concentrations of ^{238}U, ^{232}Th and ^{40}K in soil from Douala city were determined by two methods: the first, using *in-situ* gamma spectrometry and the second, at the laboratory using a NaI(Tl) detector. In addition, the measurements of indoor radon, thoron and their progeny concentrations have been carried out in Douala by using RADUET detector and thoron progeny monitor in about 71 dwellings. These measurements are followed by the determination of the equilibrium factor of thoron and the evaluation of the dose by external irradiation and by inhalation. The activity concentrations with NaI(Tl) detector varied from 18 to 47 $Bq\ kg^{-1}$ for ^{238}U, 21 to 54 $Bq\ kg^{-1}$ for ^{232}Th, and 10 to 410 $Bq\ kg^{-1}$ for ^{40}K with averages of 29, 38, and 202 $Bq\ kg^{-1}$ respectively, for *in-situ* measurements. They vary between 29-98 $Bq\ kg^{-1}$ for ^{238}U, 29-92 $Bq\ kg^{-1}$ for ^{232}Th, and 40 to 79 $Bq\ kg^{-1}$ for ^{40}K, with averages of 60, 57, and 56 $Bq\ kg^{-1}$ respectively for soil samples collected at Douala III subdivision and measured in the laboratory. The results of this current study have been compared with the world mean values of 35, 30 and 400 $Bq\ kg^{-1}$ respectively specified by the UNSCEAR. The concentrations of radon, thoron and thoron progeny were respectively found to vary from 31 $\pm$ 1 to 436 $\pm$ 12 $Bq\ m^{-3}$, 4 $\pm$ 7 to 246 $\pm$ 5 $Bq\ m^{-3}$, and 1.5 $\pm$ 0.9 to 13.1 $\pm$ 9.4 $Bq\ m^{-3}$. The arithmetic mean values of radon, thoron and thoron progeny concentrations were respectively found to be 139 $\pm$ 47 $Bq\ m^{-3}$, 80 $\pm$ 52 $Bq\ m^{-3}$, and 4.6 $\pm$ 2.9 $Bq\ m^{-3}$. The equilibrium factor of thoron varies from 0.01 $\pm$ 0.01 to 0.83 $\pm$ 1.55 with an average value of 0.11 $\pm$ 0.16. A heterogeneous distribution of absorbed dose rates in air was observed on the dose rate distribution map, and varies from 29 to 86 $nGy\ h^{-1}$ with an average of 50 $nGy\ h^{-1}$, lower than the world average value of 59 $nGy\ h^{-1}$. The total annual effective dose was evaluated and varied from 0.21 to 0.41 $mSv\ y^{-1}$ with a mean value of 0.31 $mSv\ y^{-1}$ for *in-situ* measurement, however for soil samples, the total annual effective dose varied from 0.3 to 0.7 $mSv\ y^{-1}$ with an average value of 0.42 $mSv\ y^{-1}$, which was lower than the worldwide effective dose of 0.5 $mSv\ y^{-1}$. The annual effective dose

due to exposure to indoor radon and progeny was found to vary from 0.6 to 9 $mSv\ y^{-1}$ with an average value of 2.6 $\pm$ 0.1 $mSv\ y^{-1}$ and the effective dose due to the exposure to thoron and progeny was found to vary from 0.3 to 2.9 $mSv\ y^{-1}$ with an average value of 1.0 $\pm$ 0.4 $mSv\ y^{-1}$. The total inhalation dose of radon and thoron was 3.6 $mSv\ y^{-1}$; which represents 91% of the total annual dose (4 $mSv\ y^{-1}$) received by the population of Douala. The contribution of thoron and its progeny to the total inhalation dose was found to vary from 7 to 60% with an average value of 26%. Thus thoron cannot be neglected when assessing radiation doses.

Keywords: Car-borne survey , NaI(Tl) detector , Natural radioactivity, Air absorbed dose rate, External effective dose, Radon (Rn), Thoron (Tn), Rn-Tn discriminative detector, Thoron progeny (Tnp), Equilibrium factor, Inhalation dose.

Résumé

Le but de cette étude était d'évaluer le niveau d'exposition du public à la radioactivité naturelle de la ville de Douala. La mesure de la concentration des radionucléides primordiaux ^{238}U, ^{232}Th et ^{40}K dans le sol, par spectrométrie gamma *in-situ* et de laboratoire, la mesure des débits de dose absorbée dans l'air par la méthode car-borne survey et la mesure des concentrations du radon, thoron et les filles du thoron dans les habitations utilisant les détecteurs RADUET et les moniteurs de filles de thoron ont été effectuées. Ces mesures sont suivies de la dtermination du facteur d'équilibre du thoron et de l'évaluation de la dose par irradiation externe et par inhalation. Pour la mesure *in-situ* les concentrations de ^{238}U, ^{232}Th et ^{40}K varient respectivement entre 18 - 47 , 21 - 54 et 10 - 400 $Bq\ kg^{-1}$ avec des valeurs moyennes de 29, 38 et 202 $Bq\ kg^{-1}$. Cependant, pour la mesure au laboratoire, les concentrations de ^{238}U, ^{232}Th et ^{40}K varient entre 29 - 98, 29 - 92 et 40 - 70 $Bq\ kg^{-1}$ avec des valeurs moyennes de 60, 57 et 56 $Bq\ kg^{-1}$ respectivement. Les résultats obtenus au cours de cette étude ont été comparés aux valeurs moyennes mondiales correspondantes données par l'UNSCEAR : 35, 30 et 400 $Bq\ kg^{-1}$. Par ailleurs, Les concentrations du radon et du thoron mesurées dans 71 habitations de Douala varient de 31 $\pm$ 1 Bq m^{-3} à 436 $\pm$ 12 Bq m^{-3} et de 4 $\pm$ 7 Bq m^{-3} à 246 $\pm$ 5 Bq m^{-3} avec des concentrations moyennes de 139 Bq m^{-3} et 80 Bq m^{-3} respectivement. La concentration des filles du thoron varie de 1.5 $\pm$ 0.9 Bq m^{-3} à 13.1 $\pm$ 9.4 Bq m^{-3} avec une concentration moyenne de 4.6 $\pm$ 2.9 Bq m^{-3} . Le facteur d'équilibre du thoron varie de 0.01 $\pm$ 0.01 à 0.83 $\pm$ 1.55 avec une valeur moyenne de 0.11 $\pm$ 0.16. Le débit de dose absorbée dans l'air à 1 mètre au-dessus du sol varie de 28 à 86 nGy h^{-1} avec une valeur moyenne de 50 nGy h^{-1} , inférieure à la moyenne mondiale de 59 nGy h^{-1}. La dose efficace annuelle par irradiation externe a été évalué et varie de 0.21 à 0.41 $mSv\ y^{-1}$ avec une valeur moyenne de 0.31 $mSv\ y^{-1}$ pour la mesure *in-situ*. La dose annuelle par irradiation externe évaluée à partir des concentrations de ^{238}U, ^{232}Th et ^{40}K dans le sol mesurée au laboratoire varie de 0.3 à 0.7 $mSv\ y^{-1}$ avec une valeur moyenne de 0.42 $mSv\ y^{-1}$, toutes inférieures à la valeur moyenne mondiale égale à 0.5 $mSv\ y^{-1}$. La dose totale par inhalation du radon et du thoron est de 3.6 $mSv\ y^{-1}$; ce qui représente 91% de la dose totale annuelle (4 $mSv\ y^{-1}$) reçue par la population de Douala. La contribution du thoron la dose par inhalation varie de 7 à 60% avec une moyenne de 26%. Par conséquent, le thoron ne peut être négligé dans l' évaluation de la dose totale par

inhalation.

Mots-clés : Détecteur NaI (Tl), Radioactivité naturelle, Débit de dose absorbée dans l'air, Dose efficace externe, Radon (Rn), Thoron (Tn), progéniture du thoron (Tnp) Détecteur RADUET, Facteur d'équilibre, Dose inhalée.

General Introduction

Natural ionizing radiation originates from various sources. These can affect the human body via different pathways, causing both external and internal exposure. For example at high altitude cosmic radiation, and its induced radionuclides cause elevated effective doses but at sea level the largest contribution is from terrestrial radionuclides such as radon and thoron. Radon (^{222}Rn) and thoron (^{220}Rn) isotopes, from the ^{238}U and ^{232}Th decay chains respectively, are responsible for approximately the half of the total annual effective dose from natural sources to an average human [1]. The ^{238}U and its daughters rather than ^{226}Ra and its daughter products are responsible for the major fraction of the internal dose received by humans from naturally occurring radionuclides. Even though the concentrations of these radionuclides are widely distributed in nature, they have been found to depend on the local geological conditions and as a result vary from place to place [2, 3]. This is because the specific levels are related to the type of rocks from which the soil originates. The damage caused by exposure to a radiation is determined by the type of radiation, the duration of exposure and the part of the body that is exposed. The interaction of ionizing radiation with the human body arises from either external sources or internal contamination which can lead to biological effects [1]. Radiation effects can lead to death of a cell, impairment in the natural functioning of the cell leading to somatic effects such as cancer and a permanent alteration of the cell which is transmitted to later generation i.e. genetic effect. Biological effects can also be considered in terms of stochastic effects and non stochastic effects. Stochastic effects increase with dose rate [4] while non stochastic effect has a threshold below which there is no effect. Human exposure to radiation also reduces the immunity of the person exposed [5].

Exposure due to radon is the most variable and the International Atomic Energy Agency (IAEA) has been working hand in hand with the World Health Organization (WHO) in finding means of raising the awareness of radon as a public health and radiation protection issue and to support the Member States with technical guidance for establishment and implementation of radon action plans, such a plan is currently under implementation in Cameroon through technical cooperation with IAEA. Generally, the system of radiological protection ought to deal much with exposure due to natural sources of ionizing radiation more particularly radon [6]. Scientific Committee under United Nations on the Effects of Atomic Radiation, postulated that exposure to natural sources of radiation constitutes more than 60% of the population radiation dose, whereas 50% is as a result of inhalation and ingestion of natural radioactive gas radon and its decay products. It is assessed that exposure to radon through inhalation in closed rooms is the cause of about 3-14% of all deaths from the cancer of the lung [1,7]. However studies have shown that data on the thoron since its determination is difficult [8]. Saïdou et al [9] reported Indoor radon measurements in the uranium regions of Poli and Lolodorf, Cameroon. This study showed high indoor radon distribution observed in the uranium regions of Poli and Lolodorf could stem from the combined effect of ground as floor type and building materials. Saïdou et al [10] reported Radon-thoron discriminative measurements in the high natural radiation areas of southwestern Cameroon. This showed that 30% of houses have thoron concentrations above 300 $Bq\ m^{-3}$ and the mean contribution of indoor thoron to the total inhalation was of 47%.

Further, a linkage between cancer of the lung and inhalation of radon and its progeny has been studied and recent epidemiological evidence suggests that inhalation of radon and its decay products in domestic environment initiates the cancer of the lung. Shoeib et Thabayneh [11] noted that inhalation of radon and its progeny also causes skin cancer and kidney diseases besides lung cancer and that radiological impact commenced by radionuclides is as a result of radiation exposure of the body by the gamma rays and irradiation of lung tissues from inhalation of radon and its progeny.

This research thesis is divided into 3 chapters. In chapter 1 we present fundamentals on

sources of exposure to natural radiation and the theoretical bases necessary for understanding the interaction mechanisms of electromagnetic radiation as well as the charged particles with matter and dosimetric quantities.

Chapter II presents the material and methods used to determine the activity concentration of ^{238}U, ^{232}Th, ^{40}K, ^{222}Rn, ^{220}Rn and the dosimetry of Douala population.

The results obtained on measuring radioactivity in samples of Douala, indoor radon in dwellings and on the dosimetric impact of the population will be presented in chapter III. These results will be discussed, as well as the precision and an exhaustive comparison of the literature in order to better explain our results.

CHAPTER I

LITERATURE REVIEW

I.1 Introduction

In the nature, most of atomic nuclei are stable. However, some atoms have unstable nuclei, which is due to an excess of either protons or neutrons, or both. They are said to be radioactive and are called radioisotopes or radionuclides. Radioactivity is the natural property of certain atomic nuclei to emit radiation in a spontaneous way. This emission of radiation accompanies the phenomenon of radioactive decay, which transforms the nucleus of the father element (X) into a son nucleus (Y). Thus, the nucleus of a radioactive isotope will be spontaneously transformed into a nucleus of a more stable isotope of the same element, or else into a nucleus of an isotope of another chemical element. The decay products consist of particles (alpha or beta) or photons (gamma). Radiation can be defined as a mode of propagation of energy in space, in the form of electromagnetic waves or particles. Radiation can only be detected and characterized through their interaction with the material in which they propagate. They may transfer in the medium that they cross, all or part of their energy during these interactions. Radiation can be classified according to its mode of interaction with matter in two categories:

– Directly ionizing radiation: they are consisted of charged particles which transfer directly to matter their energy, by action of the coulombian forces exerting between them and the atoms of the medium. Energy transfers depend on the masses of moving particles and it is necessary to distinguish between heavy charged particles (proton, deuteron, alpha, heavy ions) and electrons.

– Indirectly ionizing radiation: they are electrically neutral and are capable of transferring a large fraction or all of their energy in a single interaction to charged particles.

These secondary particles then ionize the medium. Ionization, in this case, is done in two stages. Electromagnetic radiation (X and γ) and neutrons fall into this category, but their mode of interaction is different [12].

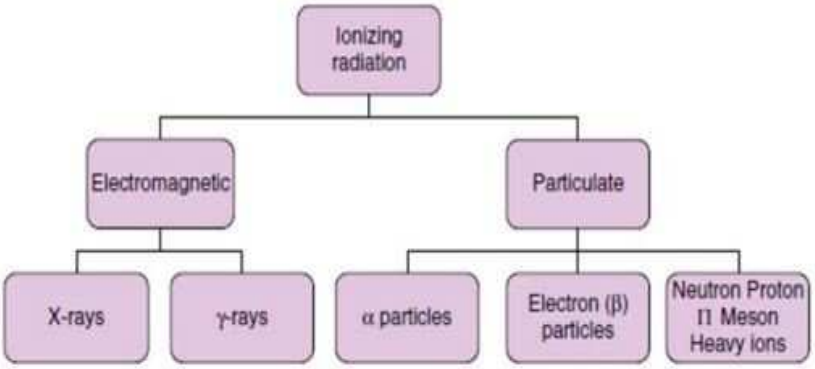

Figure 1: Ionizing Radiations [13]

I.1.1 Alpha radioactivity

Alpha radioactivity concerns heavy nuclei, whose atomic number is greater than 82 [14]. The increase in the charges indeed increases the repulsive forces and causes the expulsion of a heavy and very stable particle, formed from two protons and two neutrons, that is to say a nucleus of helium. This phenomenon occurs when the mass M of the parent nucleus is larger than the sum of the masses of the particle α and the son nucleus M_1 .

$$M > M_\alpha + M_1 \tag{I.1}$$

This emission is symbolised by the equation:

$$^{A}_{Z}X \rightarrow ^{A-4}_{Z-2}Y + ^{4}_{2}H_e + Q \tag{I.2}$$

The excess energy Q is distributed between the kinetic energy of the ejected α particle and the energy of the emitter nucleus. The kinetic energy of the ejected particle (α) is characteristic of the emitting element and can take only a small number of values very close to each other (spectrum of lines) [15]. The energy of the emitter nucleus is subjected

to a recoil movement (recoil energy From the nucleus).

Example : ${}^{238}_{92}U \rightarrow {}^{234}_{90}Th + {}^{4}_{2}H_e$

If the parent nucleus Y is produced at an excited energy level, the decay is accompanied by the emission of a gamma photon.

$$\begin{aligned} {}^{A}_{Z}X &\rightarrow {}^{A-4}_{Z-2}Y^* + {}^{4}_{2}H_e + Q \\ {}^{A-4}_{Z-2}Y^* &\rightarrow {}^{A-4}_{Z-2}Y + \gamma \end{aligned} \tag{I.3}$$

I.1.2 β^- radioactivity

During the β^- radioactivity, the parent nucleus emits an antineutrino in addition to the electron. It is admitted that the β^- electron is created following the transformation in the nucleus of a neutron made of proton according to the following disintegration equation:

$${}^{1}_{0}n \rightarrow {}^{1}_{1}p + {}^{0}_{-1}e + {}^{0}_{0}\overline{\vartheta_e} \tag{I.4}$$

Therefore, this disintegration concerns nuclei whose number of neutrons are relatively high. Thanks to antineutrino, the principle of conservation of energy is respected; in addition, its presence makes it possible to explain the continuity of the energy spectrum of the β electrons. The son nucleus has the same number of nucleons as its parent, which leads to the following decay equation:

$${}^{A}_{Z}X \rightarrow {}^{A}_{Z+1}Y + {}^{0}_{-1}e + {}^{0}_{0}\overline{\vartheta_e} \tag{I.5}$$

I.1.3 β^+ radioactivity

During β-decay, a proton nucleus transforms into a neutron, emitting a positron (energy between some keV and about 2 MeV) and a neutrino following the decay equation:

$${}^{1}_{1}P \rightarrow {}^{1}_{0}n + {}^{0}_{+1}e + {}^{0}_{0}\vartheta_e \tag{I.6}$$

This reaction concerns nuclei whose number of protons are relatively high. the son nucleus possesses the same number of nucleons, which leads to the following decay equation:

$$ {}^{A}_{Z}X \rightarrow {}^{A}_{Z+1}Y + {}^{0}_{-1}e + {}^{0}_{0}\vartheta_e \tag{I.7} $$

Example ${}^{32}_{15}P \rightarrow {}^{32}_{16}S + {}^{0}_{-1}e + {}^{0}_{0}\vartheta_e$

I.1.4 Gamma decay

The γ radiations is consists of photons, just like X-rays, but much more energetic. The photonic spectrum is discreet because it corresponds to the difference in energy between the levels of the son nucleus; it represents a unique means of identification of each radioisotope. Most γ emissions instantly are as follow:

$$ {}^{A}_{Z}X^{*} \rightarrow {}^{A}_{Z}X + \gamma \tag{I.8} $$

In the case where the emission of the photon is delayed; we are talking about isometric transition. The son nucleus has along excited period state called a metastable state. The nucleus, created at an excited level m, returns to its ground state according to the equation:

$$ {}^{Am}_{Z}X \rightarrow {}^{A}_{Z}X + h\vartheta \tag{I.9} $$

Technecium 99 is part of those elements. Its metastable excited state, ${}^{99m}_{43}Tc$, having a half-life of 6 hours, decays by emitting photons of either 0.1427, or either 0.0022 and 0.1405 MeV.

I.2 The radioactive decay laws

I.2.1 Radioactivity decay

Radioactivity is a spontaneous phenomenon, obeying the laws of statistics. Given, at a time t, a quantity of radioactive substance containing N atoms, the average number (dN) of atoms that decay in a time interval (dt) is proportional to the total number N of atoms, in a ratio of proportionality characteristic of the nature of this radioactive substance:

$$dN = -\lambda N dt \tag{I.10}$$

The sign (-) indicates that there is a gradual decrease in the number N of radioactive atoms; λ is the radioactive constant of the nuclear species considered. The integration gives the number of atoms N present at time t:

$$N(t) = N_0 e^{-\lambda t} \tag{I.11}$$

N_0 being the number of atoms at time t = 0.

I.2.2 Radioactive period or half-life

The half-life ($T_{1/2}$), or period of radioactive isotope, is the time required for half of nuclei of this isotope initially present to decay naturally. It is given by the following relation :

$$T_{1/2} = \frac{\ln 2}{\lambda} \tag{I.12}$$

where λ is the decay constant charateristic. For each time interval corresponding to a half-life, the number of nuclei is divided by two (see Figure 2) [16].

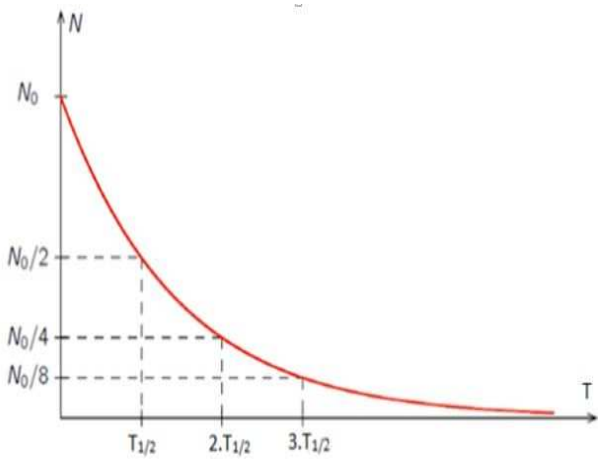

Figure 2: Radioactive decay

I.2.3 Activity

The activity of a radioactive source is the number of decays per unit of time. This activity is usually defined for a unit mass of radioactive element. It is about specific activity. The old unit of measure for radioactivity was Curie (Ci). The Curie was initially defined as the activity of about one gram of radium, natural element that we have been found back in soils with the Uranium. The current unit of activity measurement is becquerel (Bq) (1 Bq = 1 disintegration per second and 1Ci = 3.7$\times$ $10^{10} Bq$) [17]. The activity is obtained by the temporal derivation of the number of atoms of a given sample:

$$A(t) = -\frac{dN}{dt} = \lambda N_0 e^{-\lambda t} = \lambda N(t) \tag{I.13}$$

By the same reasoning, it can be shown that activity follows in the course of time the same law exponential as the decrease in the number of nuclides [18]:

$$A(t) = A_0 e^{-\lambda t} \tag{I.14}$$

I.3 Radioactive series

In the course of disintegration, all radioisotopes disintegrate when following four emission processes α, β^-, β^+, γ. The totality of radioactivity belongs to 4 families (also

called radioactive series) according to their mass number A. Thus any disintegration of a nucleus member of family gives birth to a nucleus necessarily belonging to this same family. Except few light elements such as potassium and rubidium With extremely low radioactivity, all natural radioactive elements are produced by successive decays α or β^-, from three radioactive elements ^{238}U, ^{235}U, ^{232}Th. They constitute three different families, those of radium, actinium and thorium, which contain respectively these three radioelements. Two radioelements of the same family have mass numbers that differ of a multiple of four, since disintegration leaves this number unchanged. The mass numbers have A = 4n + 2 (n integer) for the family of radium ^{226}Ra, 4n + 3 for that of actinium ^{227}Ac and 4n for that of ^{232}Th. There is a fourth family, for which A = 4n + 1, but it is composed only of artificial radioelements.

I.3.1 Uranium-238 and its decay series

According to Raad et al [19], the products of the decay are called radioactivity series. This series starts with the ^{238}U isotope, which has a half-life 4.5×10^{10} years as shown in Figure 3 [20, 21]. Since nuclides have very long half-life, this chain is still present today. The radionuclide ^{238}U decays into ^{234}Th emitting an alpha-particle, the newly formed nuclide is also unstable and decays further (Figure 3). Finally, after total of 14 such steps, emitting 8 alpha particles and 6 Beta particles, accompanied by gamma radiation, stable lead is formed ^{206}Pb. This series is said to be in secular equilibrium because all their daughters following ^{238}U have shorter half-life than the parent nuclide ^{238}U [22]. This decay series includes the ^{226}Ra which has half-lives of 1600 years and chemical properties clearly different from those of uranium.^{226}Ra decays into ^{222}Rn which is an inert noble gas that not form any chemical bonds and can escape into the atmosphere and attacks rapidly to aerosols and dust particles in the air deposited. The radiation emitted at the decay of these products, can cause damage to the deep lungs.

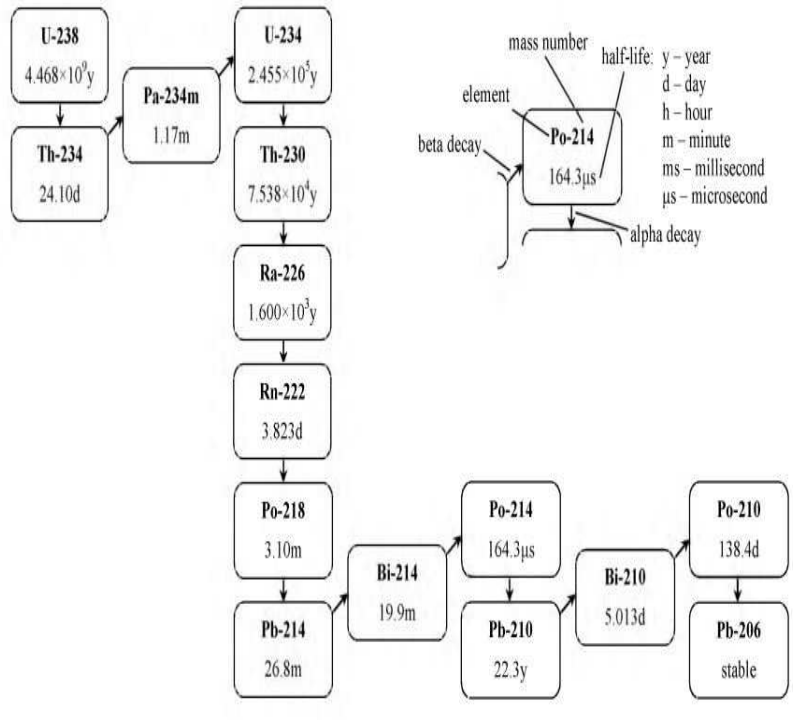

Figure 3: Uranium-238 decay series

I.3.2 Thorium-232 and its decay series

Natural thorium is 100% ^{232}Th. The decay series is shown in (Figure 4).

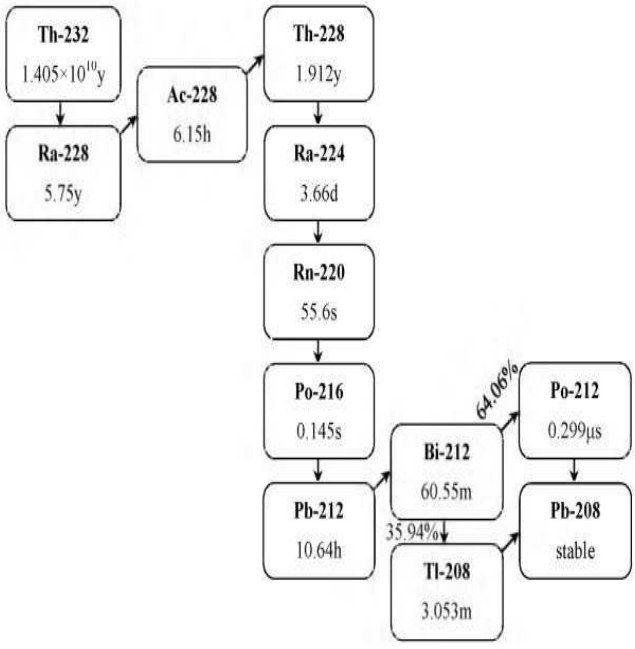

Figure 4: Thorium-232 decay series

Six alpha particles are emitted during ten decay stages. Four nuclides can be measured easily by gamma spectrometry: ^{228}Ac, ^{212}Pb, ^{212}Bi and ^{208}Tl. The decay of ^{212}Bi is branched only 35.94% of decays produce ^{208}Tl by alpha decay. The beta decay branch produces Po that cannot be measured by gamma spectrometry. If a ^{208}Tl measurement is to be used to estimate the thorium activity, it must be divided by 0.3594 to correct for the branching [23].

I.3.3 Uranium-235 and its decay series

According to Raad et al [19], it is also known as Actinium series and starts with ^{235}U and by successive transformations and up in a stable lead Pb. It comprises 0.72% of natural uranium. Although only a small proportion of the element, its shorter half-life means that, in terms of radiation emitted, its spectrometric significance is comparable to ^{238}U. The decay series, shown in (Figure 3), involves 12 nuclides in 11 decay stages and the emission of 7 alpha particles (except a number of minor decay branches). Since its abundance is very small, its dose is not taken into account in the measurements [23].

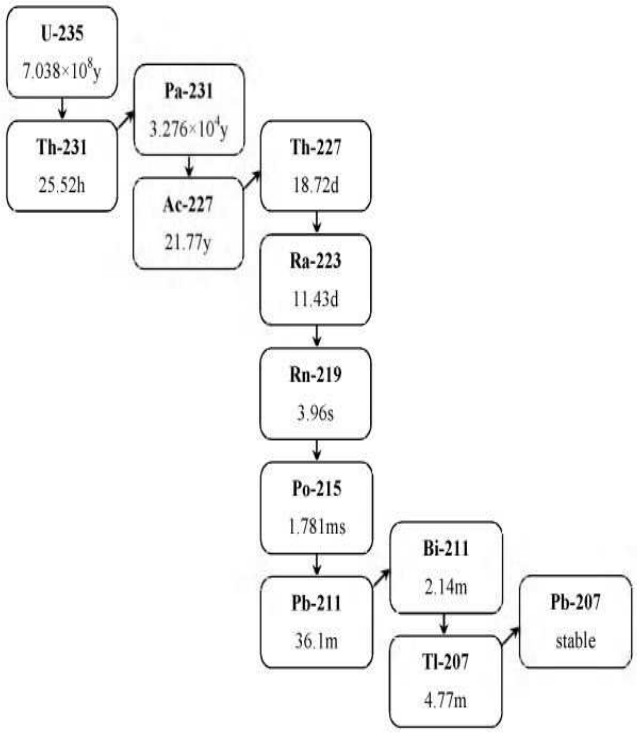

Figure 5: Uranium-235 decay series

Within this series, only ^{235}U itself can readily be measured, although ^{227}Th,^{223}Ra and ^{219}Rn can be measured with more difficulty. Even though the uncertainties may be high, measurement of the daughter nuclides can provide useful support information confirming the direct ^{235}U measurement or giving insight into the disruption of the decay series.

I.3.4 Potassium-40

According to Raad et al [19], In 1905, J.J. Thompson discovered the radioactivity in ^{40}K is what makes everybody radioactive, it is present in body tissue. This radionuclide can be decayed by three general modes:

a. Positron emission.

b. K- electron capture.

c. Beta emission.

In first mode, ^{40}K radionuclide disintegrates directly into the ground state of ^{40}Ca by then emission of Beta- particle of energy 1321 keV in probability of 88.8% of the decays and no gamma emission is associated with this type of disintegration [24]. Through the second mode,^{40}Ar by two ways, in the first one,^{40}K nuclide can be transformed into stable state (ground state) of ^{40}K disintegrates directly with one jump into ground state of ^{40}Ar with sixteen hundredths of the decays go by electron capture. In the second way, ^{40}K nuclide can be decayed indirectly into the ground state of ^{40}Ar by two stages. Firstly, ^{40}K decays into the first excited state of ^{40}Ar.

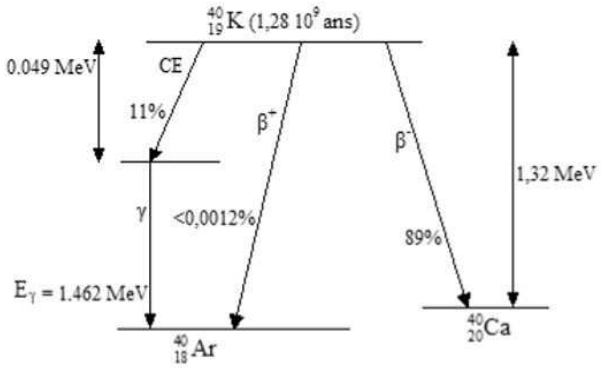

Figure 6: Potassium-40 decay chain

Secondly, the excited nuclide ^{40}Ar, decayed into ground state, accompanied by gamma

radiation of 1460 keV energy in probability of 11% of the ^{40}K atoms undergo this change. In the last one (beta emission), a proton will be decayed into positron and ^{40}K changed into ^{40}Ar with the emission probability of 0.0011%.

I.4 Bateman Equations

The Bateman equations are a mathematical relationship that describes the relative abundances and activities in a decay chain as a function of time. These govern the time evolution of all nuclear species in a radioactive chain, with the simplest case being a parent feeding a single daughter nuclide. H. Bateman [25] developed a general equation giving the number of atoms of the n^{th} isotope in the decay chain at time t in terms of the decay constants of all preceding isotopes in the chain. Typical example is the combined alpha and β^- decay processes of ^{235}U series, resulting finally into a stable isotope of lead (^{207}Pb). Before studying the case of n filiations, let us study the case of 4 bodies A, B, C, D where A, B, C are radioactive and D is stable, following the disintegration reactions:

A$\longrightarrow$B$\longrightarrow$C$\longrightarrow$D

Consider a sample composed exclusively of N_0 nuclei A at t = 0. We get the following equation system:

$$\begin{cases} \frac{dN_A}{dt} = -\lambda_A N_A \\ \frac{dN_B}{dt} = +\lambda_A N_A - \lambda_B N_B \\ \frac{dN_C}{dt} = +\lambda_B N_B - \lambda_C N_C \\ \frac{dN_D}{dt} = +\lambda_C N_C \end{cases} \tag{I.15}$$

N_A, N_B, N_C and N_D being respectively the number of nuclei present at any time t in substances A, B, C and D.

According to the resolution of the system previously, obtains:

$$N_A(t) = N_0 e^{-\lambda_A t} \tag{I.16}$$

$$N_C(t) = \lambda_A \lambda_B N_0 \left[\frac{e^{-\lambda_C t}}{(\lambda_A - \lambda_C)(\lambda_B - \lambda_C)} + \frac{e^{-\lambda_A t}}{(\lambda_B - \lambda_A)(\lambda_C - \lambda_A)} + \frac{e^{-\lambda_B t}}{(\lambda_A - \lambda_B)(\lambda_C - \lambda_B)} \right] \tag{I.17}$$

In the case of a filiation at n particles, a general expression of the solution concerning the n^{th} radioactive element is:

$$N_n(t) = N_0 \sum_{i=0}^{n} \left[\frac{e^{-\lambda_i t}}{\prod_{j\neq i}^{n} {}_{j=0}(\lambda_j - \lambda_i)} \right] \prod_{i=0}^{n-1} \lambda_i \tag{I.18}$$

In the case where we consider that sample consists of N_0^0 nucleus of X_0 and N_1^0 nucleus from X_1 at t = 0, then the solution for the elements $X_{n\geq 1}$ will be the sum of the solutions for $(N_0(0) = N_0^0,\ N_{(n\neq 0)}(0) = 0)$ and $(N_1(0)) = N_1^0, N_{n\neq 0}(0) = 0)$. In fact, if N_i^0 is the initial quantity of X_i at t = 0, the general solution for the n^{th} element is:

$$N_n(t) = \sum_{k=0}^{n} \left[N_k^0 \sum_{i=k}^{n} \left(\frac{e^{-\lambda_i t}}{\prod_{j\neq i}^{n} {}_{j=0}(\lambda_j - \lambda_i)} \right) \right] \prod_{i=0}^{n-1} \lambda_i \tag{I.19}$$

The activity of n^{th} element is given by

$$A_n(t) = N_0 \sum_{i=0}^{n} \left[\frac{e^{-\lambda_i t}}{\prod_{j\neq i}^{n} {}_{j=0}(\lambda_j - \lambda_i)} \right] \prod_{i=0}^{n-1} \lambda_i \tag{I.20}$$

I.5 Secular Equilibrium

According to Abubakar [26], If we consider the case of secular equilibrium where the activity of the parent does not decrease measurably during many subsequent half-lives of the daughter nucleus, then a chain of n, subsequent short-lived radionuclides can all be in secular equilibrium with the initial long-lived parent. The daughter nuclides decay at the same rate at which they are formed, such that: $\lambda_1\ N_1$ = $\lambda_2\ N_2$ = ... =$\lambda_n\ N_n$. The activity of each member of the chain equals that of the parent while the total activity is n times the activity of the original parent. To illustrate this, consider the first three stages of the ^{232}Th (i.e.$^{232}Th \rightarrow {}^{228}Ra \rightarrow {}^{228}Ac$) and ^{238}U (i.e. $^{238}U \rightarrow {}^{234}Th \rightarrow {}^{234m}Ra$) decay series (see figs. 3 and 4). In the case of each parent/daughter pair, the half-life of the parent is much greater than that of the daughter and thus a secular equilibrium established between each pair. The activity of ^{234}Th and ^{234}Pa + ^{234m}Pa (the activity will

be shared between the two nuclides based on their respective branching ratios), will be equal to that of ^{238}U and activity of ^{228}Ra and ^{228}Ac will be equal to that of ^{232}Th. The total activity will be three times that of the ^{238}U and ^{232}Th, respectively. Secular equilibrium occurs if the half-life of the parent nuclide is very long compared to that of the daughter.

I.6 Sources of exposure

Radiation exposure that reaches the body can be either external or internal. External exposure to radiation causes external irradiation. It stops as soon as the body is no longer in the path of radiation. When radioactive substances are inside the body, there is internal exposure. Internal contamination ceases when radioactive substances have disappeared from the body after a longer or shorter time. The removal of the contamination can be done either by radioactive decay, or by natural elimination, or by treatment.

I.6.1 External exposure

I.6.2 Exposure of cosmic origin

This type of radiation is produced as a result of the continuous interaction of cosmic-ray particles with nitrogen in the atmosphere. The types of radionuclides produced are known as cosmogenic radionuclides. Typically, they include: ^{3}H, ^{7}Be, ^{14}C and ^{22}Na as shown in Table 1 [1]. The production of these radionuclides is highest in the upper stratosphere but some energetic cosmic-rays neutrons and protons which survive in the lower stratosphere are able to produce the cosmogenic radionuclides as well. The annual average effective dose worldwide at sea level has been estimated to be 320 μSv with the directly ionizing and indirectly ionising radiation component contributing 270 μSv and 48 μSv respectively. The dominant component of the cosmic ray field at the ground level is muons with energies between 1 and 20 GeV [1] and this contribute about 80 % of the absorbed dose rate in free air from the directly ionizing radiation. The population-

Table 1: Cosmogenic radionuclides [1] ([a] altitude weighting factors applied at sea level for directly ionising (1.25) and neutrons (2.5).)

Element	Isotope	Half-life	Decay mode
Hydrogen	^{3}H	12.33 a	Beta (100%)
Beryllium	^{7}Be	53.29 d	EC^{a} (100%)
	^{10}Be	1.51×10^{6} a	Beta (100%)
Carbon	^{14}C	5730 a	Beta (100%)
Sodium	^{22}Na	2.602 a	EC (100%)
Aluminium	^{26}Al	7.41×10^{5}a	EC (100%)
Silicon	^{32}Si	172 a	Beta (100%)
Phosphorus	^{32}P	14.26 d	Beta (100%)
	^{35}P	25.34 d	Beta (100%)
Sulphur	^{35}S	87.51 d	Beta (100%)
Chlorine	^{36}Cl	3.01×10^{5} a	EC(1.9%),Beta (100%)
Argon	^{37}Ar	35.04 d	EC (100%)
	^{39}Ar	269 a	Beta (100%)
Kryptor	^{81}Kr	2.29×10^{5} a	EC (100%)

weighted average absorbed dose rate from the directly ionizing and photon components of cosmic radiation at sea level is estimated to be 31 $(nGy\ h^{-1})$ $(280Sv\ y^{-1})$ [1]. It is however more difficult to estimate the neutron radiation component at the sea level because of the low response of instruments to high energy photons, which is the important component of the spectrum. The annual world average of the neutron components contribution to the cosmic radiation is estimated to be 120 μSv. The global value of the annual collective dose is about 2×10^{6} man-Sv and two thirds of the world population that live at altitude of 0.5 km receive about one half of this dose [1]. Previous UNSCEAR reports on the assessment of the cosmogenic radionuclides have reported annual effective doses of 12 μSv for ^{14}C, 0.15 μSv for ^{22}Na, 0.01 μSv for ^{3}H and 0.03 μSv for ^{7}Be. These cosmogenic radionuclides are relatively homogenously distributed on the surface of the earth [1,27].

I.6.3 Exposure from telluric origin

It originates from gamma emitting radionuclides present in rocks and soils. ^{40}K and the gamma-emitting descendants of the ^{238}U and ^{232}Th series are the main isotopes responsible for external terrestrial irradiation of telluric origin of populations [28]. The

existence of a gaseous chemical element, radon, in the two families of uranium and thorium contributes to reduce, because of its exhalation of soils and rocks, the telluric exposure attributable to gamma emitters post-emanation present in both families (Tab 2). The irradiation of telluric origin is on average 60 $nGy\ h^{-1}$. It can vary between 10 and 200 $nGy\ h^{-1}$ depending on the ^{40}K and gamma emitting radionuclide concentrations of the ^{238}U and ^{232}Th series present in soils. Another cause of rapid variation is due to the deposition on the ground, in the event of rain, of solid descendants gamma emitter post-emanation, ^{222}Rn in particular. The average annual dose associated with natural radiation from land-based sources is estimated at 74 μSv for an individual staying 20% of his time outdoors.

Table 2: The global average annual effective dose from natural radiation sources [29]. Note: relative values are given in brackets (%)

Sources of irradiation	External (mSv)	Internal (mSv)	Total
Cosmic rays	0.410(17)		0.410(17)
Cosmogenic radionuclides		0.015(1)	0.015(1)
Natural sources :			
^{40}K	0.150(6)	0.180(7)	0.330(13)
^{238}U - series	0.100(4)	1.239(51)	1.339(55)
^{232}Th - series	0.160(7)	0.176(7)	0.336(14)
Total	0.820(34)	1.616(66)	2.436(100)

I.7 Internal exposure

I.7.1 Exposure to Radon

According to Robin Corrigan [30] The main sources of radon in dwellings are rocks and soil, with secondary contributions from building materials which happen to contain ^{226}Ra, and water from well. Figure (7) illustrates the main concepts and sequences of steps associated with the process through which humans receive radiological doses from radon gas in dwellings. For radon originating from rocks and soil, the main pathway into the dwellings is through cracks in the foundation and walls. Outdoor levels

of radon gas may also contribute to residential concentrations through windows or air exchange systems, though ventilation is generally beneficial in reducing radon exposure since indoor concentrations are normally higher than outdoors. Once radon enters the residence, the occupants may be exposed to the gas and its short-lived progeny. Residential exposure occurs when the occupants are inside their residences, estimated to be approximately 70% of time for average members of the population [31]. Radon exposures are therefore multiplied by an Occupancy Factor to account for the fraction of time exposed. The properties that allow radon to accumulate in dwellings(e.g. inert gas, 3.82 d half life) also imply that most radon breathed into the lungs is expelled. However, the unstable radon progeny are solids with electrostatic charge and may attach to airborne particulates and aerosols. These may adhere to the surface of the lungs following inhalation, resulting in a reduced chance of being cleared before decaying. Thus, it is the progeny, rather than radon itself, which exerts the greatest dose associated with radon exposure. Therefore, for a given radon concentration, it is important to know what concentration of progeny is implied. These proportions are related by the Equilibrium Factor, F. If an enclosed volume was constantly supplied with radon gas, the concentration of the short-lived progeny would increase until they are in secular equilibrium. They are decaying at the same rate that they are created (i.e. the same rate at which the ^{222}Rn is decaying). In such a scenario, the relative contributions to radioactivity from radon and from its progeny at steady-state are known based on the type and energy of the emissions from the radionuclides. In practice, the steady-state proportions are different from the situation described above because radon progeny can be removed from the pool by means other than decay, which includes attachment of the progeny to walls, floors, or other surfaces, as well as deposition of unattached progeny. These phenomena reduce the concentration of radon progeny but not the concentration of radon gas, thereby reducing the equilibrium ratio. The Equilibrium Factor is the ratio of the radon progeny activity to radon activity in the scenario of interest. For typical homes, the Equilibrium Factor has been estimated to be approximately 40% by Hopke et al. [32]. Figure 7 indicates an indoor concentration of radon gas and radon progeny with some of the radon

progeny becoming attached to airborne particles and eventually being inhaled into the lungs where they may attach to the lining of the lungs.

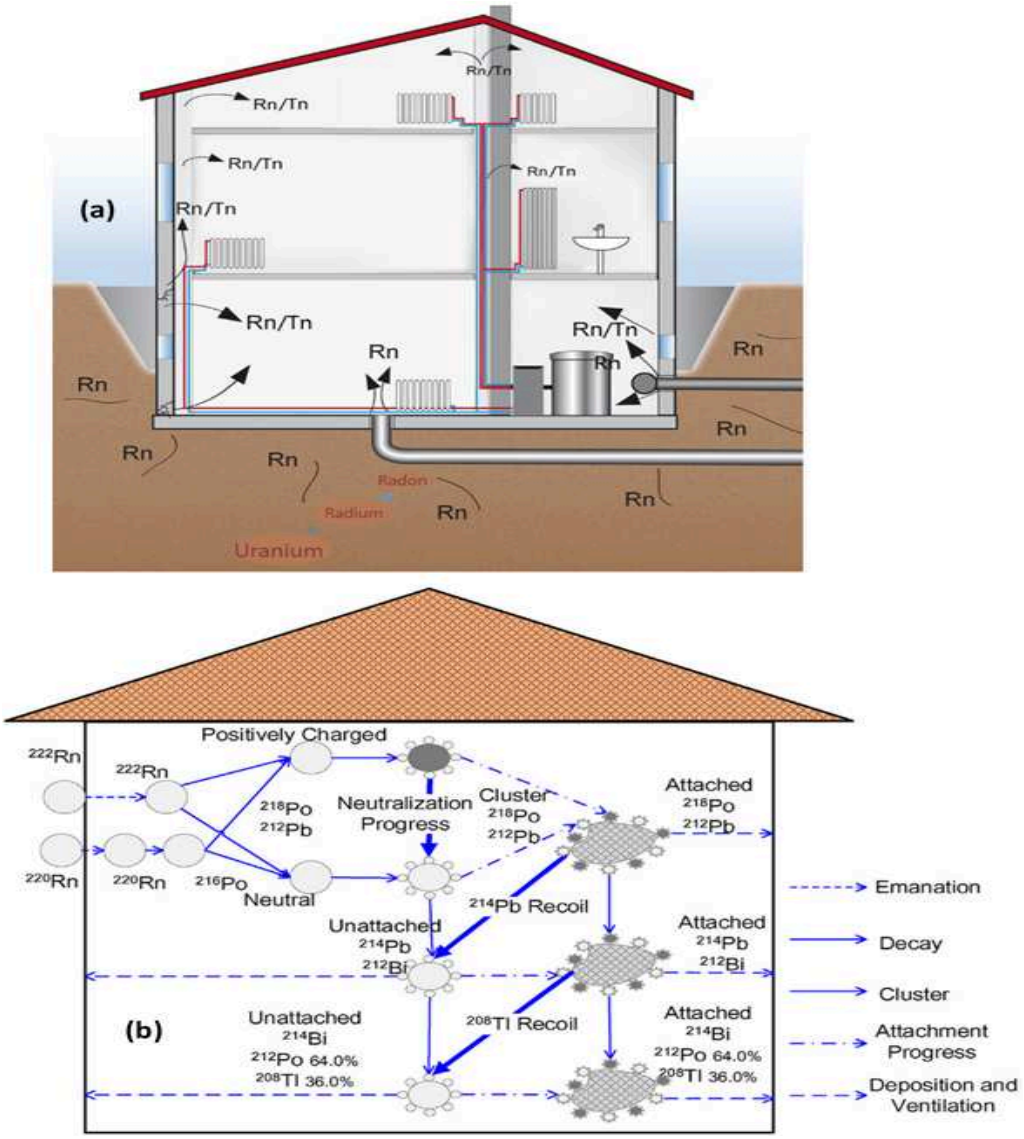

Figure 7: The sources of indoor ^{222}Rn (Rn) (a) and ^{220}Rn (Tn), Illustration of the behaviors of indoor ^{222}Rn, ^{220}Rn and their progenies (b). [33]

I.7.2 Radon and Thoron decay series

There are 39 known isotopes of radon with atomic mass numbers ranging from 193 to 231.

For instance, when some amount of ^{222}Rn decays to ^{218}Po, which is also radioactive and has half-life of 3.10 minutes [36], half of polonium atoms will decay in 3.10 minutes.

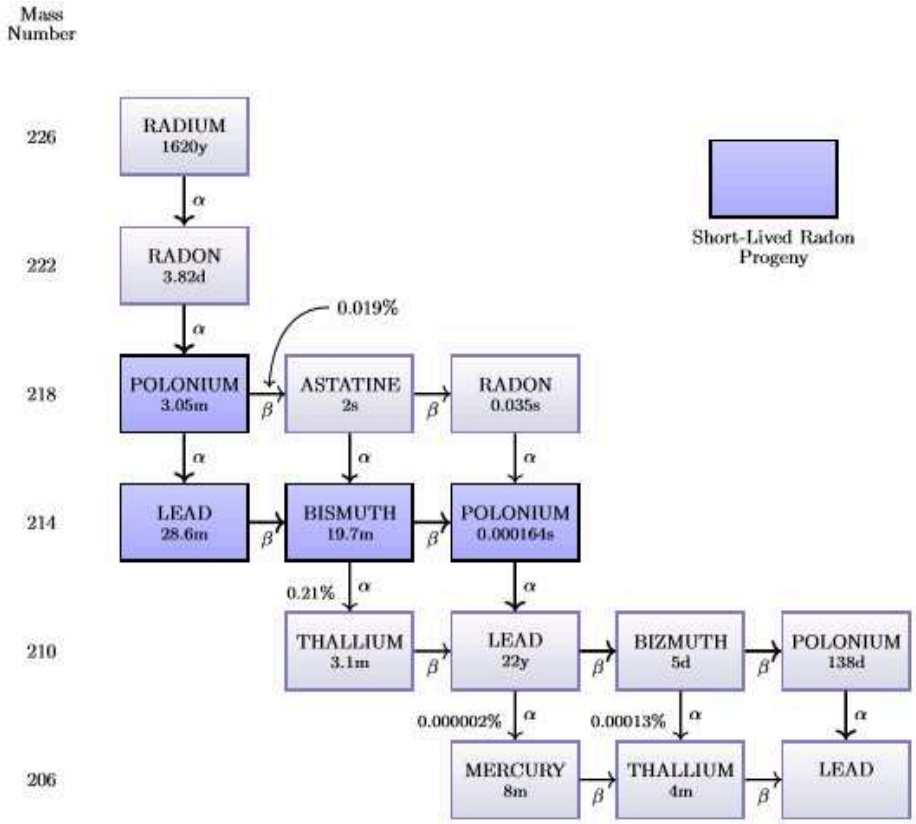

Figure 8: Radon decay chain

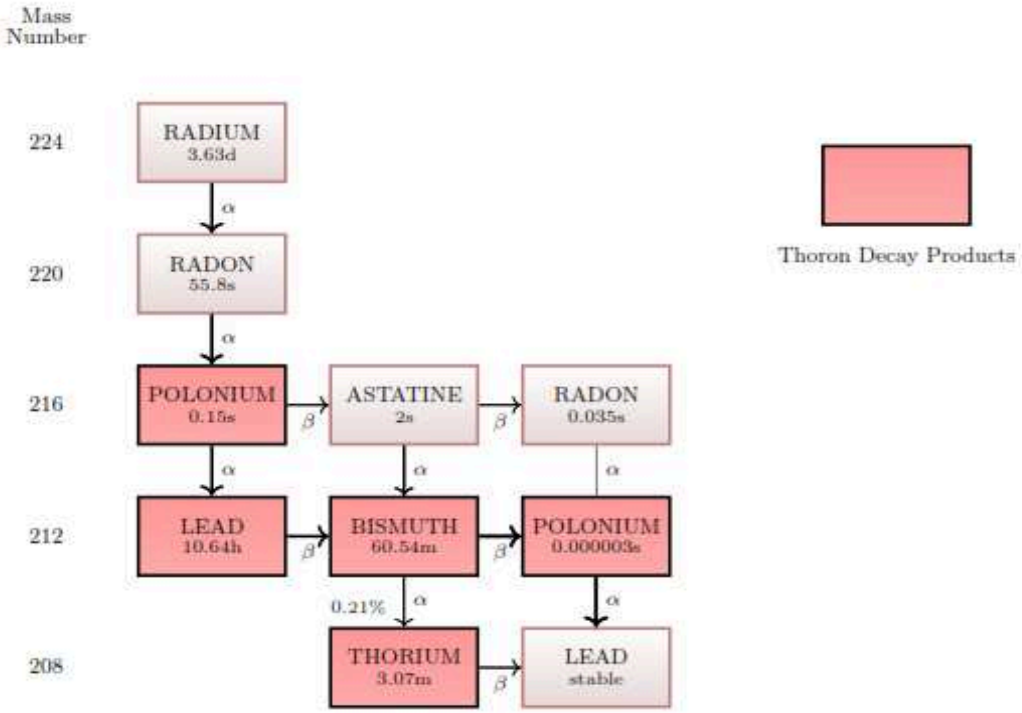

Figure 9: Thoron decay chain

Thus, ^{218}Po cannot accumulate, but it will reach an equilibrium amount. Since ^{218}Po half-life is much shorter than the one of ^{222}Rn, this example demonstrates a case of secular equilibrium. This means that after a period of time, quantity of polonium will remain constant (will decrease only due to decrease of radon amount). In this case, polonium production rate is equal to its decay rate. While moving down the decay chain, it is obvious, that the amount of each next isotope produced, depends on the activity of its parent. When the half-live of progeny is not short enough, compared to the parent's half-life, only transient equilibrium can be achieved. Finally, when the half-life of the daughter isotope is longer, than the one of the parent, no equilibrium can occur.

I.8 Gamma-rays interaction with matter

Gamma rays are photons that originate from the nuclei of radioactive atoms undergoing decay. They have no mass and no charge. They are quanta of electromagnetic energy that travel at the speed of light and can travel long distances in air un-attenuated. When these photons interact with matter, free electrons are generated and as these electrons are slowed down by matter, they create charge pairs. The photon detectors use the charge pairs generated to determine the photon energy by measuring the quantity of charge produced by these pairs [37]. The knowledge of interactions of gamma rays with detector scintillation material is essential for the understanding of how the gamma photons are detected and attenuated in the detectors. Gamma-ray photons interact with matter in three processes.

I.8.1 Photoelectric Absorption

According to Todsadol [38] In the process of photoelectric absorption, a photon interacts with a bound electron in an absorber material in which the photon is completely absorbed. Then, an energetic electron called photoelectron is ejected from one of the electron shells with a kinetic energy given by the incident photon energy $(h\upsilon)$ minus the

binding energy of the electron in its origin shell (E_b). For typical gamma-ray energies, the emission of the photoelectron is likely to originate from the most tightly bound or, K-shell, of the atom. The binding energies of these K-shell electrons vary from a few keV for low-Z materials to tens of keV for material with higher atomic number [39]. The photoelectric absorption process is shown schematically in the diagram below.

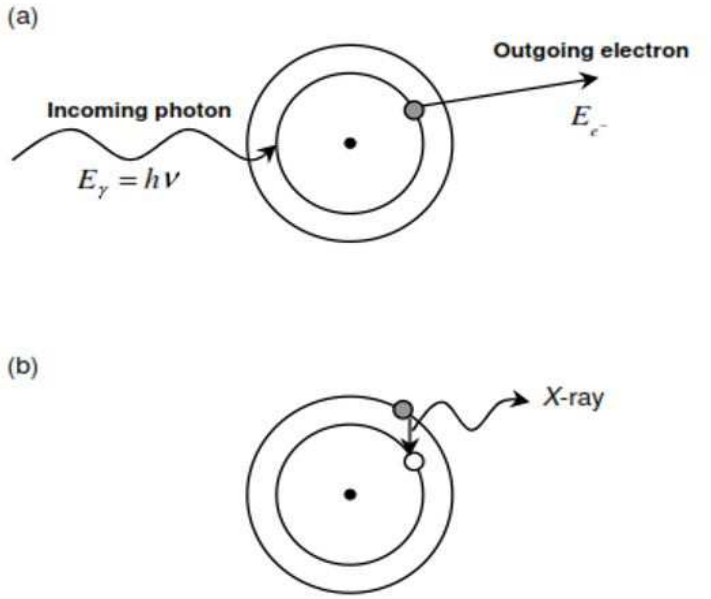

Figure 10: Schematic of the photoelectric absorption process.

As can be seen in Figure 10.a, the outgoing electron is ejected with a kinetic energy given by [40–43]:

$$E_{e^-} = h\vartheta - E_b \tag{I.21}$$

The photoelectron emission also creates a vacancy in a shell of the atom resulting in an excited state. The de-excitation of the atom can occur by the electron rearrangement from higher shells to fill in a vacancy leading to the emission of characteristic X-ray shown in Figure 10.b. Alternatively, the excitation energy can be carried away by the release of other, less tightly bound electrons known as Auger electrons. The interaction cross section (τ) of the photoelectric process varies in a complex manner with E and with the value of Z of the absorber. A single analytic expression cannot describe the

probability of this process, but an approximation can be given by [39, 44, 45]:

$$\tau \cong const.\frac{Z^n}{E_\gamma^m} \tag{I.22}$$

where the power indices n and m are numbers ranging from 3 to 5 over the gamma-ray energy region of interest. The photoelectric absorption probability strongly depends on photon energy and atomic number of an absorber material. The strong Z dependence indicates that a high-Z material is very effective in the absorption of photons. The strong dependence on the photon energy is the reason why the photoelectric process is significant at low energy of photons, but becomes less dominant at higher energies.

I.8.2 Compton Scattering

The Compton scattering process describes a collision between the incident gamma-ray photon and weakly bound or free electron in the absorbing material. Instead of giving up its entire energy, only a portion of the photon energy is transferred to the electron. The result of this interaction is that the incoming gamma-ray photon is degraded in energy and deflected from its original direction and an electron known as a recoil electron is created. From the laws of conservation of total mass-energy and linear momentum, the energies of the scattered photon and recoil electron are related to the angles at which they are emitted. Figure 11 shows a schematic of the Compton scattering process.

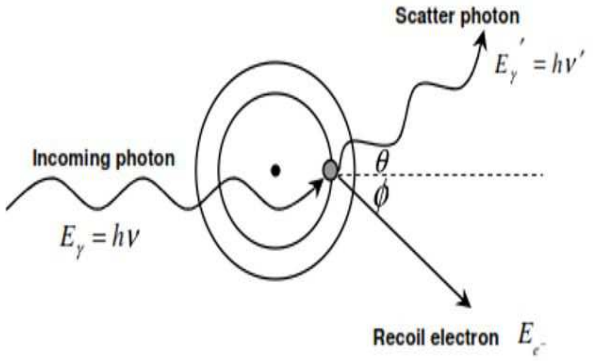

Figure 11: Schematic of the Compton scattering process.

The energy of the scattered gamma-ray $h\upsilon'$, is related to its scattering angle θ by

the expression [42,43,46,47]:

$$h\vartheta' = \frac{h\vartheta}{1+\alpha(1-\cos\theta)} \tag{I.23}$$

where $\alpha = \frac{h\vartheta}{m_0c^2}$, m_0c^2=511 Kev represents the rest mass energy of the electron. It then follows that the kinetic energy of the recoil electron is given by [40,48]:

$$E_e = h\vartheta - h\vartheta' = h\vartheta\left(\frac{\alpha(1-\cos\phi)}{1+\alpha(1-\cos\phi)}\right) \tag{I.24}$$

The energy of the recoil electron can vary from zero $(\theta = 0)$ up to a maximum value $(\theta = \pi)$ depending upon the angle of scatter. The maximum energy of the recoil electron is given by

$$E_{e(\max)} = \frac{h\vartheta}{1+\frac{m_0c^2}{2h\vartheta}} \tag{I.25}$$

The Compton cross section (σ) can be described by the Klein-Nishina formula for a differential solid angle $d\Omega$ at an angle θ as [39].

$$\frac{d\sigma}{d\Omega} = Zr_0^2\left(\frac{1}{1+\alpha(1-\cos\theta)}\right)^2\left(\frac{1+\cos^2\theta}{2}\right)\left(1+\frac{\alpha^2(1-\cos\theta)^2}{(1+\cos^2\theta)[1+\alpha(1-\cos\theta)]}\right) \tag{I.26}$$

where, r_0 is the classical electron radium. The probability of Compton scattering depends strongly on the number of electrons per unit mass of the interacting material. It also depends on the incoming gamma-ray energy as function of $1/E_\gamma$ [44,48]. Compton scattering is the dominant interaction process for gamma-ray energies ranging from 0.1 to 10 MeV [42]. At higher energy, another interaction mechanism, known as 'pair production' becomes more significant.

I.8.3 Pair Production

The third significant interaction mechanism of gamma-rays with matter is pair production. This process becomes increasingly important when the incident gamma-ray photon has energy significantly greater than twice the rest mass energy of an electron

$(2m_0c^2 = 1.022MeV)$. This interaction occurs within the Coulomb field of a nucleus in which the gamma-ray photon is absorbed into the vacuum and is converted into an electron-positron pair. Since an initial photon energy of at least m_0c^2 is required for the creation of the electron-positron pair, any excess energy $(E_\gamma - m_0c^2)$ carried in by the photon above 1.022 MeV is imparted to and shared equally by the positron and the electron as kinetic energy, given by [39, 40, 49]:

$$E_{e^+} = E_{e^-} = \tfrac{1}{2}(h\vartheta - 2m_ec^2) \tag{I.27}$$

After electron and positron pair is created, they can traverse the medium, losing their kinetic energy by collisions with electrons in the surrounding material through ionization, excitation and/or bremsstrahlung. Once, the positron slows down, it can combine with an atomic electron in the surrounding material and subsequently annihilate to form two photons, called annihilation photons, each with energies of about m= 0.511 MeV. In order to conserve linear momentum these two photons must be emitted in opposite direction. The interaction cross section (k) for pair production is related to

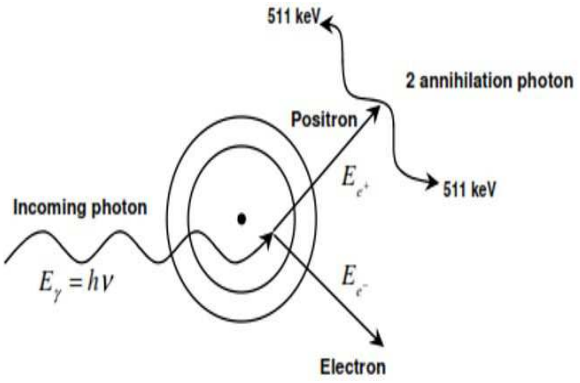

Figure 12: Schematic of the pair production process and annihilation.

the atomic number of the material as approximately proportional to Z^2 [39, 48, 49]. The probability of pair production mechanism depends on the gamma-ray energy above the threshold $(at\ 1.022MeV = 2m_0c^2)$ and becomes the dominant interaction process for gamma-ray energies greater than 10 MeV [39, 42]. Figure 13 represents the importance of the three principal gamma-ray interaction processes as a function of γ-ray energy and

the value of Z of the absorber.

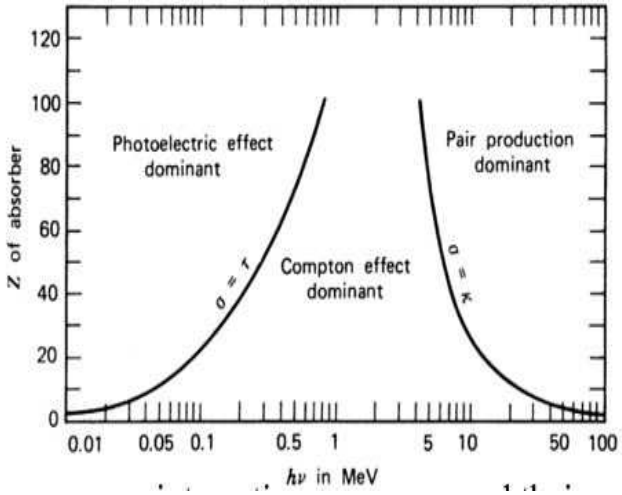

Figure 13: The three gamma-ray interaction processes and their regions of dominance [39].

I.9 Interactions of heavy charged particles

The heavy charged particles (protons, deuterons, α particles), having the energy of order of a few MeV, are emitted by nuclear reactions, spontaneous radioactive decays or reactions caused by nucleus bombardment with accelerated particles, or artificially accelerated with cyclotrons (energies of several tens of MeV). A heavy charged particle that passes through the material looses energy mainly through the ionization and excitation of the atoms. A heavy charged particle can transfer only a small fraction of its energy during a single electronic collision. His deflection during the collision is negligible. All heavy particles travel essentially along a direct path in matter [50]. Heavy charged particles $(m \gg me)$, such as α-particles, protons, or ionized atom cores, interact primarily through coulombic forces between their own positive charge and the negative charge of the orbital electrons of the atoms of the absorber material. The direct interaction of these particles with the nuclei (Rutherford diffusion) is possible, but much more rare and therefore in practice negligible to model their slowing down. The very high value of stopping power has important consequences: the path of the heavy particles is, at the same energy, much smaller than that of the electrons and the TEL along the

trajectory is very high, which gives these particles high biological efficiency [51,52].

I.10 Interactions of light charged particles

Electrons are light particles carrying an elementary electric charge, negative for negatons and positive for positrons [53]. An electron crossing a material medium loses energy by: - "Collisions" that is to say Coulomb interactions with the electrons of the atoms of the Middle crossed, which leads to the ionization or the excitation of these atoms, two cases of figure can appear: electrons act either with electrons of the atoms constituting the middle, or either with their nucleus [54]. In the case of an "electron-electron" interaction, we will speak of a collision. There exist two types: ionization and excitation; in the case of an "electron-core" interaction, we will talk about braking radiation.

I.11 Phenomenon of excitation and ionization

These interactions are most likely. The incident electron transfers part of its kinetic energy to the atomic electron; depending on the value of the quantity of energy transferred, one or the other of these reactions will take place [55]: Let ΔE denote the kinetic energy of the incident electron and W_L the electron binding energy of the target atom. Depending on whether or not ΔE is sufficient to eject the electron from its orbit, two phenomena can occur: [53]. If $\Delta E \geq W_L$: the electron of the target is ejected from its orbit with kinetic energy ($\Delta E - W_L$), and an ionization of the target atom occurs. The ejected electron, called the secondary electron, can in turn create other ionizations if its kinetic energy is sufficient.

If $\Delta E < W_L$: the transfer of energy ΔE cannot produce any ionization but, can carry the target electron to a higher energy level, with excitation of the target atom.

If $\Delta E \ll W_L$: this excitation results to a heat dissipation (by increasing the translation energy, rotation or vibration of the target molecules.

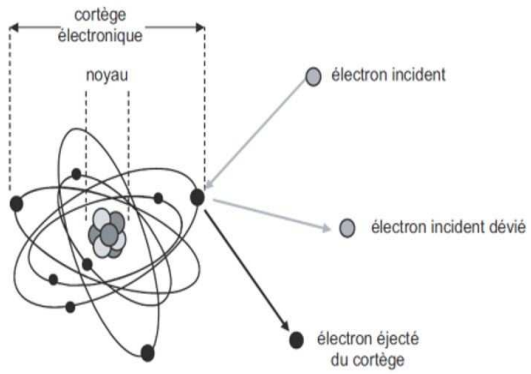

Figure 14: Ionization phenomenon.

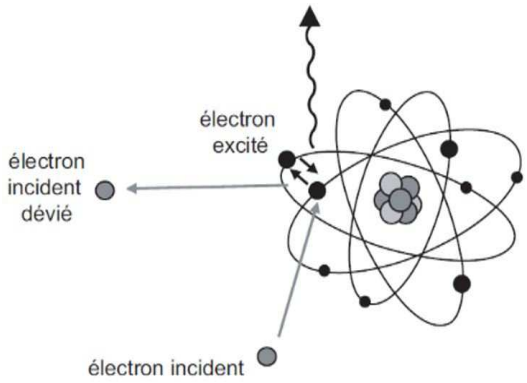

Figure 15: Excitation phenomenon.

I.12 Bremsstrahlung

More rarely, incident electrons can interact with the nuclei of the atoms of the substance being passed through. They are influenced by the coulombic field of the nucleus: they are then deviated and yield some of their energy to the nucleus. This manifests itself as a slowdown or braking. The lost energy is emitted in the form of X-ray radiation, known as ”braking”. In the literature, the term ”bremsstrahlung” (”braking radiation”, in German) is also used. This phenomenon is important only in the case of electrons of high energy (greater than 1 MeV) passing through a material made up of heavy atoms (high atomic number Z) [55].

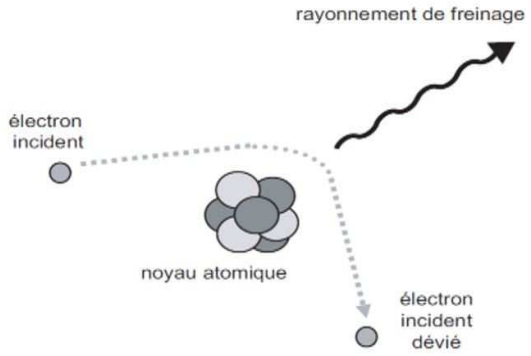

Figure 16: Braking phenomenon.

I.13 Dosimetry of ionizing radiation

The heterogeneity of the emission of the source of radiation, the characteristics of radiation use, the distances of the source with respect to the different parts of the volume of the treated products and the structure of the product do not make it possible to obtain an identical dose in all the volume of the product. Hence the need to proceed to dosimetry [56]. The biological effect obtained during irradiation of living matter with radiation depends essentially on the nature of the radiation and the energy absorbed by the irradiated material. Dosimetry have as purpose to determine this absorbed energy. This determination is essential:

- To estimate the potential danger of diagnostic techniques using in vivo ionizing radiation.

- To predict in radiotherapy, the effects of treatment on tumor tissues and adjacent healthy tissues.

- To define the norms of individual and collective radioprotection [57].

I.14 Quantities and dosimetric units

Dosimetric quantities characterize the physical effect of radiation on matter in terms of transferred energy or energy deposition.

I.14.1 Exposure

The exposure applies only to indirectly ionizing radiation and among these only to X and gamma rays. This amount of exposure is defined by ICRU (International Commission on Radiation Units and Measurements) as the quotient of charge ΔQ by mass air volume Δm [57–59]:

$$X = \frac{\Delta Q}{\Delta m} \tag{I.28}$$

The unit is: $C\ kg^{-1}$ The old unit used was Roentgen (R), $1R = 2.58.10^{-4} C\ kg^{-1}$ where ΔQ is the total electrical charge of all the ions of a given sign produced in the air when all the secondary electrons released by the photons in an air volume of mass Δm are completely stopped by the air. The ions produced by the absorption of the braking radiation emitted by highy energetic secondary electrons do not enter the charge ΔQ.

I.14.2 Kerma

Kerma (Kinetic Energy Released in Matter) is used to characterize indirectly ionizing radiation such as photons and neutrons. It defines the transfer of energy to directly ionizing charged secondary particles and the sum of the initial kinetic energies of the charged particles set in motion by the incident radiation in a volume of mass dm.

$$K = \sum \frac{dE}{dm} \tag{I.29}$$

I.14.3 Absorbed dose

The activity of a radioactive source is expressed in Becquerel (Bq) which is also the number of nuclei that spontaneously transform per second. When radiation interacts with matter, it transmits energy to it. This transfer is defined by the absorbed dose of which the unit is gray (Gy) which is also the deposit of 1 J/Kg. The energy deposited at a point makes it possible to define the importance of an irradiation. The absorbed dose D_{abs} or

radiation at a point, corresponds to the energy which is deposited (dE) per unit mass (dm). The absorbed dose is given by the following relation

$$D_{abs} = \frac{dE}{dm} \tag{I.30}$$

The activity of a source is not directly related to the absorbed dose because D_{abs} varies according to the radioelements and therefore the nature of the emitted radiation. Depending on the type of radiation, it is possible to obtain different biological effects at equivalent absorbed dose. For example, when α-beams enter the material, they are braked more rapidly by the γ or X radiation. They are therefore more disruptive because they spread less their energy deposition. To take into account the nature of the radiation emitted, it is therefore necessary to use an equivalent dose.

I.14.4 Absorbed dose rate

The absorbed dose rate, D_{abs} (nGy h^{-1}) is the quotient of dD by dt, where dD is absorbed dose increment during the corresponding dt time interval:

$$\dot{D}_{abs} = \frac{dD}{dt} \tag{I.31}$$

I.14.5 Equivalent dose

Biological detriment to an organ depends not only on the physical average dose received by the organ but also on the pattern of the dose distribution that results from the radiation type and energy [24]. For the same dose to the organ a or neutron radiation will cause greater harm compared to γ-rays or electrons. Effectiveness of the given radiation in inducing health effect is expressed in equivalent dose. Equivalent dose H_T as per equation 32 [1] is the product of the absorbed dose D and the radiation weighting factor of the radiation. The radiation weighting factors are related to the particular type

of radiation and depend on the ionizing capacity and density.

$$H_T = \sum_R W_R D_{T,R} \tag{I.32}$$

where $D_{T,R}$ is the absorbed dose in tissue T due to radiation R. In 2007, the ICRP defined W_R values that are grouped in the table.

Table 3: Recommended radiation weighting factors from ICRP [60]

particule	Energie (E)	W_R (E en MeV)
X et γ	All energy	1
n	$<$ 1 Mev	2.5 + 18.2$e^{-\frac{\ln^2(E)}{6}}$
	1 to 50 Mev	5 + 17$e^{-\frac{\ln^2(2E)}{6}}$
	$>$ 50 Mev	2.5 + 3.25$e^{-\frac{\ln^2(0.04E)}{6}}$
A fragments of fission	All energy	20
e^-	All energy	1
p	All energy	2

The equivalent dose rate (H_T) is the equivalent dose based on the exposure time $(Sv\ yr^{-1})$.

I.14.6 Effective dose

Various organs and tissues in the body differ in their response to radiation. For the same equivalent dose the detriments from the exposure of different organs or tissues are different. Equivalent dose in each tissue or organ is multiplied by a tissue weighting factor W_T and the sum of these products over the whole body is the effective dose, given by following equation [1].

$$E = \sum_T W_T H_T = \sum_T W_T \sum_R W_R D_{T,R} \tag{I.33}$$

The effective equivalent dose rate (E) is also the effective dose based on the exposure time $(Sv\ yr^{-1})$.

Table 4 lists the tissue weighting factors for tissues and organs of the human body. These factors were obtained from a reference population of equal numbers of men and

Table 4: Tissue weighting factors according to ICRP [60],$(*)$ Remaining tissues: Adrenals, extrathoracic region, gall bladder, heart, kidneys, lymphatic nodes, muscle, oral mucosa, pancreas, prostate (man), small intestine, spleen, thymus, uterus/cervix (woman)

Tissue	Tissue weighting factor W_T	$\Sigma\, W_T$
Bone-marrow (red), colon, lung, stomach, breast, remaining tissues(*)	0.12	0.72
Gonads	0.08	0.08
Bladder, Oesophagus, Liver, Thyroid	0.04	0.16
Bone surface, Brain, Salivary glands, Skin	0.01	0.04
	Total	1.00

women ranging in age. Because of the normalization of all tissue weighting factor values is unity, the effective dose equals an uniform equivalent dose over the whole body [61, 62]. The SI unit of effective dose is also the Sievert (Sv).

I.15 Natural radioactivity in the world

According to Elijah [64], There are several studies that have been carried out to access the dangers of human exposure to radiations from naturally occurring radionuclides in the environment. In Cyprus, a survey was carried out to determine activity concentration levels and associated dose rates from the naturally occurring radionuclides ^{232}Th, ^{238}U and ^{40}K in the various geological formations by means of high-resolution gamma ray spectrometry. From the measured spectra, activity concentration were found to be ^{232}Th (range from 1.0×10^{-2} to 39.8 $Bq\, kg^{-1}$), ^{238}U (from 1.0×10^{-2} to 39.3 $Bq\, kg^{-1}$) and ^{40}K (from 4.0×10^{-2} to 565.8 $Bq\, kg^{-1}$). Gamma absorbed dose rates in air were calculated to be in the range of 1.1×10^{-2} to 51.3 $nGy\, h^{-1}$ with an overall mean of 8.7 $nGy\, h^{-1}$ which was below the world average of 60 $nGy\, h^{-1}$. Effective dose rates equivalent to population were calculated to be between 1.3×10^{-2} and 62.9 μSv y^{-1} with a mean of 10.7 μSv y^{-1} [65]. In Nigeria exposure to workers and villagers in and around some quarry sites in Ogun state was done using radiation detection methods. The results obtained from the study show that annual exposure rate was found to be 49.1 μSv y^{-1} which is below

the world average of 70 μSv y^{-1}, but recommended that workers at quarry sites should always put on masks to reduce the amount of radioactive inhalation [66]. A study on the activity concentration and the gamma absorbed dose of the primordial naturally occurring radionuclides was done for sand samples collected from the Baoji Weihe sands park, China using gamma-ray spectrometry. The natural radioactivity concentration of sand ranged from 10.2 to 38.3 $Bq\ kg^{-1}$ for ^{226}Ra, 27.0 to 48.8 $Bq\ kg^{-1}$ for ^{232}Th and 635.8 to 1,126.7 $Bq\ kg^{-1}$ for ^{40}K with mean value of 22.1, 39.0 and 859.1 $Bq\ kg^{-1}$ respectively. The radium equivalent activity values of all sand samples were lower than the limit of 370 $Bq\ kg^{-1}$. The mean outdoor air absorbed dose rate was 69.6 $nGy\ h^{-1}$ and the corresponding outdoor effective dose rate was 0.085 $mSv\ y^{-1}$ [67]. A study on the distribution of natural radionuclides concentrations in sediment samples in Didim and Izmin Bayin Turkey has been done. The results showed that the concentrations of activity in the sediment samples were 9±0.6 $Bq\ kg^{-1}$ to 12±0.7 $Bq\ kg^{-1}$,7±0.4 $Bq\ kg^{-1}$ to 16±1.0 $Bq\ kg^{-1}$,6±0.3 $Bq\ kg^{-1}$ to 16±1.0 $Bq\ kg^{-1}$ and 250±13 $Bq\ kg^{-1}$ to 665±33 $Bq\ kg^{-1}$ [68] for ^{226}Ra,^{238}U,^{232}Th and ^{40}K, respectively which were in the same order as international levels. In Kenya, various studies have been done to asses the level of human exposure to ionizing radiation. Study on natural radioactivity in some building materials in Kenya and the contribution to the indoor external doses has been done. Typical activity concentration encountered was in the range of; 50 to 1500 $Bq\ kg^{-1}$ for ^{40}K, 5 to 200 $Bq\ kg^{-1}$ for ^{226}Ra; and 5 to 300 $Bq\ kg^{-1}$ for ^{232}Th [69]. The concentration levels of ^{238}U, ^{232}Th and ^{40}K in Mombasa, Malindi and Gazi along the coast was measured and found that Mombasa had the highest of 22.8±1.8 $Bq\ kg^{-1}$ for ^{238}U, 26.2±1.7 $Bq\ kg^{-1}$ for ^{232}Th and 479.8±24.2 $Bq\ kg^{-1}$ for ^{40}K. The effective dose rate in Mombasa was found to have a mean of 0.12±0.01 $mSv\ y^{-1}$ [70].

I.15.1 Natural radioactivity in Cameroon

Ngachin et al. [71] presented a study on external exposure to construction materials used in Cameroon. This study revealed that all the materials examined could be used

as building materials according to the criteria of the Organisation for Economic Cooperation and Development [72] . Saïdou et al. [73] reported measurements of radioactivity and an evaluation of the total dose in the Poli uranium region in northern Cameroon. Most of the estimated total dose was attributed to radon consumption and high levels of ^{210}Po and ^{210}Pb in vegetables and food products consumed by local populations. In addition, soil samples collected at Awanda, Bikoué and Ngombas in the southwestern region of Cameroon by Ele Abiama et al. [74] revealed high concentrations of ^{238}U, ^{232}Th and ^{40}K at some points; this proves that the areas studied have a very high level of radioactivity. In the same region, Beyala Ateba et al. [75] measured the concentration of uranium in the rocks and soils collected at the sites where a radiometric anomaly was detected during an investigation. The analysis, carried out by gamma spectrometry in the laboratory using a Germanium detector, showed a high uranium content in the soil and rock samples and that the areas studied have uranium mining potential. A study on the Determination of ^{226}Ra, ^{232}Th, ^{40}K, ^{235}U and ^{238}U activity concentration and public dose assessment in soil samples from bauxite core deposits in Western Cameroon has been done, the results show that the radiological safe parameters were relatively higher than the recommended safe limits of UNSCEAR, Nguelem et al. [76].

I.16 Conclusion

This chapter has shown the different pathways of human exposure in nature to ionizing radiation, and the mechanisms of interaction of its radiation with matter. Its radiation destroys irradiated cells according to their nature. Thus, the dosimetric quantities to evaluate the effects of its radiation on the health of the human beings were also discussed.

CHAPTER II

MATERIAL AND METHODS

II.1 Introduction

In this chapter, the geographical location and the geology of the study area, the materials used as well as the methods used for sampling, sample preparation and measurements are discussed. Also, the dose and radiological risk assessments are discussed in this section.

II.2 Description of the study area

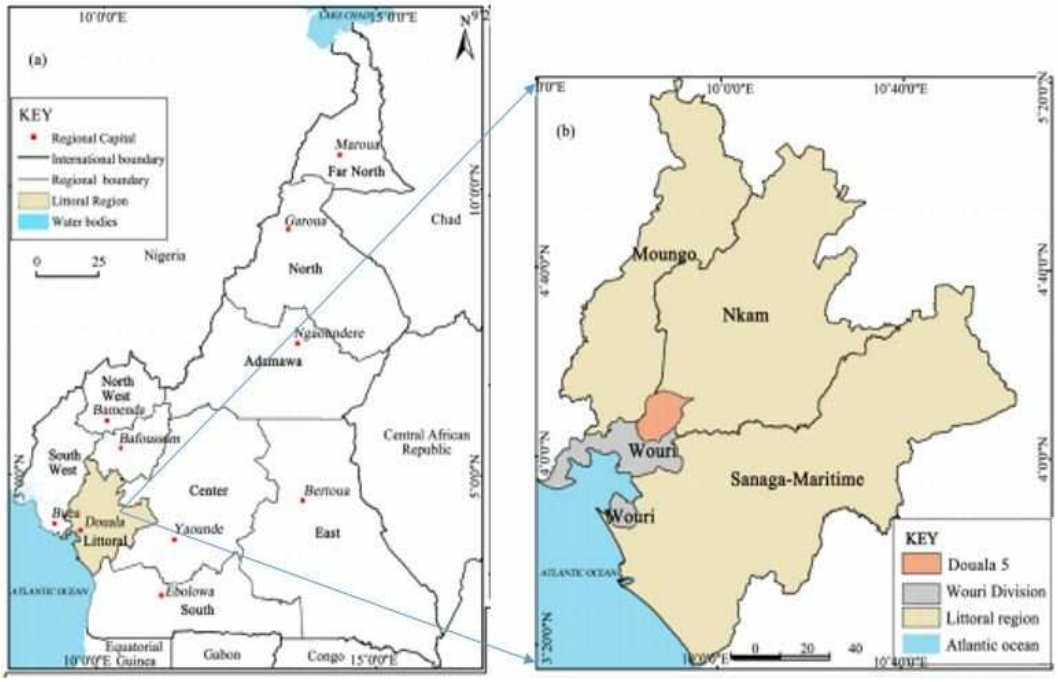

Figure 17: Map of Douala.

Douala is a coastal city, the economic capital of Cameroon, the main business center and the largest city of the country; with approximately 4 million inhabitants. It

is the chief town of the Littoral Region and the Wouri Division. Located on the edge of the Atlantic Ocean, at the bottom of the Gulf of Guinea, at the mouth of the Wouri River, Douala has the largest port in the Cameroon and one of the most important in Central Africa. The annual rainfall ranges between 3000 and 5000 mm, and the annual average temperature is 26^0C [77]. The geology of the region consists of sedimentary rocks, mainly, tertiary and quaternary sediments [78].

II.3 *In-situ* measurement of natural radioactivity

II.3.1 Generality on *in-situ* gamma spectrometry

G.BALEA [79] reported in its article entitled Theory of *in-situ* gamma-ray spectrometry that, the technique of *in-situ* spectrometry had its origins during the time of atmospheric nuclear weapons testing where it was found to provide quick, reliable information on the components of the outdoor environment. It provided a means to separate natural background from man-made sources and gave quantitative results. Over the years, it has been employed by various groups for assessing radiation sources in the environment not only via ground based detectors, but with aircraft systems as well. It proved particularly useful following the Chernobyl accident and was employed by a number of European laboratories. It should prove adaptable to site assessments in the current era of environmental rescue.

Kevin M et al [80] reported: The power in the technique of *in-situ* spectrometry lies in the fact that a detector placed over a ground surface measures gamma radiation from sources over an area of several hundred square meters. As an example of the effective ground area being measured by a detector at 1 m above the ground. Figure 18 shows the relative contribution to the fluence from different rings of ground area about the detector for a typical source of fallout ^{137}Cs (gamma energy of 662 keV) in the environment. The "field of view" for the detector would be larger for higher energy sources and for sources closer to the soil surface. In contrast, a soil sample would represent an area of

but a few tens or hundreds of square centimeters. In practice, an effective characterization of a site would involve *in-situ* spectrometry in conjunction with soil sampling. As part of an overall program, *in-situ* spectrometry provides a means to assess the degree of contamination in areas during the course of operations in the field, thus guiding the investigator on where to collect samples. It can also substantially reduce the number of samples that need to be collected and subsequently analyzed. Some of the limitations of *in-situ* spectrometry need to be pointed out from the start. Due to the nature of radiation transport through matter (the soil and air), it is for the most part limited to the measurement of gamma and, to some extent, x-ray emitters. Even so, the attenuation properties of soil are such that buried sources are not likely to be detected with measurements performed above ground.

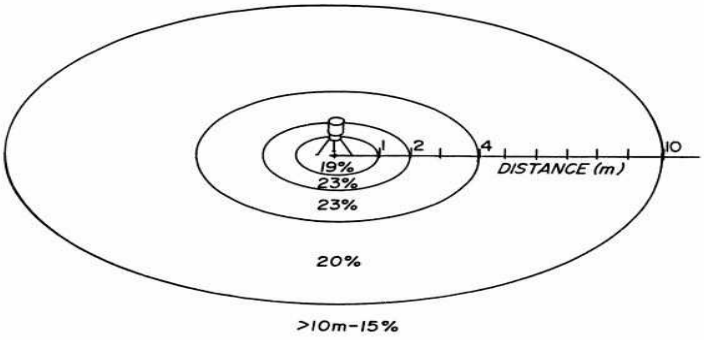

Figure 18: Contribution to total 662 keV primary flux at 1 m above ground for a typical ^{137}Cs source distribution [80].

II.3.2 Basic Calibration Parameters

For sample analysis in the laboratory, calibrations are generally performed with solutions in the same counting geometry or spicked matrices such as soil and vegetation. In principle, one could calibrate a Ge, NaI(Tl) detector for field use with very large (approaching an infinite half-space) calibrated areas as well. In practice, a far more convenient and flexible approach is to calculate the flux distribution on the detector for a given source geometry, to determine the detector response with calibrated point sources and then perform an integration [80]. The fundamental quantities used for *in-situ* spectrom-

etry include full absorption peak count rate (N), fluence rate (Φ), and source activity (A). In practice, one would like a single factor to convert from the measured peak count rate in a spectrum to the source activity level in the soil or the dose rate in air. This factor can be calculated from three separately determined terms as follows [81]:

$$\frac{N_f}{A} = \frac{N_f}{N_0}\frac{N_0}{\Phi}\frac{\Phi}{A} \tag{II.1}$$

where N_f/A is the full absorption peak count rate at some energy E, from a gamma transition for a particular isotope per unit activity of that isotope in the soil, N_0/Φ is the full absorption peak count rate per unit fluence rate for a plane parallel beam of photons at energy E, that is normal to the detector face, N_f/N_0 is the correction factor for the detector response at energy E, to account for the fact that the fluence from an extended source in the environment will not be normal to the detector face but rather distributed across some range in angles and Φ/A is the fluence rate at energy E, from unscattered photons arriving at the detector due to a gamma transition for a particular isotope per unit activity of that isotope in the soil. The term N_0/Φ is purely detector dependent while the term N_f/N_0 is dependent on both the detector characteristics and the source geometry. These two terms will be covered in the following chapter on detector calibration. The terms Φ/A is not dependent on the detector characteristics but rather on the source distribution in the soil.

II.3.3 Measuring device

The measuring device of natural radioactivity in environment by *in-situ* measurement is showed in figure below.

Figure 19: *In-situ* measurement of natural radioactivity in environment using 3" $\times$ 3" Nal (TI) detector .

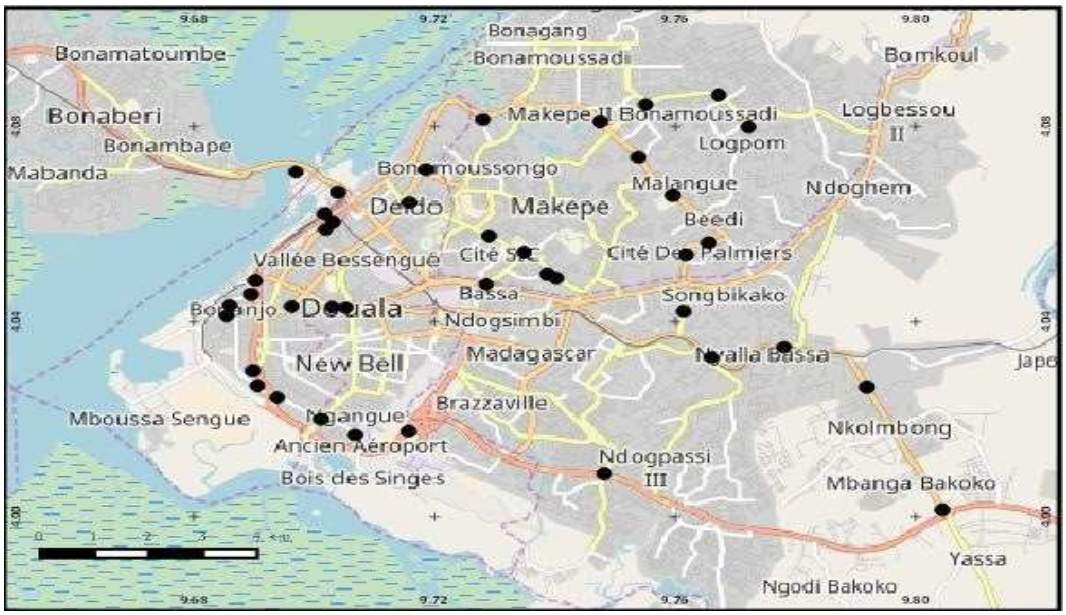

Figure 20: *In-situ* Measurement points (39) of gamma-ray pulse height distribution using a NaI(Tl) scintillation spectrometer

II.4 Car-borne survey and methodology of the activity calculation of ^{238}U, ^{232}Th and ^{40}K

II.4.1 Car-borne survey

A car-borne survey was carried out using a mobile vehicle moving at a speed of approximatively 40 $km\ h^{-1}$, in which was positioned a measuring system consisting of a sodium iodide detector 3-in $\times$ 3-in NaI(Tl), a global positioning system (GPS) to record coordinates at each measuring point, a computer to analyze gamma-ray spectra (EMF-211, EMF Japan Co, Japan). Absorbed dose rate measurements inside the vehicle were performed every 30 seconds along the way and corrected by multiplying with a shielding factor with the aim of representing the unshielded external dose rate. The shielding factor (Figure 36) was evaluated in order to be able to convert the values measured inside the vehicle to ambient dose rate outside of the car, and was estimated by making measurements inside and outside the vehicle at 10 measurement points and correcting them with count rates inside. The absorbed dose rates in air were calculated using a dose rate conversion factor based on the correlation of dose rate $(nGy\ h^{-1})$ and total count rate (cpm) from 0 to 1023 channels in the gamma-ray pulse height distribution [82,83]. Commonly, the gamma-ray pulse height distribution is obtained by 15 min measurements at each point. Measurements of gamma-ray pulse height distributions were carried out at 1m above the ground surface at 39 measurement points in Douala City. The gamma-ray pulse height distributions were unfolded using a 22 x 22 response matrix for the estimation of absorbed dose rate in air [84,85]. The dose rate conversion factor of the scintillation spectrometer used in the present survey was determined to be $1.7510^{-3} nGy\ h^{-1}\ cpm^{-1}$. Figure 34 gives the relationship between absorbed dose rate $(nGy\ h^{-1})$ which was calculated by software using the response matrix method and total count rates outside the vehicle. Absorbed dose rate in air (D_{out}) 1m above the ground surface at each measurement point can be estimated by the following equation [86]:

$$D_{out} = 2D_{in} \times 1.62 \times 0.00175 \tag{II.2}$$

where (D_{in}) is the count rate inside the car (cps) obtained by the measurements for 30 seconds. Since the dose rate conversion factor was given as a dose rate $(nGy\ h^{-1})$ for counts per minute (cpm), it is necessary to double D_{in} in order to convert into the counts per minute.

Following *in-situ* measurements, external effective dose in Douala was assessed using the following equation [87]:

$$E_{ext}(mSv/y) = F_c \times [Q_{in} \times R + Q_{out}] \times \sum_{i=1}^{3} A_i \times (KCF)_i \times t \tag{II.3}$$

where, E is the external effective dose (mSv y^{-1}), $D_{out}$is the absorbed dose rate in air (nGy h^{-1}), DCF is the dose conversion factor from the dose rate to the external effective dose for adults (0.748 $\pm$ 0.007Sv Gy^{-1}) [88] t is 8766 h, Q_{in} and Q_{out} are indoor (0.6) and outdoor (0.4) occupancy factor respectively. R (1.11) is the ratio of indoor and outdoor dose rate (figure 39b).

II.4.2 Activity concentrations of ^{238}U, ^{232}Th and ^{40}K and their contribution to the air absorbed dose rate

The evaluation of activity concentrations and the contribution of ^{238}U, ^{232}Th and ^{40}K to the absorbed dose rate in air were obtained by measuring the spectra of gamma-ray pulse height distributions and using a 22 $\times$ 22 response matrix conceived by Minato [85, 89]. The gamma-ray pulse height distribution obtained by measurements was converted to the energy bin spectrum of incident gamma-ray which is a distribution of gamma-ray flux density to each energy bin. The energy ranges from 0 to 3.2 MeV, energies above 3.2 MeV were not included for evaluation because the maximum value of the gamma-ray energy from natural radionuclides is 2.615Mev emitted by ^{208}Tl (^{232}Th-series). The gamma-ray lines utilized for natural radionuclides are: 1.464 MeV for ^{40}K,

1.768 MeV and 2.205 MeV for ^{214}Bi (^{238}U-series) and also 2.615 MeV for ^{208}Tl (^{232}Th-series). The 22 $\times$ 22 matrix for the 3-in $\times$ 3-in NaI(Tl) scintillator for an isotropic field was calculated using the Monte Carlo code, SPHERIX [90,91]. The gamma-ray flux density and dose rate per unit solid angle are considered almost isotropic in the natural environment [92]. The calculation of gamma-ray flux densities per unit activity concentrations of ^{238}U-series, ^{232}Th-series and ^{40}K are necessary, in order to evaluate each activity concentrations of natural radionuclides from an energy bin spectrum. This calculation assumed that a semi-infinite volume source was formed in the ground [85]. The primary and scattered gamma-ray flux density per unit activity concentrations could be calculated using one-dimensional Monte Carlo gamma transport code, MONARIZA/G2 [93,94]. A total of a million histories were traced for each natural radionuclide. The nuclear data of gamma-ray energies and disintegration rates used the reported values by Beck [95] and Beck et al. [81] for this Monte Carlo simulation. The activity concentration of each natural radionuclide was evaluated by a successive approximation which used a 3 $\times$ 3 matrix determined by Minato [85] to the values of energy bins for ^{238}U-series, ^{232}Th-series and ^{40}K. The statistical errors for absorbed dose rates in air and activity concentrations for ^{40}K, ^{238}U-series and ^{232}Th-series obtained using this software depend on the integral air kerma $(nGy\ h^{-1})$ at each measurement point [90], and these were evaluated in this study as 2%, 2%, 68% and 45%, respectively.

II.5 Natural radioactivity measurements in the soil samples

II.5.1 Soil sampling and conditioning

The measurement of natural radioactivity in the environmental samples is carried out first of all by a sampling of soil samples and this sampling must obey the representativity of the samples so that the measurement is precise. After sampling, packaging is necessary regardless of the measurement technique.

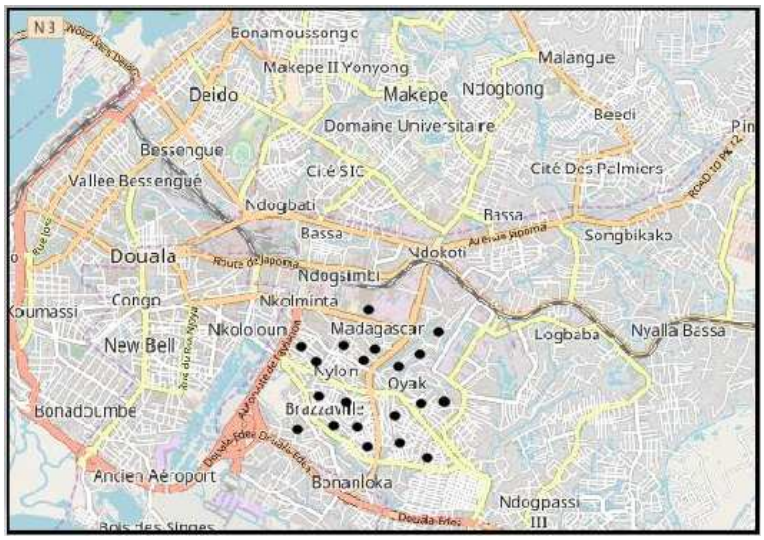

Figure 21: Location of sampling point (20) pulse

II.5.2 Soil sampling

Before taking soil samples, it is necessary to start with the identification of the sampling point. Then we define a square of 1 m side on a surface void of plant cover. A dibbler was used to collect at each peak of the square a thickness of 0-5 cm of soil, the 04 layers of soil collected constitute a sample of about 1000 g dry mass also varying from one sampling site to another. The procedure described allows for representative sample from those collected in the whole square and also ensures a uniform average distribution of radionuclides at the sampling point. During the sampling, the elements having a size greater than 2 cm, the plant roots and the plastics are eliminated. All the samples taken from the square of 1 m are introduced into a plastic bag, labeled and hermetically sealed.

II.5.3 Conditioning

The samples collected were dried in an oven at a temperature of 70^0C for a period of 48 hours and then grounded into fine particles. Plastic boxes of $500cm^3$ of volume (Marinelli Beaker) were partially filled in order to leave the space for gaseous releases (radon). The mass of soil sample finally used was about 1 kg. All the boxes were subse-

quently sealed to prevent any escape of radon. The boxes were stored for a minimum of one month in order to reach the secular balance between radium-226 and its daughters.

Figure 22: Sample preparation for direct gamma spectrometry.

II.6 Radioactivity measurements by γ-spectrometry

II.6.1 Fundamentals of γ-spectrometry

The development of γ-spectrometry began with the development of nuclear science and technology to meet the needs for control, characterization and analysis of radioactive materials. This measurement technique exploits a fundamental property observed by most unstable nuclei: the emission of radiation consecutive to the process of nuclear disintegration. It is therefore called "non-destructive" because it allows to respect the integrity of the object to be analyzed. The interest of γ-spectrometry has been increasing for years, so far as the metrological and applications point of view. This growth was made possible thanks to a better understanding of the process of interaction of photons with matter and especially thanks to the appearance of semiconductor detectors in the

1960. γ- spectrometry then became a powerful tool to study disintegration schemes with which measurement uncertainties of the order of 10^{-6} (in relative terms) can be reached. It is used today in very various sectors (Dating, Climatology, Astrophysics, Medicine) and in almost all stages of the nuclear fuel cycle.

II.6.2 Measuring device

According to Gasser [96], In γ-spectrometry, a measurement chain consists of a detector, a preamplifier, an amplifier, an analog to digital converter, an electronic acquisition system and an analysis software.

By means of a high voltage delivered to the detector, a quantity of electric charges proportional to the energy deposited by the photon in the crystal is collected. The charge carriers are collected using a charge preamplifier whose functions are the conversion of the charge into electrical voltage and a first amplification. Signal shaping and a second amplification are performed by the amplifier.

The amplitude of the pulse analyzer is performed by a multi-channel analyzer. The choice of the number of channels necessary for acquisition depends on the resolution of the detector and the energy range. For a NaI detector (Tl), a resolution in energy generally requires a coding on 10-bit, or 1024 channel to cover a range of energy between 0 and 3 MeV. A PC of acquisition, associated with an analyzer, records the energy of the event by incrementing the corresponding channel. A spectrum is thus collected then analysed by GENIE 2000 software.

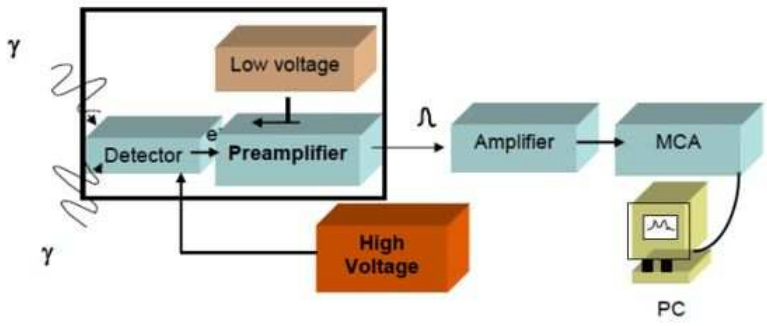

Figure 23: Typical gamma-ray spectrometry system.

II.7 Analysis of γ-lines

II.7.1 Generalities on γ-lines

According to Saïdou [97] The direct measurement of ^{238}U by γ-spectrometry at the 49.5 keV (0.084%) line is very difficult because of the low emission probability and the self-absorption effect. However, if it is in secular equilibrium with its daughters, ^{238}U can be determined by the 63.3 keV (4.5%) line and the doublet 92.6 keV (92.4 + 92.8 keV, 2.6 + 2.6%) of ^{234}Th and 766.4 keV (0.21%) and 1001.0 keV (0.83%) lines of ^{234m}Pa [98]. The fact that ^{234}Th and ^{234m}Pa are short-lived radionuclides ($T_{1/2} = 24.1d$ for ^{234}Th and $T_{1/2} = 1.17min$ for ^{234m}Pa) is a great advantage because the secular equilibrium is reached about six months. after sampling for ^{234}Th in relation to ^{238}U and ten minutes for ^{234m}Pa compared to ^{234}Th. However, the 766.4 keV line of ^{234m}Pa is of low emission probability and may interfere with line 768.3 keV (4.8%) of ^{234}Bi. In environmental samples, the 1001.0 keV line, although less affected by the autoabsorption effect, has a low emission probability which, combined with the low efficiency of HPGe detectors at high energies, gives rise to significant uncertainties [99, 100]. The 92.6 keV doublet of ^{234}Th coincides with the 93 keV line of the Xk photon of thorium and the 93.3 keV line of ^{235}U (4.5%). So, for samples with a high uranium and thorium content, the 93 keV line does not give an accurate indication of the activity of ^{238}U. 63.3 keV line of ^{234}Th interferes with 63.9 keV line (0.255%) of ^{232}Th, 63.9 keV (0.023%) of ^{231}Th and 62.9 keV (0.018%) of ^{234}Th. In natural environmental samples, these different interferences at 63.3 keV line can be neglected [99]. The method generally used to measure directly consists in using its only 186.2 keV exploitable line (3.53%). However, this line interferes with 186.05 keV (0.009%) of ^{230}Th, 186.15 keV (1.76%) of ^{234}Pa and 185.7keV (57.2%) of ^{235}U [101]. Because of the low branching ratio of ^{234}Pa and the low emission probability of the ^{230}Th line, the first two contributions can be neglected. The main interference is ^{235}U which has other exploitable lines at 143.7 keV (10.9%), 163.3 keV (5%) and 205.3 keV (5%). Since ^{235}U activity in most soil samples is low, ^{235}U is best determined by alpha

spectrometry [102,103]. The activity of ^{226}Ra can be deduced from the 186 keV multiplet after subtracting the ^{235}U contribution. Alternatively, the ^{226}Ra can be determined from the emission of its daughters by avoiding the emanation of ^{222}Rn [103]. For ^{232}Th, the only line potentially exploitable at 59 keV (0.15%) is of low intensity and strongly subject to the self-absorption effect in environmental samples. Therefore, it must be determined by the emissions of his daughters ^{228}Ac, ^{212}Pb or ^{212}Bi.

Table 5: Main lines used in the present work(blue) in γ-spectrometry for the measurement of the activity of natural radionuclides.

^{238}U series	^{234}Th	63.3(4.5)	92.6(5.4)		
	^{234m}Pa	765(0.21)	1001(0.7)		
	^{226}Ra	186(3.3)			
	^{214}Pb	242(7.43)	295.2(19.2)	351.8(37.2)	
	^{214}Bi	609.3(46.6)	1120.3(15.1)	1764(15.9)	
	^{210}Pb	46.5(4.1)			
^{232}Th series	^{228}Ac	338.3(11.4)	911.6(27.7)	969.1(16.6)	940.3(44.3)
	^{212}Pb	238.5(43.6)	300.1(3.23)		
	^{212}Bi	727.2(6.7)	1620.6(1.5)		
	^{208}Tl	510.8(21.6)	583(86.3)	860.4(12.5)	2614.7(100)
Others	^{40}K	1460.8(10.7)			

II.7.2 Counting statistics

The contents (N) of the observed γ lines are numbers resulting from a counting experiment, which are partially superimposed on a high background. This produces an uncertainty of the result which can seriously degrade the precision with which the net peak counts is measured. Counting statistics is applied to estimate this uncertainty which is expressed by the standard deviation of the result. For any counting experiment the result (N) of which is governed by a Poisson distribution, the standard deviation is:

$$\sigma = \sqrt{N} \tag{II.4}$$

The above equation expresses the fact that a repetition of a counting experiment would in about 2/3 of the cases give a result in the range of N $\pm\sigma$. For the analysis of a peak without background this is sufficient. But to subtract a background, the Pois-

son distribution should be approximated by a Gaussian distribution. This can be done without large errors for numbers of counts (N) greater than about 10 [104]:

$$N_{net} = N_{tot} - N_{BG} \tag{II.5}$$

$$\sigma = \sqrt{\sigma^2_{Ntot} + \sigma^2_{BG}} = \sqrt{N_{tot} - N_{BG}} \tag{II.6}$$

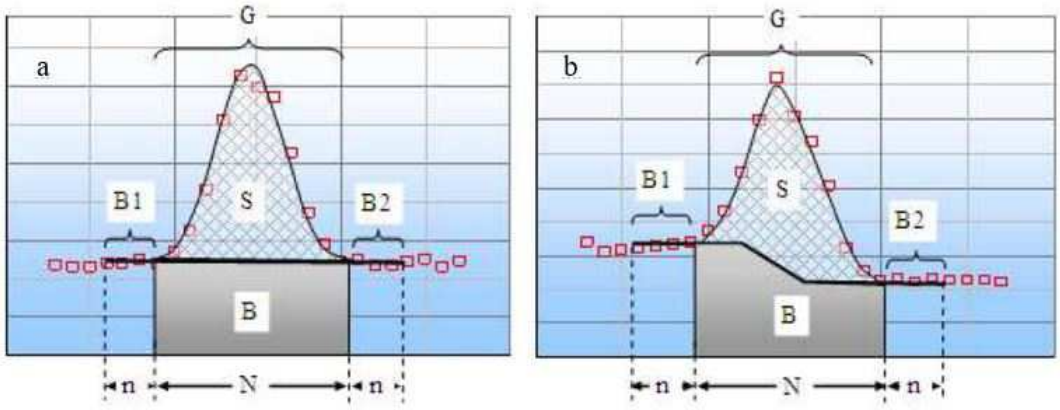

Figure 24: Net Area Determination [105]

The background according to the profile type is:

-For a linear profil

$$B = \frac{N}{2n}(B_1 + B_2) \tag{II.7}$$

-For a staircase profil

$$B = \sum_{i=1}^{N}\left(\frac{B_1}{n} + \frac{(B_2 - B_1)}{nG}\sum_{j=1}^{i} y_j\right) \tag{II.8}$$

where, - B is the value of the background, N the number of channels of the region of interest, n the number of channels taken into account on the left and right of the region of interest to calculate the background, B_1 and B_2 the sum of the contents of the n channels on the left and on the right, y_j value of the channel j.

II.8 Detector calibration

The calibration serves to connect the results delivered by the chain with the certified values corresponding to the standard and / or the reference materials.

II.8.1 Energy calibration

According to Saïdou et al [106], in many routine applications, the expected energy lines in the spectrum are known in advance and can be easily identified. On the other hand, in other applications one can meet spectra whose peaks are not identifiable. In such cases, the energy calibration of the detector is essential. Accurate calibration requires a multi-line standard source or several standard sources with E_γ energies that are not far from those to be measured in the spectrum.

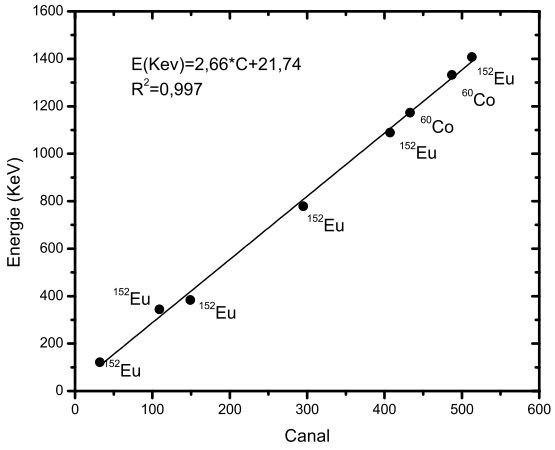

Figure 25: Energy calibration curve.

Given the problems of non-linearity that may exist in some channels of the detector, it is useful to have several standard sources to better take them into consideration. The energy calibration can be adjusted by a 2^{nd} degree polynomial [107]:

$$E(x) = a_1 + a_2 x + a_3 x^2 \tag{II.9}$$

where x is a detector channel and E is its corresponding energy. The parameters a_1, a_2 and a_3 depend on the fit of the points (E, x).

II.8.2 Efficiency calibration

The traditional approach for full energy peak (FEP) efficiency determination involves measurement of test sources and calculating efficiencies for given geometry and energy as:

$$\varepsilon_i = \frac{N_i}{AP_\gamma t} \tag{II.10}$$

where N is FEP net count, t is counting live time, A is source activity and P_γ probability of emission of the particular gamma line. Experimental efficiency curves for each detector in the Laboratory had been constructed for "standard geometries". These include for liquid samples Marinelli beakers of several sizes and plastic bottles filled into defined heights (density 1 g cm^{-3}) and for solid samples (soil) pressed pellets, Marinelli beakers (different sizes and density 1.5 and 2.0 g cm^{-3}) and a standard filter geometry. Efficiencies for these geometries had been measured using calibrated solution (or a solid calibration source prepared using calibrated solution mixed with a solid matrix) of gamma emitters mixture over a wide range of energies.

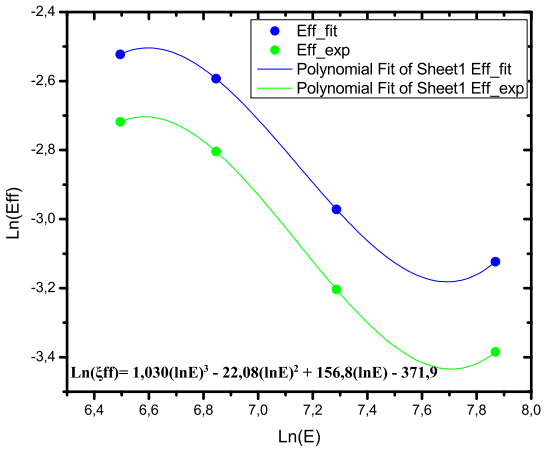

Figure 26: Efficiency calibration curve.

The energy efficiency calculation for each radionuclide of the reference material makes it possible to establish the equation efficiency curve:

$$\log \varepsilon = a(\log E)^3 + b(\log E)^2 + c(\log E) + d \tag{II.11}$$

Note: The sample is conditioned in a geometry identical to that of the standard or the reference material. Corrections must be made in case the geometry is different.

II.9 Decision thresholds, detection limits and Minimum Detectable Activity

The detection capabilities associated with measuring and analysing radioactivity levels vary according to the instrumentation and analytical techniques used [108]. For a low-level counting system, it is necessary to determine the detection limit above which counts are statistically significant of the measurement. The concept of a decision limit (or critical level) and detection limit was established by Currie in 1968 [109, 110]. The critical level L_C, can be defined as a decision level above which the net counts present represent some detected activity, with a certain degree of confidence.

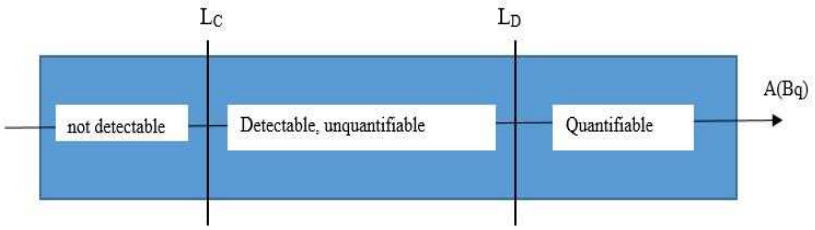

Figure 27: Diagram showing the Critical Limit L_C and the detection limit L_D.

Mathematically, the critical level can be given by [109] :

$$L_C = k_\alpha \times \sigma_0 \tag{II.12}$$

where k_α is the expansion factor corresponding to the $1-\alpha$ confidence level of the probability law.

σ_0 is the standard deviation of the number of counts when a blank sample is measured to determine the background level.

The limit of detection (L_D) according to NF T90-210-2012: is the smallest true value of the measurand which is associated with the statistical test and hypothesis (made for the Critical Limit) by the following characteristics: If in reality the true value is equal to or exceeds the detection limit, the probability of wrongly not rejecting the hypothesis (error of the second kind) shall be at most (error of the second kind) shall be at most equal to a given value β. According to ISO 11929-3: [111] of July 2000, the detection limit specifies the minimum contribution of the sample that can be detected, with a given probability of error. This value is directly related to the measurement conditions (count in the region of interest, duration of the measurement) and must be established for each spectrum [112]. The L_D is defined by:

$$L_D = L_C + k_\beta \times \sigma_D \tag{II.13}$$

where k_β is the expansion factor corresponding to the $1-\beta$ confidence level of the probability distribution.
σ_D is the standard deviation corresponding to the net area of the peak considered when this area is equal to L_D. The experimenter determines in advance the degree of confidence at which the decision will be made to accept the peak as truly present. It chooses two levels of confidence $1-\alpha$ and $1-\beta$ which are in general of 95% with the corresponding quantiles k_α = k_β= 1.645. In practice σ_0, σ_D are of the same order of magnitude; for that, we fix k_α = k_β = k, this which simplifies the expression. We obtain :

$$L_D = 2L_C \tag{II.14}$$

Thus, the decision threshold (L_C) and the detection limit (L_D) can be expressed in $Bq\ L^{-1}$ and $Bg\ kg^{-1}$, respectively.

It is possible to adapt the counting time to obtain depending on the background of the device, the desired detection limit for high counting rates. If BDF is the counting rate of the background, t_{BDF} is its counting time, t is a counting time of the sample and ε the detection efficiency, the detection limit is given by:

$$LD = \frac{\sqrt[4]{\frac{2BDF}{t_{BDF}}}}{\sqrt{t.\varepsilon}} \tag{II.15}$$

The smallest measurable activity that can be detected using γ-ray counting with a certain degree of confidence is called MDA [113]. This value can be determined for de-ionized water filled in Marinelli beaker, and can be calculated by the following equation:

$$MDA = \frac{L_d}{\varepsilon\gamma t} \tag{II.16}$$

where L_d is the detection limit (the level of true net counts that, if present, will be detected with a given probability); γ is the emission probability per disintegration of the selected gamma-ray line; ε is the absolute efficiency of the corresponding gamma line; and t is the live time of the spectrum. MDA is calculated in term of activity (Becquerel), which depends on the γ-ray energies of the sample and the counting efficiency of the detector [113].

II.10 Methodology for determining Activity concentrations and uncertainties of ^{238}U, ^{232}Th and ^{40}K in soil samples

II.10.1 Concentrations of ^{238}U, ^{232}Th and ^{40}K

The activity of a radioelement is proportional to the number of events in the total absorption peak. This activity is defined by the international standard (International

Organization for Standardization) NT ISO 18589-3 of [114] which includes several parts, including the measurement of γ-emitting radionuclides in the soils. This activity is expressed in Becquerel per kg and is defined according to the equation:

$$A = \frac{n_{N,E}}{t_g \times P_E \times \varepsilon_E \times m \times K} \tag{II.17}$$

with $n_{(N,E)}$: number of net coups the total absorption peak,

t_g: counting time expressed in seconds,

P_E: Emission probability of radionuclide of interest,

ε_E: detection efficiency for a given energy E,

m: is the sample mass,

K:The correction factor and $K = K_1.K_2.K_3.K_4.K_5$

K_1 is the correction factor for the nuclide decay from the time the sample was collected to the start of the measurement given as:

$$K_1 = \exp\left(-\frac{\ln 2 \bullet \Delta t}{T_{1/2}}\right) \tag{II.18}$$

where Δt is the elapsed time from the sample that was taken to the beginning of the measurement and $(T_{1/2})$ is the radionuclide half life.

K_2 is the correction factor for the nuclide decay during counting period given as:

$$K_2 = \frac{T_{1/2}}{\ln 2 t_r}\left(1 - \exp\left(-\frac{\ln 2 t_r}{T_{1/2}}\right)\right) \tag{II.19}$$

where t_r is the real time of the sample spectrum collection in seconds.

K_3 is the correction factor for a self-attenuation in the measured sample compared with the calibration sample. The self-attenuation factor K_3 is defined as the ratio of the full energy peak efficiency $\varepsilon(\mu, E)$ for a sample with the linear attenuation coefficient μ and the full energy peak efficiency $\varepsilon(\mu_{ref}, E)$ for a sample with the linear attenuation μ_{ref}:

$$K_3 = \frac{\varepsilon(\mu,E)}{\varepsilon\left(\mu_{ref},E\right)} \tag{II.20}$$

Evidently, if the matrix of both the calibration sample and the measured sample is the same, then K_3 = 1.

If more than one photon is absorbed by the detector during a pulse sampling cycle, the sum of the energies of two (or more) is recorded in the spectrum instead of two (or more) different signals. Any full-energy photon that is summed with another pulse is not recorded in the single photon peak and represents a loss of counts or efficiency. This loss is count rate dependent.

K_4 is the correction factor for pulses loss due to random summing:

$$K_4 = \exp\left(-2R\tau\right) \tag{II.21}$$

where τ is the resolution time of the measurement system and R is the mean count rate. For low count rates this correction factor could be taken as 1. K_5 is the coincidence correction factor for those nuclides decaying through a cascade of successive photon emission. If the nuclide has no cascade of gamma-rays then K_5 =1.

The absolute uncertainty on the activity is defined as follows:

$$\sigma_A = A\sqrt{\left(\frac{\sigma_{n_{N,E}}}{n_{N,E}}\right)^2 + \left(\frac{\sigma_{t_g}}{t_g}\right)^2 + \left(\frac{\sigma_{P_E}}{P_E}\right)^2 + \left(\frac{\sigma_{\varepsilon_E}}{\varepsilon_E}\right)^2 + \left(\frac{\sigma_m}{m}\right)^2 + \left(\frac{\sigma_K}{K}\right)^2} \tag{II.22}$$

If a radionuclide possessing several lines does not interfere with another radioelement, the result of the calculation of the activity corresponds then to a weighted average on its lines:

$$A = \frac{\sum_n^{i=1} \frac{A_i}{\sigma^2_{A_i}}}{\sum_n^{i=1} \frac{1}{\sigma^2_{A_i}}} \tag{II.23}$$

with

$$\sigma_A = \sqrt{\frac{1}{\sum_n^{i=1} \frac{1}{\sigma^2_{A_i}}}} \tag{II.24}$$

II.11 Radium equivalent and uncertainty

The term R_{aeq} has been used to define the activity of a radionuclide having a biological effect equivalent to 1 mg of ^{226}Ra. In practice, radium sources are often measured in milligrams rather than millicuries [115] because the "curie" has been defined according to the activity of 1g of radium. R_{aeq} has for 40 years [116–119] been able to assess radiological risks due to radioactivity in environmental materials. The R_{aeq} concept is also used to assess the radiological risks of environmental components [120,121].

According to Beretka [117], the natural radioactivity of building materials is generally determined from the families of ^{226}Ra and ^{232}Th, as well as from ^{40}K. It has been observed that 98.5% [122] of the radiological effects of elements of the uranium series (^{238}U) are due to ^{226}Ra and its descendants. For this reason, the construction of the precursors between ^{238}U and ^{226}Ra can be neglected. The radiation dose is defined by taking into account the measured activity of the radionuclide and the dose rate conversion models [120].

The Krisiuk model [116] predicts that a concentration of ^{226}Ra activity of 370 $Bq\ kg^{-1}$ ($1Ci\ g^{-1}$) evenly distributed in a material, gives an annual dose of 1.5 mGy [123,124] at a distance 1 m of this material.

Krisiuk considers a house as a cavity with walls of infinite thickness to obtain a formula that combines the dose rate inside with the content of radioactivity of building materials. So the R_{aeq} is given by the following equation:

$$R_{a_{eq}} = \frac{370}{370}A_{R_a} + \frac{370}{259}A_{Th} + \frac{310}{4810}A_K \tag{II.25}$$

In this equation, the activity of ^{226}Ra (370$Bg\ kg^{-1}$), ^{232}Th (259 $Bg\ kg^{-1}$) and ^{40}K (4810 $Bg\ kg^{-1}$) represent the same effective dose of γ radiation.

Uncertainty is given by the following equation:

$$\mu^2_{Ra_{eq}} = \mu^2_{A_{Ra}} + \left(\frac{370}{259}\right)^2 \mu^2_{A_{Th}} + \left(\frac{370}{4810}\right)^2 \mu^2_{A_K} \tag{II.26}$$

It is also necessary to evaluate the internal and external risks specific to man that are due to the contribution of radionuclides emitting γ-radiation present in building materials. The effective radiation dose limit for building materials established by the UNSCEAR report [1] is 1 $mSv\ y^{-1}$.

II.12 External and Internal hazard index

The hazard index were defined by a model [116, 125, 126] taking into account the maximum activity of R_{aeq} (370 $Bg\ kg^{-1}$).The external hazard index (H_{ex}) is used to evaluate the danger of natural gamma radiation and its purpose is to restrict the radiation dose to permissible dose equivalent limit of 1 $mSv\ y^{-1}$ and is defined by the equation below [127]:

$$H_{ex} = \frac{A_{Ra}}{370} + \frac{A_{Th}}{259} + \frac{A_K}{4810} \leq 1 \tag{II.27}$$

The respiratory organs are threatened because of the decrease of ^{226}Ra in ^{222}Rn and its descendants. The maximum allowable activity for ^{226}Ra is therefore reduced by half, ie 185 $Bg\ kg^{-1}$.

Similarly The internal hazard index (H_{in}), is definied as [123]:

$$H_{in} = \frac{A_{Ra}}{185} + \frac{A_{Th}}{259} + \frac{A_K}{4810} \leq 1 \tag{II.28}$$

where A_{Ra}, A_{Th} and A_K are the activity concentrations $Bg\ kg^{-1}$ of ^{226}Ra, ^{232}Th and ^{40}K respectively. For construction materials to be considered safe for construction of dwellings, the value of this index must be less than unity in order to keep the radiation hazard insignifiant.

II.13 Estimation of absorbed dose rate in air and external effective dose

The external terrestrial gamma-radiation absorbed dose rates in air at a height of about 1 m above the ground are calculated by using the conversion factor 0.0417 (nGy/h) (Bq/kg)$^{-1}$ for ^{40}K, 0.462 (nGy/h)(Bq/kg)$^{-1}$ for ^{238}U and 0.604 (nGy/h)(Bq/kg)$^{-1}$ for ^{232}Th [1]. Assuming that, ^{137}Cs, ^{90}Sr and the ^{235}U decay series can be neglected as they contribute very little to the total dose from the environmental background [128–130]:

$$D(nGy/h) = 0.462A_U + 0.604A_{Th} + 0.0417A_K \tag{II.29}$$

where A_U, A_{Th} and A_K are the mean activity concentrations of ^{238}U, ^{232}Th and ^{40}K, respectively in (Bq kg^{-1}). In the estimation of external effective dose, the conversion coefficient and occupancy factor must be taken into account. In the present work, a conversion factor of 0.7 Sv Gy^{-1} and occupancy factors Q have been used to convert the absorbed rate to human effective dose equivalent with an outdoor Q_{out} and indoor Q_{in} occupancy of 40% and 60% respectively. However, since the materials used in the construction of most these buildings also contain radionuclides, R (1.11) is the ratio of indoor and outdoor dose rate. It should be noted that the dwellings were built mainly using locally made soil bricks. A_i are average activity concentrations of ^{238}U, ^{232}Th and ^{40}K. $(KCF)_i$ are corresponding air kerma conversion factors given previously. The external effective dose is determined as follows [131]:

$$E_{ext}(mSv/y) = F_c \times [Q_{in} \times R + Q_{out}] \times \sum_{i=1}^{3} A_i \times (KCF)_i \times t \tag{II.30}$$

II.14 Radon, thoron and thoron progeny measurements

Radon is a rare gas that is chemically inert. The main natural isotopes being radon (^{222}Rn, $T_{1/2}$ = 3.8d), thoron (^{220}Rn, $T_{1/2}$ = 55.6s) and actinon (^{219}Rn, $T_{1/2}$ = 3.98s) re-

spectively from the isotope decay chains: ^{238}U, ^{232}Th and ^{235}U. These radioactive gases decay by alpha transition to produce aerosol-forming solid descendants in the air that are radioactive isotopes of lead, polonium, and bismuth.

II.14.1 E-PERM Electret Ion Chambers (EICs)

Figure 28: Electret Ion Chambers (EICs) (left) and electret voltage reader (right).

An electret instrument includes a measurement chamber to which air from the room diffuses through a filter that removes radon daughters. The chamber walls are electrically conductive. The chamber contains an electret, an electrostatically charged sheet of Teflon. The electret is positively charged on the surface that is facing the chamber. The opposite side is negatively charged and is connected to the walls of the chamber. Alpha particles from the decay of radon and daughters ionize the air in the chamber. Electrons freed at the ionization moves in the electric field towards the surface of the electret while the positive ions move toward the walls. The electrostatic charge becomes reduced and the potential can be measure by a voltmeter. If a chamber with screw cap is used the electret is an integrating method that can for example be used to measure only during daytime. The electret method has to be corrected for gamma radiation.

II.14.2 Raduet detector

To determine radon and thoron concentrations, passive integrated radon-thoron discriminative detector developed at the National Institute of Radiological Sciences (NIRS) in Japan (Commercially Raduet) were used. These detectors have two diffusion cham-

bers with different ventilation rates and each chamber contains a CR-39 chip $10 \times 10mm^2$ in size (RADUET, Radosys Ltd., Hungary, Fig.29) [132] which was used to detect the alpha particles emitted from radon and thoron as well as their progeny.

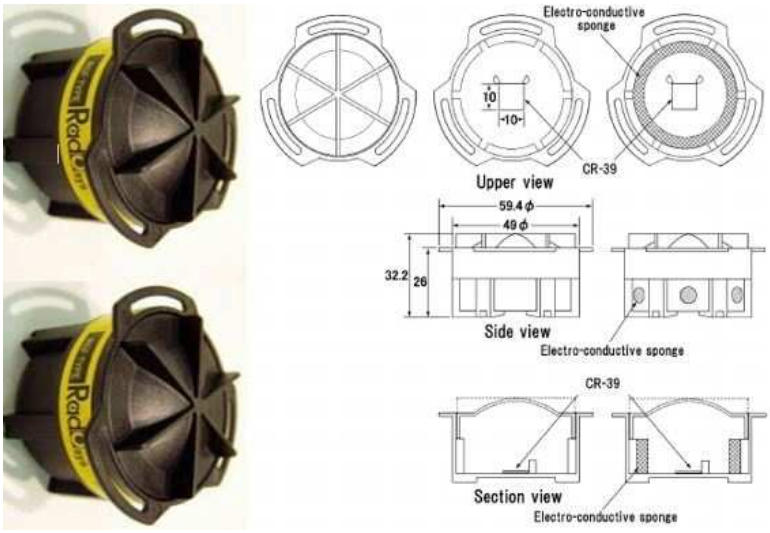

Figure 29: Schematic drawings of the passive type radon and thoron discriminative detector (RADUET) (Tokonami et al [132]).

The low diffusion rate chamber is made of electron conductive plastic with an inner volume of 30 cm^3. The high diffusion rate chamber is also made of the same material, but it has six holes in the wall and has electroconductive sponge covering the holes to prevent radon and thoron progeny, and aerosols from infiltrating inside. While one chamber measures radon only, the other chamber detects radon and thoron combined. Thoron concentration is then determined by substracting the result of one detector from the other. The difference in track density between the two CR-39 chips makes it possible to estimate radon and thoron concentrations separately. After the exposure, the CR-39 plates were chemically etched for 24 h in a 6 M NaOH solution at 60^0C, and alpha tracks were counted with an optical microscope [133].

II.14.3 Thoron progeny monitors

The thoron progeny monitors also used CR-39 mounted on a stainless stell plate and covered with a thin sheet of absorbed [134, 135]. The prototype of a thoron progeny monitor was developed by Zhuo and Iida [136]. The CR-39 pieces are covered with

an aluminium-vaporised Mylar lm of 71 mm of air equivalent thickness. The thickness of the Mylar lm allows the detection of only the 8.8 MeV alpha particles emitted from ^{212}Po (thoron progeny). According to Janik et al [137], the lower limit of detection (LLD) is calculated on the basis of an ISO Guideline, these LLD depends on the concentration of both gases and on the exposure period. For example, when a radon concentration of 15 Bq m^{-3} and a thoron concentration of 15 Bq m^{-3} are given with a measurement period of 90 days, the detection limits are estimated to be 5 Bq m^{-3} and 7 Bq m^{-3}, respectively. While detection limit of thoron progeny concentration is 0.005 Bq m^{-3}.

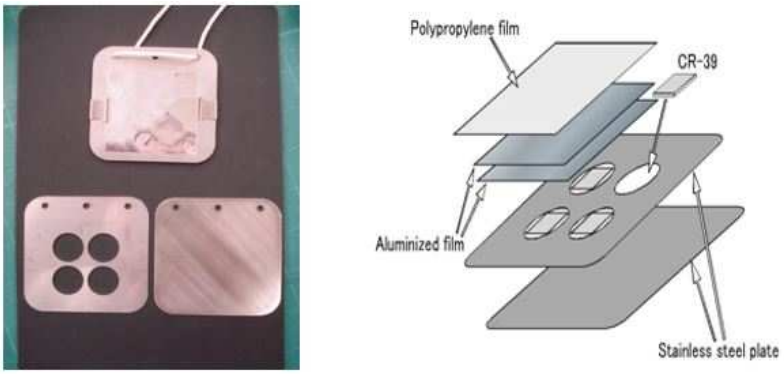

Figure 30: Thoron progeny monitor and Schematic drawings of the passive type thoron progeny monitor (Kudo et al [138]).

II.15 ^{222}Rn Activity concentrations and uncertainty

II.15.1 Radon concentrations using E-PERM Electret Ion Chambers

The evaluation of the radon concentration using the measurements taken in the field is obtained first by determining the calibration factor of the detector (type E-perm):

$$CF = A + B\frac{I+F}{2} \tag{II.31}$$

expressed in $V/pCi.j.l^{-1}$. I and F being initial and final voltages of the electret expressed in V while A and B are constants given by the manufacturer [139].

The concentration of radon in the air is given by:

$$C_{R_n} = \left(\frac{I-F}{CF.D} - BG\right) f_{corr}^{alt} \left({}^{pCi}/_{l}\right) \tag{II.32}$$

$$C_{R_n} \left({}^{pCi}/_{l}\right) = \frac{1}{37} C_{R_n}(Bq/m^3) \tag{II.33}$$

D is the duration of the exposure (days), BG is the background due to the ambient dose expressed in radon equivalent concentration ($pCi\ l^{-1}$), f_{corr}^{alt} is the correction factor taking into account of the dwelling altitude (alt) above sea level. The fitting parameters A and B are given by the manufacturer A =0.02383 and B = 0.0000112.

$$f_{corr} = 0.996 + 0.00016 \bullet alt(m) \tag{II.34}$$

EICs are sensitive to background gamma radiation. The equivalent radon signal in picoCuries per liter ($pCi\ l^{-1}$) per unit background radiation in micro-roentgens per hour (μR h^{-1}) is determined by the manufacturer depending on the type of EIC. This is specic to the chamber and not to the electret used in the chamber. This parameter is 0.12 for L chambers [139]. This value must be multiplied by the gamma radiation level at the site (in μR h^{-1}) and the product (in equivalent $pCi\ l^{-1}$) subtracted from the apparent radon concentration. The gamma radiation level at the site was 0.12μSv h^{-1} = 11 μR h^{-1}.

$$BG = [0.12 \times (PCi.l^{-1}) \,/\, (\mu R/h)] \times 11\mu R/h \tag{II.35}$$

The minimum voltage before exposing the EIC is fixed at 200 V. The accuracy of measurements is ensured by using reference electrets for quality control checking before each set of electret readings using the Electret Voltage Reader. The voltage of the reference chamber when provided by the manufacturer is (248 ± 1) V. This voltage is supposed to decrease less than 1 V each year and should not be used for many years. Three sources of uncertainty were identified:

•Uncertainty on the active volume and electret thickness of the EIC estimated at 5%;

•Uncertainty related to the initial and final readings of the electret estimated at 1.4 V;

•Uncertainty on the gamma external radiation estimated between 0.1 and 0.2 $pCi\ l^{-1}$.

•Uncertainty on the temperature, humidity, and ventilation system was neglected.

$$\mu(C_{R_n}) = \sqrt{E_1^2 + E_2^2 + E_3^2} \tag{II.36}$$

where E_1, E_2 and E_3 are 5%, 1.4 V et 0.1-0.2 pCi/l respectively.

II.15.2 Radon and thoron concentrations using Raduet detector

The average radon $\overline{(\mathrm{C_{Rn}})}$ and thoron $\overline{(\mathrm{C_{Tn}})}$ concentration are calculated using the following formulae [141]:

$$\begin{aligned}\overline{(\mathrm{C_{Rn}})} &= \left(d_L - \overline{b}\right) \frac{f_{Tn2}}{t.(f_{Rn1}.f_{Tn2} - f_{Rn2}f_{Tn1})} - \left(d_H - \overline{b}\right) \frac{f_{Tn1}}{t.(f_{Rn1}.f_{Tn2} - f_{Rn2}f_{Tn1})} \\ &= \left(d_L - \overline{b}\right).w_1 - \left(d_H - \overline{b}\right).w_2\end{aligned} \tag{II.37}$$

with $w_1 = \frac{f_{Tn2}}{t.\varepsilon}$ and $w_2 = \frac{f_{Tn1}}{t.\varepsilon}$ where $\varepsilon = f_{Rn1}.f_{Tn2} - f_{Rn2}f_{Tn1}$

$$\begin{aligned}\overline{(\mathrm{C_{Tn}})} &= \left(d_H - \overline{b}\right) \frac{f_{Rn1}}{t.(f_{Rn1}.f_{Tn2} - f_{Rn2}f_{Tn1})} - \left(d_L - \overline{b}\right) \frac{f_{Rn2}}{t.(f_{Rn1}.f_{Tn2} - f_{Rn2}f_{Tn1})} \\ &= \left(d_H - \overline{b}\right).w_3 - \left(d_L - \overline{b}\right).w_4\end{aligned} \tag{II.38}$$

with $w_3 = \frac{f_{Rn1}}{t.\varepsilon}$ and $w_4 = \frac{f_{Rn2}}{t.\varepsilon}$

where d_L and d_H were alpha track densities for low and high air-exchange rate chamber in tracks per square centimetre $(track\ cm^{-2})$ respectively. $\overline{b}$ is track density due to background in $(track\ cm^{-2})$. t sampling duration (h). f_{Rn1} and f_{Tn1} , were calibration factor for ^{222}Rn, ^{220}Rn in a low air-exchange rate chamber in $(tracks\ cm^{-2}h^{-1})/(Bqm^{-3})$, respectively. f_{Rn2} and f_{Tn2} were calibration factor for ^{222}Rn, ^{220}Rn in a high air-exchange rate chamber in $(tracks\ cm^{-2}h^{-1})/(Bqm^{-3})$.

According to ISO/IEC Guide 98-3, the standard uncertainty of $\overline{(\mathrm{C_{Rn}})}$ is calculated as given in formula following:

$$u\left(\overline{C_{Rn}}\right) = \left(\begin{array}{l} w_1^2\left(u^2\left(d_L\right) + u^2\left(\overline{b}\right)\right) - 2w_1w_2u^2\left(\overline{b}\right) + w_2^2\left(u^2\left(d_H\right) + u^2\left(\overline{b}\right)\right) \\ + \left(d_L - \overline{b}\right)^2 u^2\left(w_1\right) + \left(-d_H + \overline{b}\right)^2 u^2\left(w_2\right) \end{array} \right)^{-1/2} \quad \text{(II.39)}$$

with

$$u^2\left(w_1\right) = \frac{1}{\varepsilon^4 t^2}\left\{\left(\varepsilon - f_{Rn2}f_{Rn1}\right)^2 u^2\left(f_{Tn2}\right) + f_{Tn2}^4 u^2\left(f_{Rn1}\right) + f_{Tn1}^2 f_{Tn2}^2 u^2\left(f_{Rn2}\right) + f_{Rn2}^2 f_{Tn2}^2 u^2\left(f_{Tn1}\right)\right\} \quad \text{(II.40)}$$

and

$$u^2\left(w_2\right) = \frac{1}{\varepsilon^4 t^2}\left\{\left(\varepsilon + f_{Rn1}f_{Tn2}\right)^2 u^2\left(f_{Tn1}\right) + f_{Tn2}^4 u^2\left(f_{Rn2}\right) + f_{Tn1}^2 f_{Tn2}^2 u^2\left(f_{Rn1}\right) + f_{Rn1}^2 f_{Tn1}^2 u^2\left(f_{Tn2}\right)\right\} \quad \text{(II.41)}$$

the standard uncertainty of $\overline{(\mathrm{C_{Tn}})}$ is calculated as give in formula following:

$$u\left(\overline{C_{Tn}}\right) = \left(\begin{array}{l} w_3^2\left(u^2\left(d_H\right) + u^2\left(\overline{b}\right)\right) - 2w_3w_4u^2\left(\overline{b}\right) + w_4^2\left(u^2\left(d_L\right) + u^2\left(\overline{b}\right)\right) \\ + \left(d_H - \overline{b}\right)^2 u^2\left(w_3\right) + \left(-d_L + \overline{b}\right)^2 u^2\left(w_4\right) \end{array} \right)^{-1/2} \quad \text{(II.42)}$$

with

$$u^2\left(w_3\right) = \frac{1}{\varepsilon^4 t^2}\left\{\left(\varepsilon - f_{Rn1}f_{Tn1}\right)^2 u^2\left(f_{Rn1}\right) + f_{Rn1}^4 u^2\left(f_{Tn2}\right) + f_{Rn1}^2 f_{Tn1}^2 u^2\left(f_{Rn2}\right) + f_{Rn1}^2 f_{Rn2}^2 u^2\left(f_{Tn1}\right)\right\} \quad \text{(II.43)}$$

and

$$u^2\left(w_4\right) = \frac{1}{\varepsilon^4 t^2}\left\{\left(\varepsilon + f_{Rn2}f_{Tn1}\right)^2 u^2\left(f_{Tn2}\right) + f_{Rn2}^4 u^2\left(f_{Tn1}\right) + f_{Rn2}^2 f_{Tn2}^2 u^2\left(f_{Rn1}\right) + f_{Rn1}^2 f_{Rn2}^2 u^2\left(f_{Tn2}\right)\right\} \quad \text{(II.44)}$$

where the uncertainty of the exposure time is neglected.

The calculation of the characteristic limits (ISO 11929) requires the calculation of $\tilde{u}\left(\tilde{C}_{Rn}\right)$ and $\tilde{u}\left(\tilde{C}_{Rn}\right)$ i.e. the standard uncertainty of $\overline{C_{Rn}}$ and $\overline{C_{Tn}}$ as a function of their true value, calculated as given in following formulae respectively:

$$\tilde{u}\left(\tilde{C}_{Rn}\right)=\left(\begin{array}{l} w_1^2\left(u^2\left(d_L\right)+u^2\left(\overline{b}\right)\right)-2w_1w_2u^2\left(\overline{b}\right)+w_2^2\left(u^2\left(d_H\right)+u^2\left(\overline{b}\right)\right) \\ +\frac{\left(d_H^2-2\overline{b}d_H+\overline{b}^2\right)w_2^2+\tilde{C}_{Rn}\left(2d_H-2\overline{b}\right)w_2+\tilde{C}_{Rn}^2}{w_1^2}u^2\left(w_1\right)+\left(-d_H+\overline{b}\right)^2u^2\left(w_2\right) \end{array}\right)^{-1/2} \quad \text{(II.45)}$$

$$\tilde{u}\left(\tilde{C}_{Tn}\right)=\left(\begin{array}{l} w_3^2\left(u^2\left(d_H\right)+u^2\left(\overline{b}\right)\right)-2w_3w_4u^2\left(\overline{b}\right)+w_4^2\left(u^2\left(d_L\right)+u^2\left(\overline{b}\right)\right) \\ +\frac{\left(d_L^2-2\overline{b}d_L+\overline{b}^2\right)w_4^2+\tilde{C}_{Tn}\left(2d_L-2\overline{b}\right)w_4+\tilde{C}_{Tn}^2}{w_1^2}u^2\left(w_3\right)+\left(-d_L+\overline{b}\right)^2u^2\left(w_4\right) \end{array}\right)^{-1/2} \quad \text{(II.46)}$$

The decision threshold $\overline{C}_{Rn}^{*}$ and $\overline{C}_{Tn}^{*}$ are obtained from the formulae of w_3, w_4 and $\overline{(\mathrm{C_{Rn}})}$ for $\tilde{C}_{Rn}=0$, $\tilde{u}\left(d_L=0\right)$, $\tilde{C}_{Tn}=0$ and $\tilde{u}\left(d_H=0\right)$ (see ISO 11929).

we obtain:

$$\overline{C}_{Rn}^{*}=k_{1-\alpha}.\tilde{u}\left(0\right)=k_{1-\alpha}\left(\begin{array}{l} w_1^2u^2\left(\overline{b}\right)-2w_1w_2u^2\left(\overline{b}\right)+w_2^2\left(u^2\left(d_H\right)+u^2\left(\overline{b}\right)\right) \\ +\frac{\left(d_H^2-2\overline{b}d_H+\overline{b}^2\right)w_2^2}{w_1^2}u^2\left(w_1\right)+\left(-d_H+\overline{b}\right)^2u^2\left(w_2\right) \end{array}\right)^{-1/2} \quad \text{(II.47)}$$

$$\overline{C}_{Tn}^{*}=k_{1-\alpha}.\tilde{u}\left(0\right)=k_{1-\alpha}\left(\begin{array}{l} w_3^2u^2\left(\overline{b}\right)-2w_3w_4u^2\left(\overline{b}\right)+w_4^2\left(u^2\left(d_L\right)+u^2\left(\overline{b}\right)\right) \\ +\frac{\left(d_L^2-2\overline{b}d_L+\overline{b}^2\right)w_4^2}{w_1^2}u^2\left(w_3\right)+\left(-d_L+\overline{b}\right)^2u^2\left(w_4\right) \end{array}\right)^{-1/2} \quad \text{(II.48)}$$

$\alpha=0.05$ with $k_{1-\alpha}=1.65$ often chosen by default.

The detection limit, $\overline{C}_{Rn}^{\#}$ and $\overline{C}_{Tn}^{\#}$, are calculted as given in following formulae (see ISO 11929):

$$\overline{C}_{Rn}^{\#} = \overline{C}_{Rn}^{*} + k_{1-\beta}.\left(\begin{array}{l} w_1^2\left(u^2\left(d_L\right)+u^2\left(\overline{b}\right)\right) - 2w_1w_2u^2\left(\overline{b}\right) + w_2^2\left(u^2\left(d_H\right)+u^2\left(\overline{b}\right)\right) \\ +\frac{\left(d_H^2-2\overline{b}d_H+\overline{b}^2\right)w_2^2+\tilde{C}_{Rn}\left(2d_H-2\overline{b}\right)w_2+\tilde{C}_{Rn}^2}{w_1^2}u^2\left(w_1\right)+\left(-d_H+\overline{b}\right)^2u^2\left(w_2\right) \end{array} \right)^{-1/2} \quad \text{(II.49)}$$

$$\overline{C}_{Tn}^{\#} = \overline{C}_{Tn}^{*} + k_{1-\beta}.\left(\begin{array}{l} w_3^2u^2\left(\overline{b}\right) - 2w_3w_4u^2\left(\overline{b}\right) + w_4^2\left(u^2\left(d_L\right)+u^2\left(\overline{b}\right)\right) \\ +\frac{\left(d_L^2-2\overline{b}d_L+\overline{b}^2\right)w_4^2}{w_1^2}u^2\left(w_3\right)+\left(-d_L+\overline{b}\right)^2u^2\left(w_4\right) \end{array} \right)^{-1/2} \quad \text{(II.50)}$$

The detection limit can be calculated by solving formulae of $\tilde{u}\left(\tilde{C}_{Tn}\right)$ and $\overline{C}_{Rn}^{*}$ for $\overline{C}^{\#}$ or, more simply, by iteration with a starting approximation $\overline{C}^{\#} = 2 \times \overline{C}^{*}$ in terms of the right side of following formulae. One obtains $\overline{C}^{\#}$ with $k_{1-\alpha}$ = $k_{1-\beta}$ = k:

$$\overline{C}_{Rn}^{\#} = \frac{2.\overline{C}_{Rn}^{*}+k^2\left\{\frac{\left(2d_H-2\overline{b}\right)w_2u^2(w_1)}{w_1^2}\right\}}{1-k^2\frac{u^2(w_1)}{w_1^2}} \quad \text{(II.51)}$$

$$\overline{C}_{Tn}^{\#} = \frac{2.\overline{C}_{Tn}^{*}+k^2\left\{\frac{\left(2d_L-2\overline{b}\right)w_4u^2(w_3)}{w_1^2}\right\}}{1-k^2\frac{u^2(w_3)}{w_3^2}} \quad \text{(II.52)}$$

Values α=β=0.05 and therefore $k_{1-\alpha}$ = $k_{1-\beta}$ =1.65 are often chosen by default.

II.16 Radon and Thoron progeny concentrations

The concentrations of progeny are determined through Equilibrium Equivalent Radon and Thoron Concentration (EERC and EETC). EERC was calculated by following equation:

$$EERC = F_R \times C_{Rn} \quad \text{(II.53)}$$

where C_{Rn} is concentration of radon calculated using track density from Raduet detector and F_R equilibrium factor for radon (0.4). However EETC was measured by thoron progeny monitors [136], these monitors also used CR-39 mounted on a stainless

stell plate and covered with a thin sheet of absorbed [134].

II.17 Equilibrium Factor

ICRU [142] reported that, because radon progeny in the air can be removed by deposition on surfaces and ventilation, the activity concentrations of the short-lived radon progeny in the air are not in equilibrium with that of the radon gas. This is quantified by the equilibrium factor, F, which is a measure of the degree of disequilibrium between the radon gas and its progeny. The inhaled decay products and not radon gas deliver the majority of the alpha particle dose to the bronchial airways. Thus, the equilibrium factor is of dosimetric importance because it is used to estimate the progeny activity concentration in air when measurements of radon and not progeny are made.
The equilibrium factors for radon, thoron and their progeny were then simply calculated by using the following expressions [143]:

$$F_{Rn} = \frac{EERC}{C_{Rn}} \tag{II.54}$$

$$F_{Tn} = \frac{EETC}{C_{Tn}} \tag{II.55}$$

where EERC and EETC are the equilibrium equivalent concentration $(Bq\ m^{-3})$ of radon and thoron.

II.18 Total inhalation dose assessment

The total inhalation dose due to exposure to indoor radon, thoron and their progeny has been calculated using the relation given by UNSCEAR [144]:

$$E_{Rn}(mSv/y) = (0.17 + 9 \times F_R) \times C_{Rn} \times t \times F_{occ} \times 10^{-6} \tag{II.56}$$

$$E_{Tn}(mSv/y) = (0.11 \times C_{Tn} + 40 \times EETC) \times t \times F_{occ} \times 10^{-6} \quad \text{(II.57)}$$

where F_R is the equilibrium factor for radon. C_{Rn} and C_{Tn} are respectively radon and thoron concentrations in Bq m^{-3}. $EETC$ is the equilibrium equivalent thoron concentration. The quantities 0.17 and 9 are dose conversion factors for radon and its progeny concentrations, respectively, while 0.11 and 40 are the dose conversion factors for thoron and its progeny concentrations in nSv respectively [144]. The exposure time t was 8766 h, and the indoor occupancy factor (F_{occ}) was assumed to be 0.6. The multiplication factor 10^{-6} is used to convert nSv into mSv.

II.19 Risk assessment

The cancer and hereditary risks due to low doses without threshold dose known as stochastic effect were estimated using the ICRP cancer risk assessment methodology [60, 63]. In its 1990 recommendations, risks from radiation induced cancers were derived from observations of people exposed to high doses using a dose and dose rate effectiveness factor (DDREF). Risk estimates based on the observations of people exposed to low doses has associated large uncertainties and therefore will contribute to quantitative risks estimates [63]. The lifetime risks of fatal cancer recommended in the 1990 recommendations by the ICRP are 5×10^{-2} Sv for the members of the public and $4 \times 10^{-2} Sv^{-1}$ for occupationally exposed workers [63].

In its latest recommendations of 2007, the Commission has retained its fundamental hypothesis for the induction of stochastic effects of linearity of dose and effect without threshold and a dose and dose-rate effectiveness factor (DDREF) of 2 to derive the nominal risk coefficients for low doses and low dose rates. In its latest recommendations, the system of regulations for radiological protection based on the 1990 recommendations has not changed [60].

However, a new set of nominal risk coefficient has been derived to be used for the es-

timation of fatal cancer as well as hereditary effects. The recommended nominal risk coefficients in its 2007 recommendations are given in table 6. The new nominal risk coefficients were derived based upon data on cancer incidence weighted for lethality and life impairment whereas the 1990 values were based upon fatal cancer risk weighted for non-fatal cancer, relative life years lost for fatal cancers and life impairment for non-fatal cancer. However the combined detriment from stochastic effects in the new values has remained unchanged at around $5\%Sv^{-1}$ [60].

Table 6: Detriment-adjusted nominal risk coefficients for stochastic effects after exposure to radiation at low dose rate (10^{-2}) [60]

Exposed	Cancer		Heritable effects		Total detriment	
Population	2007	1990	2007	1990	2007	1990
Whole	5.5	6.0	0.2	1.3	5.7	7.3
Adult	4.1	4.8	0.1	0.8	4.2	5.6

The risk of exposure to low doses and dose rates of radiation to members of the public in Douala were estimated as using the 2007 recommended risk coefficients [60] and an assumed 70 years lifetime of continuous exposure of the population to low level radiation.

Fatality cancer risk = total annual effective dose (Sv) $\times$ cancer nominal risk factor.

Hereditary effect = total annual effective dose (Sv) $\times$ hereditary nominal effect factor.

II.20 Conclusion

The purpose of this chapter, was to present the material used for natural radioactivity measurements, as well as the methodology used to determine the concentration of the following primordial radionuclides: ^{238}U, ^{232}Th and ^{40}K then, concentration of the radon gas (^{222}Rn and ^{220}Rn) and their progeny.

CHAPTER III

RESULTS AND DISCUSSION

III.1 Introduction

The concentrations of the primordial radionuclides were calculated in the soil samples and, indoor radon and thoron were measured in the dwellings of the Douala city. In this part of the work, the results obtained will be presented, discussed and compared to other works on the one hand and, at their different corresponding global average values on the other hand.

III.2 Measurement of natural radioactivity by *in-situ* gamma spectrometry

III.2.1 *In-situ* activity concentrations of ^{238}U, ^{232}Th and ^{40}K and their contribution to air absorbed dose rate

According to Table 7, Activity concentrations for primordial radionuclides range between 18-47 $Bq\ kg^{-1}$, 21-54 $Bq\ kg^{-1}$ and 110-410 $Bq\ kg^{-1}$ for the ^{238}U series, ^{232}Th series and ^{40}K respectively, with corresponding average values of 29 $Bq\ kg^{-1}$, 38 $Bq\ kg^{-1}$ and 202 $Bq\ kg^{-1}$. For ^{238}U and ^{232}Th, 7/39 and 32/39 measurement points have respectively activity concentrations higher than the world average value [1]. For ^{40}K, 1/39 measurement point has activity concentrations higher than the world average.

By comparing the average *in-situ* activity concentrations of ^{238}U, ^{232}Th and ^{40}K in Douala with the average values in other areas of Cameroon and other countries as shown in Table 9, it should be noted that the mean activity concentration of ^{238}U is

Table 7: *In-situ* Activity concentrations and the contributions of ^{40}K ,^{238}U and ^{232}Th to air absorbed dose rates in Douala using the car-borne survey method.

Point	Latitude	Longitude	Absorbed dose rate in air	Contribution to the dose rate (%)			Activity concentrations (Bq kg^{-1})		
	N	E	(nGy h^{-1})	^{40}K	^{238}U	^{232}Th	^{40}K	^{238}U	^{232}Th
Douala	N4.05883	E9.701882	50±1	12	28	60	146±3	33±2	48±2
Douala	N4.060352	E9.703057	50±1	23	25	53	292±6	31±2	44±2
Douala	N4.062082	E9.701685	59±1	27	33	40	386±8	45±3	36±2
Douala	N4.06649	E9.703935	32±1	34	24	40	290±6	18±1	21±1
Douala	N4.070663	E9.696892	45±1	36	23	41	410±8	25±3	30±2
Douala	N4.048405	E9.690173	32±1	23	23	53	185±4	18±1	27±1
Douala	N4.045582	E9.689423	41±1	17	28	54	187±4	29±2	37±2
Douala	N4.043308	E9.685862	29±1	15	28	57	110±2	20±1	28±1
Douala	N4.041148	E9.685378	39±1	12	30	58	129±3	30±2	39±2
Douala	N4.029897	E9.68979	45±1	16	26	59	184±4	28±2	44±2
Douala	N4.026803	E9.690527	36±1	14	26	60	130±3	24±2	36±2
Douala	N4.024398	E9.693795	52±1	13	30	58	177±4	39±3	51±3
Douala	N4.019988	E9.701103	40±1	20	26	55	210±4	26±2	37±2
Douala	N4.016748	E9.706783	33±1	16	29	55	146±3	25±2	32±2
Douala	N4.05417	E9.734857	48±1	16	25	58	208±4	31±2	47±2
Douala	N4.057508	E9.729035	41±1	23	26	51	246±5	27±2	35±2
Douala	N4.064372	E9.715773	49±1	15	29	56	200±4	36±3	47±2
Douala	N4.071107	E9.718553	36±1	23	26	52	208±4	22±2	31±2
Douala	N4.081412	E9.728038	31±1	16	29	56	131±3	23±2	30±2
Douala	N4.080985	E9.747512	37±1	13	27	60	124±2	26±2	38±2
Douala	N4.084458	E9.755105	44±1	13	29	59	143±3	30±2	42±2
Douala	N4.086427	E9.767235	46±1	23	21	56	286±6	25±2	44±2
Douala	N4.079912	E9.772208	32±1	15	28	57	130±3	18±1	32±2
Douala	N4.073662	E9.753895	35±1	13	28	59	125±3	25±2	36±2
Douala	N4.065873	E9.759602	33±1	16	27	57	139±3	23±2	32±2
Douala	N4.056127	E9.765598	43±1	15	25	61	167±3	27±2	44±2
Douala	N4.053658	E9.761817	52±1	15	25	61	201±4	33±2	54±3
Douala	N4.042078	E9.761412	42±1	16	24	59	176±4	25±2	42±2
Douala	N4.032633	E9.766025	42±1	22	25	53	237±5	26±2	37±2
Douala	N4.03475	E9.778138	49±1	15	25	60	194±4	31±2	50±3
Douala	N4.026533	E9.791902	44±1	16	25	60	184±4	28±2	45±2
Douala	N4.00135	E9.804472	40±1	22	24	54	223±4	24±2	36±2
Douala	N4.049702	E9.738715	50±1	24	25	51	312±6	31±2	43±2
Douala	N4.048875	E9.740258	48±1	16	25	59	200±4	30±2	47±2
Douala	N4.047623	E9.728583	31±1	20	27	54	155±3	20±1	28±1
Douala	N4.04285	E9.705237	43±1	20	44	36	231±5	47±3	26±1
Douala	N4.043018	E9.702948	47±1	29	33	39	359±7	39±3	31±2
Douala	N4.043115	E9.696225	44±1	17	35	48	197±4	39±3	36±2
Douala	N4.017505	E9.715673	40±1	12	36	52	127±3	37±3	36±2

higher than the average value measured in other areas of Cameroon such as Bakassi and Poli, and lower than those measured in Lolodorf and Douala quarries. The same comparison can be made with those measured in Lagos state in Nigeria, in Itagunmodi and Canakkale in Turkey, and in Kerala in India. For ^{232}Th, the average activity concentration found out in the present study is higher than those of Bakassi and Poli, and lower than those measured at Douala-quarriers and Lolodorf. This value is also higher than those of Itagunmodi and Lagos State and lower than that of Kerala. The average value of ^{40}K is higher than that is obtained in Bakassi and less than the average values found at Douala-quarriers, Lolodorf and Poli. Compared to other studies in the world, this value is higher than that of Canakkale, lower than those of Lagos state, Itagunmodi and Kerala. Figure 31 shows a weak correlation between thorium and uranium (correlation coefficient =0.09).

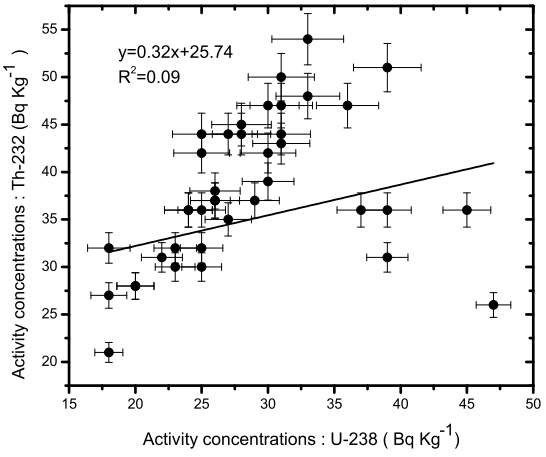

Figure 31: Correlation between ^{232}Th and ^{238}U activity concentrations.

The contributions of ^{238}U, ^{232}Th and ^{40}K to the absorbed dose rates in air range respectively between 21-44%, 36-61% and 12-36% with the average values of 27%, 54% and 19% respectively. The highest contributions of ^{238}U, ^{232}Th and ^{40}K to the absorbed dose rate were respectively found at Akwa (44%) (N4.04285, E9.705237), Beedi (61%) (N4.053658, E9.761817) and SCDP (36%) (N4.06649, E9.703935) while the lowest contri-

butions were found at Makepe (36%) (N4.04285, E9.705237) and Akwa (12%) (N4.017505, E9.715673) for ^{232}Th and ^{40}K respectively.

III.3 Natural radioactivity measurement in soil samples by gamma spectrometry

III.3.1 Activity Concentrations of ^{238}U, ^{232}Th and ^{40}K in Soil Samples

Activity concentrations of natural radionuclides ^{238}U, ^{232}Th and ^{40}K in 20 soil samples using gamma spectrometry in laboratory are listed in Table 8.

Table 8: Activity concentrations of natural radionuclides ^{238}U, ^{232}Th and ^{40}K in 20 soil samples using gamma spectrometry in laboratory.

	Location		**Activity concentration (Bq kg^{-1})**			**Absorbed dose rate**	**Annual effective dose**
Sample code	**Latitude**	**Longitude**	^{40}K	^{238}U	^{232}Th	**(nGy h^{-1})**	**(mSv y^{-1})**
STN-16-39	04°01′640″	09°44′424″	40±8	88±17	82±18	92±13	0.6±0.1
STN-16-40	04°01′625″	09°44′510″	41±9	52±10	53±12	58±9	0.4±0.1
STN-16-41	04°01′642″	09°44′345″	43±9	66±13	64±14	72±10	0.5±0.1
STN-16-42	04°01′395″	09°44′284″	53±11	39±08	37±8	43±6	0.3±0($\prec$ 0.1)
STN-16-43	04°01′342″	09°44′240″	42±9	52±10	48±11	55±8	0.4±0.1
STN-16-44	04°01′136″	09°44′239″	77±16	29±06	29±6	34±5	0.2±0 ($\prec$0.1)
STN-16-45	04°00′995″	09°44′766″	44±9	65±13	68±15	73±11	0.5±0.1
STN-16-46	04°00′907″	09°44′810″	47±10	69±14	69±15	76±11	0.5±0.1
STN-16-47	04°00′835″	09°44′746″	60±13	39±08	36±8	43±6	0.3±0 ($\prec$0.1)
STN-16-48	04°00′769″	09°44′619″	59±13	52±10	54±12	59±9	0.4±0.1
STN-16-49	04°00′822″	09°44′595″	62±13	43±08	42±9	48±7	0.3±0 ($\prec$0.1)
STN-16-50	04°00′861″	09°44′702″	43±9	56±11	58±13	63±9	0.4±0.1
STN-16-51	04°01′047″	09°44′320″	51±11	58±11	51±11	60±8	0.4±0.1
STN-16-52	04°01′016″	09°44′089″	64±13	62±12	54±12	65±9	0.4±0.1
STN-16-53	04°01′258″	09°44′046″	74±16	61±12	55±12	65±9	0.4±0.1
STN-16-54	04°01′302″	09°44′055″	67±14	40±08	38±8	45±6	0.3±0 ($\prec$0.1)
STN-16-55	04°01′433″	09°44′016″	79±17	66±13	62±14	72±10	0.5±0.1
STN-16-56	04°01′421″	09°43′763″	68±14	82±16	74±16	86±12	0.6±0.1
STN-16-57	04°01′371″	09°43′740″	52±11	81±16	79±17	88±13	0.6±0.1
STN-16-58	04°01′188″	09°43′941″	46±10	96±19	92±20	102±15	0.7±0.1

They range respectively between 29-96 $Bq\ kg^{-1}$, 29-92 $Bq\ kg^{-1}$ and 40-79 $Bq\ kg^{-1}$

with respective average values of 60 $Bq\ kg^{-1}$, 57 $Bq\ kg^{-1}$ and 56 $Bq\ kg^{-1}$. The world average values of ^{238}U, ^{232}Th and ^{40}K in the earths crust are 35, 30 and 400 $Bq\ kg^{-1}$, respectively [1]. It appears that average values of ^{238}U and ^{232}Th are higher than the corresponding world average activity concentrations. Figure 32 shows a good correlation between thorium and uranium in soil samples (correlation coefficient =0.97). The highest ^{238}U and ^{232}Th activity concentrations were found at Brazzaville (96 $Bq\ kg^{-1}$) and Dakar for ^{40}K (79 $Bq\ kg^{-1}$). The lowest activity concentrations of ^{238}U and ^{232}Th were found at Bilongue (29 $Bq\ kg^{-1}$) and Oyack for ^{40}K (40 $Bq\ kg^{-1}$). The results of activity concentrations of natural radionuclides in soil samples taken from Douala III at different locations and in other parts of the world are displayed in Table 9. It clearly appears that activity concentrations of ^{238}U and ^{232}Th were higher than those of other areas in Cameroon (Bakassi, Poli and Douala-quarries) except Lolodorf and other countries (Lagos state, Itagunmodi, Canakkale).

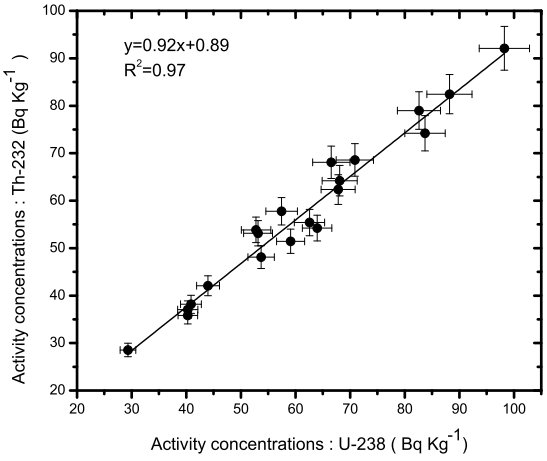

Figure 32: Correlation between ^{232}Th and ^{238}U activity concentrations.

III.4 Radiological Hazard Indices

Following The calculated R_{aeq} values for all soil samples and *in-situ* measurement points presented in Table (10), it may be seen that Raeq oscillates between 69 and 126

Table 9: Comparison of activity concentrations of ^{238}U, ^{232}Th and ^{40}K in soil samples from Douala littoral region following laboratory and *in-situ* measurements with values from other areas around the world.

Country			Activity (Bq kg^{-1})			References
			^{238}U	^{232}Th	^{40}K	
Nigeria	Lagos state		1.20-55.30 (23)	2.18-60.33 (23)	44.74-489.96 (204)	Ojo and Gbadegesin. [145]
	Itagunmodi		18.5-90.3 (55)	12.5-52.4(26)	200.5-901.2 (501)	Augustine Kolapo et al. [146]
Turkey	Canakkale		14.9-118 (42)	18.7-146(53)	197.1-1033.4 (54)	S.Turhan et al. [147]
India	Kerala		25-1269	42-2374	22-964	Hosoda et al. [148]
Cameroon	Poli		12-57 (24)	15-58(28)	112-1124 (506)	Saïdou et al. [131]
	Bakassi		17-23 (19)	27-38(32)	93-138 (110)	Saïdou et al. [149]
	Lolodorf		60-270 (130)	100-700(390)	370-1530 (850)	Saïdou et al. [131]
	Douala (quarries)		11.8-146.7 (40)	8-102.9(43)	54-928 (342)	Ghuembou et al [150]
	Douala	In-situ	18-47 (29)	21-54(38)	110-410 (202)	Present work
		Labo	29-96 (60)	29-92(57)	40-79 (56)	Present work
	World		16-110 (35)	11-64 (30)	140-850 (400)	Unscear [1]

with an average of 98 $Bq\ kg^{-1}$, between 76 and 231 with an average of 146 $Bq\ kg^{-1}$ for *in-situ* measurement and laboratory measurement respectively. It is observed that the values of R_{aeq} were less than the acceptable safe limit of 370 $Bq\ kg^{-1}$ [29]. In addition, the calculated values of hazard index for *in-situ* measurement points were ranged from 0.2 to 0.3 with an average value of 0.3 and from 0.2 to 0.5 with an average value of 0.3 for external (H_{ex}) and internal (H_{in}) respectively as mentioned in table (10). However for the soil samples, the hazard index were ranged from 0.2 to 0.6 with an average value of 0.4 and from 0.3 to 0.9 with an average value of 0.6 for external (H_{ex}) and internal (H_{in}) respectively (table 10). These values are lower than the agreed value of unity.

Table 10: Radium Equivalent (R_{aeq}) and Hazard index (H_{ex} and H_{in}) ($Bq\ kg^{-1}$).

	In-Situ measurement			**Laboratory measurement**		
	Raeq	Hex	Hin	Raeq	Hex	Hin
	113	0.3	0.4	209	0.6	0.8
	116	0.3	0.4	131	0.4	0.5
	126	0.3	0.5	161	0.4	0.6
	70	0.2	0.2	96	0.3	0.4
	99	0.3	0.3	124	0.3	0.5
	71	0.2	0.2	76	0.2	0.3
	96	0.3	0.3	166	0.4	0.6
	69	0.2	0.2	171	0.5	0.6
	96	0.3	0.3	95	0.3	0.4
	105	0.3	0.4	134	0.4	0.5
	85	0.2	0.3	108	0.3	0.4
	126	0.3	0.4	142	0.4	0.5
	95	0.3	0.3	136	0.4	0.5
	82	0.2	0.3	144	0.4	0.6
	114	0.3	0.4	146	0.4	0.6
	96	0.3	0.3	100	0.3	0.4
	119	0.3	0.4	161	0.4	0.6
	82	0.2	0.3	193	0.5	0.7
	76	0.2	0.3	198	0.5	0.8
	90	0.2	0.3	231	0.6	0.9
	101	0.3	0.4			
	110	0.3	0.4			
	74	0.2	0.2			
	86	0.2	0.3			
	79	0.2	0.3			
	103	0.3	0.4			
	126	0.3	0.4			

	99	0.3	0.3			
	97	0.3	0.3			
	117	0.3	0.4			
	107	0.3	0.4			
	93	0.3	0.3			
	117	0.3	0.4			
	113	0.3	0.4			
	72	0.2	0.2			
	102	0.3	0.4			
	111	0.3	0.4			
	106	0.3	0.4			
	98	0.3	0.4			
Min-Max	69-126	0.2-0.3	0.2-0.5	76-231	0.2-0.6	0.3-0.9
Moyenne	98	0.3	0.3	146	0.4	0.6
Médiane	99	0.3	0.3	143	0.4	0.5

III.5 Indoor radon and equilibrum factor of thoron

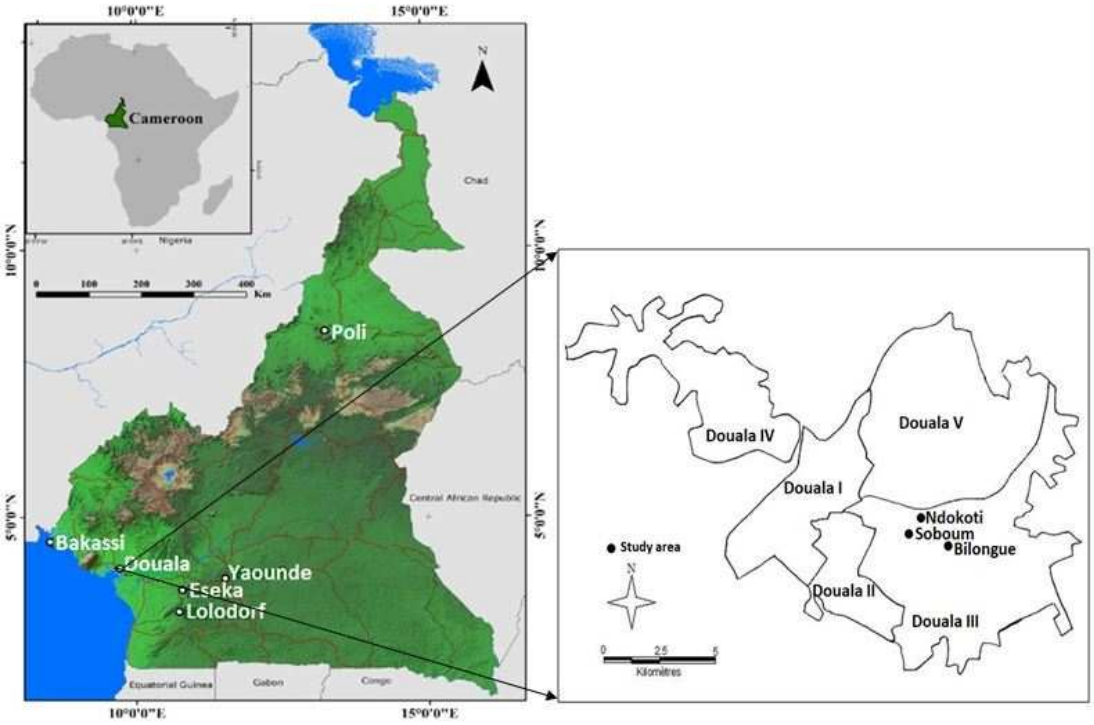

Figure 33: Location of the study area.

Radon measurements were made using E-perm detectors, Raduet detectors and Thoron progeny monitors in more than 100 dwellings in Douala. These measurements took place in three phases where the first two used the detectors of types E-perm and

last, detectors of types Raduets and monitors progeny of thoron.

III.5.1 Radon concentration measured with E-perm detector

After three months of exposure, the table below gives us the results of radon concentrations in the first and second phase of measurements.

Table 11: Indoor activity concentration of radon in dwellings of Douala using E-perm detector.

Statistics	Radon Concentration (Bq m^{-3})	
	Rainy season	Dry season
Minimum	91	15
Maximum	8204	1901
Arithmetic Mean (AM)	2989	423
Standard deviation (SD)	1864	444
Geometric Mean (GM)	2292	243
Geometric standard deviation(GSD)	2.4	3.08
Median	2753	251

The activity concentration of radon in the first phase of measurement was found to vary between 91 to 8204 $Bq\ m^{-3}$, with an average value of 2989 $Bq\ m^{-3}$ which is ten time that given by ICRP (300 $Bq\ m^{-3}$). However, in second phase of measurement radon concentration was found to range between 15 to 1901 $Bq\ m^{-3}$ with an average value of 423 $Bq\ m^{-3}$, value slightly above the reference value limit. Sorimachi et al [151] reported, it is known that radon measurement with electret monitors may be affected by environmental parameters, e.g., temperature, relative humidity (RH), elevation, the presence of ions in the room, air drafts, gamma radiation, thoron in the air, and external dust. However for the continuation of the work we used the RADUET detectors as far as to have the best results.

III.5.2 Indoor radon and thoron concentration mesured with Raduet detector

Table 12 summaries the results obtained for radon and thoron in 71 dwellings of Douala.. The measured values of radon and thoron concentrations vary from 31 ± 1 to

436 ± 12 Bq m^{-3} with an arithmetic mean of 139 ± 47 Bq m^{-3} and from 4 ± 7 Bq m^{-3} to 246 ± 5 Bq m^{-3} with an arithmetic mean of 80 ± 52 Bq m^{-3}, respectively.The geometric mean of C_{Rn} and C_{Tn} result 118 Bq m^{-3} and 62 Bq m^{-3} respectively, which are lower than the international indoor geometric mean of 45 Bq m^{-3} [144]. According to Ćurguz et al [152], the geometric means of radon depends on building materials. In our study, the indoor geometric mean radon is different from other parts of the world because the building material of dwellings in Douala is hardly comparable..

Table 12: The ranges, arithmetic mean, geometric mean and median of the indoor radon, thoron and progeny:levels and the equilibrium factor of thoron..

	Min	Max	AM $\pm$ SD	GM(GSD)	Median
Radon (Bq m^{-3})	31 ± 1	436 ± 12	139 ± 47	118(1.3)	139
Thoron (Bq m^{-3})	4 ± 7	246 ± 5	80 ± 52	62(2.1)	71
FTn	0.01 ± 0.01	0.83 ± 1.55	0.11 ± 0.16	0.07(9.90)	0.07
(EETC) (Bq m^{-3})	1.5 ± 0.9	13.1 ± 9.4	4.6 ± 2.9	3.9(1.8)	3.6
(EERC) (Bq m^{-3})	12 ± 1	174 ± 5	51 ± 21	47(1.6)	55

Less than 2% of dwellings among those surveyed had radon concentration higher than the permissible level of 300 Bq m^{-3} [153]. 32% and 34% of dwellings have respectively radon concentrations below 100 Bq m^{-3} [154], and 148 Bq m^{-3} [155]. Only 32% of dwellings have radon concentrations below 200 Bq m^{-3}, as recommended by EU countries [156]. In the uranium-bearing region of Lolodorf and Poli, Saïdou et al. [9] measured radon concentrations using electret ionization chambers in a range between 24-4390 Bq m^{-3} for Lolodorf, and 29-2240 Bq m^{-3} for Poli with arithmetic means of 687 Bq m^{-3} and 294 Bq m^{-3} respectively. These values are higher than the corresponding values reported in the present study. Figure 34 shows the radon concentrations plotted against thoron concentrations, but they do not correlate each other. In Cameroon, there are not yet reference levels for radon indoors. However, the national radon action plan is being elaborated..

Similar studies were carried out worldwide. Results of the radon and thoron activity concentrations, the EERC and the EETC in several countries are summarized in Table 13. Prasad et al [157] reported a study of radiation exposure due to radon, thoron and

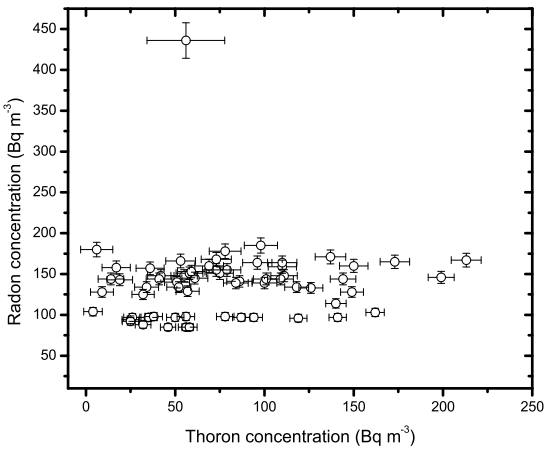

Figure 34: Scatter plots of radon-thoron concentration.

progeny in the indoor environment of Yamuna and tons valleys of Garhwal Himalaya. Visnuprasad et al [159] reported the contribution of thoron and progeny towards inhalation dose in a thorium abundant beach environment in Kerala, India.Gierl et al. [160] performed a similar study on thoron and thoron progeny measurements in German clay houses.

The results show that gas concentrations range between 20 and 160 Bq m^{-3} for radon and between 10 and 90 Bq m^{-3} for thoron 20 cm from the wall. This study showed that increased thoron gas concentrations as well as thoron progeny concentrations can be found in houses built of unfired clay. The traditional Chinese residential dwelling is constructed with loam bricks or mud walls (so called raw-soil building) for which Shang et al. [161] determined the radon and thoron concentrations (Table 13). The value of equilibrium factor of indoor thoron for concrete and brick houses is higher (0.020-0.038) than in soil-structure houses (0.004-0.007). These results point to high thoron concentrations in Chinese traditional residential dwellings constructed with loam bricks or soil wall. Indoor thoron contributes 13-57% to the total inhalation dose. The radon and thoron concentrations in Douala investigated within our study are compared to the above worldwide results. General radon concentrations are greater than the associated thoron levels based upon numerous studies (see Table 13).

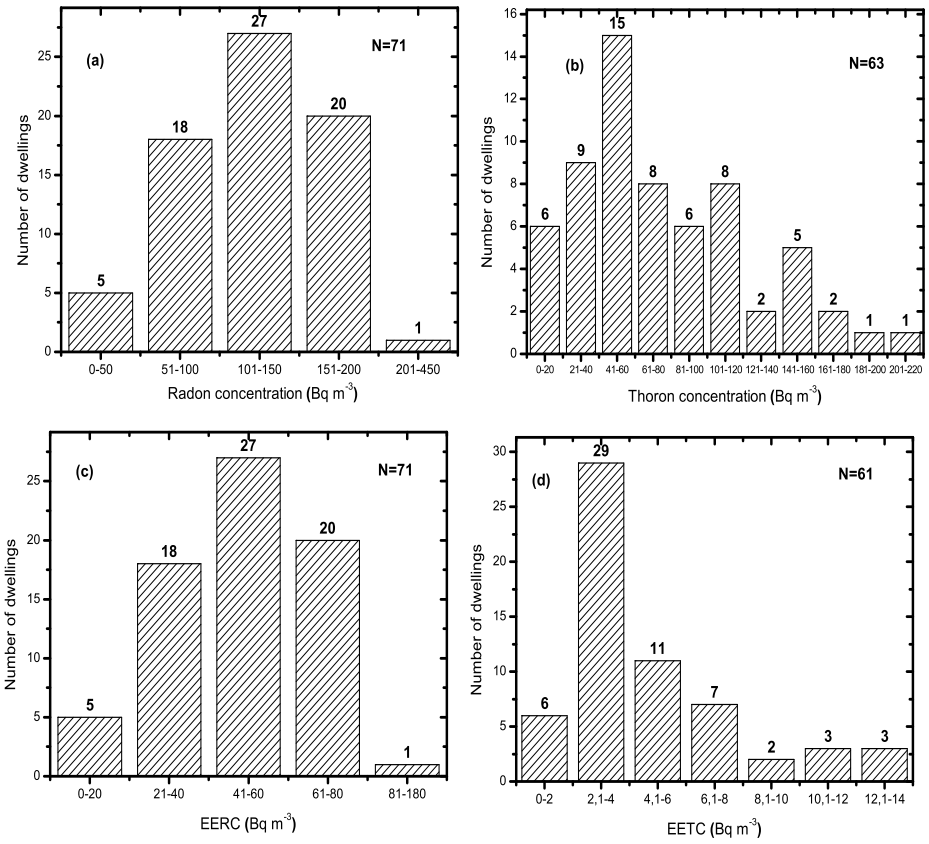

Figure 35: Frequency distribution of radon and its progeny (a and c), thoron and its progeny (b and d) in the dwellings of Douala.

From Figure 35(a) we can see that the highest frequencies of the C_{Rn} results are in intervals lower than 150 Bq m^{-3}. It should be mentioned that one of the surveyed dwellings appears to have annual C_{Rn} higher than 400 Bq m^{-3}. In all dwellings C_{Tn} was lower than 300 Bq m^{-3} as well as in Figure 35(b).

III.5.3 Indoor radon and thoron progeny concentration

The equilibrium equivalent radon concentration (EERC) and equilibrium equivalent thoron concentration (EETC) have been found to vary from 12 to 174 Bq m^{-3} with an arithmetic mean of 51 $\pm$ 21 Bq m^{-3} and from 1.5 $\pm$ 0.9 to 13.1 $\pm$ 9.4 with an arithmetic mean of 4.6 $\pm$ 2.9 Bq m^{-3}, respectively. The geometric mean of EERC and EETC are

respectively 47 Bq m^{-3} and 4 Bq m^{-3} with the geometric standard deviation (GSD) of 1.6 and 1.8 respectively. The frequency distribution of the radon, thoron and progeny concentrations in the 71 dwellings of the investigated area are shown in figure 35.

Results of the radon, thoron activity concentrations, the EERC, and the EETC in several countries are summarized in Table 13.

III.5.4 Equilibrium factor of thoron

The average equilibrium factor for thoron was calculated from the measurements of the AM of 0.1 $\pm$ 0.1 (Table 12). This mean value is higher than the value (0.02) given by UNSCEAR [144]. The distribution of equilibrium factor for thoron is shown in Figure 36. About 20% of the dwellings have F_{Tn} values less than or equal to 0.02. Harley et al. [162] reported an equilibrium factor of 0.04 $\pm$ 0.01 for indoor thoron using a large database obtained by a long-term measurement of thoron and its progeny. However, Hosoda et al [163] presented widely ranged EETCs from 0.008 to 0.07 obtained by the recent measurements in several countries. These results vary because the equilibrium factor depends largely on the environment conditions such as hours, humidity, time, place and modes of ventilation etc. [164,165].

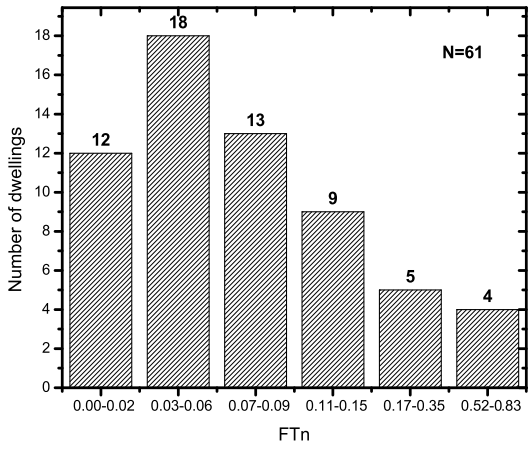

Figure 36: Frequency distribution of the equilibrium factor between thoron and its progeny.

Table 13: Results of measurements of the radon, thoron activity concentration, the EERC and the EETC.

		CRn (Bq m^{-3})		CTn (Bq m^{-3})		EERC (Bq m^{-3})		EETC (Bq m^{-3})		Reference
Country/area		Range(AM)	GM	Range(AM)	GM	Range(AM)	GM	Range(AM)	GM	
South Africa	West	28-465(132)	-	-	-	-	-	-	-	[166]
	East	8-98(37)								
India	Himalaya	4.2-174.3(37.6)	24.3	1-108.2(24.6)	18.3	1.6-76.1(17.4)	13.2	0.1-3.6(0.9)	0.7	[157]
Canada	Ottawa	8-1525(110)	74	5-924(56)	19	-	-	-	-	[158]
India	Kerala	7.8-89(24.2)	21.6	3.7-129(36.7)	28.1	1.9-31.5(10.9)	9.50	0.1-11.4(1.6)	1.1	[159]
German		20-160	-	10-90	-	-	-	2-10	-	[160]
Chinese		11.6-427(72.4)	57.5	LLD-1,860(318)	162	-	-	LLD-15.8(3.8)	-	[161]
Cameroon	Poli	46-143(82)	-	24-238(94)	-	-	-	4-9(6.4)	-	[167]
	Lolodorf	27-937(97)		6-700(160)				0.4-36(10.3)		
	Betare oya	88-282(133)		4-383(92)				0.6-19(6)		

III.6 Dose calculations to the public

III.6.1 *In-situ* measurements

III.6.2 Shielding factor and dose rate conversion factor

The relationship between count rates inside and outside the car is shown in figure 37, and the shielding factor and standard uncertainty [168] were found to be 1.62 and 0.03, respectively. However the shielding factor is influenced by the type of car, number of passengers and detector position inside the car.

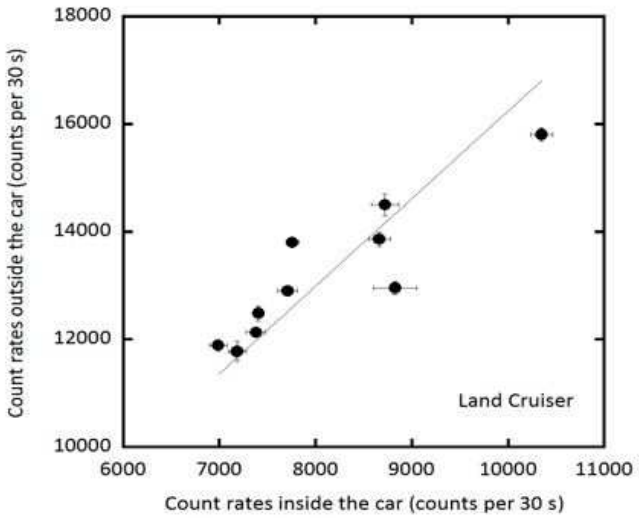

Figure 37: Correlation between count rates outside and inside the car. This regression formula was used as the shielding factor of the car body.

Figure 38 shows the correlation between absorbed dose rates in air ($nGy\ h^{-1}$) calculated using the 22 $\times$ 22 response matrix method and count rate outside the car (cps) (that is corrected count rate inside the car). The dose conversion factor and uncertainty were found to be 0.00175 nGy h^{-1} cps^{-1} and 0.01, respectively. Thus the absorbed dose rate in air D_{out} outside the car 1 m above the ground surface at each measuring point can be estimated using the following equation [86]:

$$D_{out} = 2D_{in} \times 1.62 \times 0.00175 \tag{III.1}$$

where D_{in} is count rate inside the car (cps) obtained by measurements for 30 seconds.

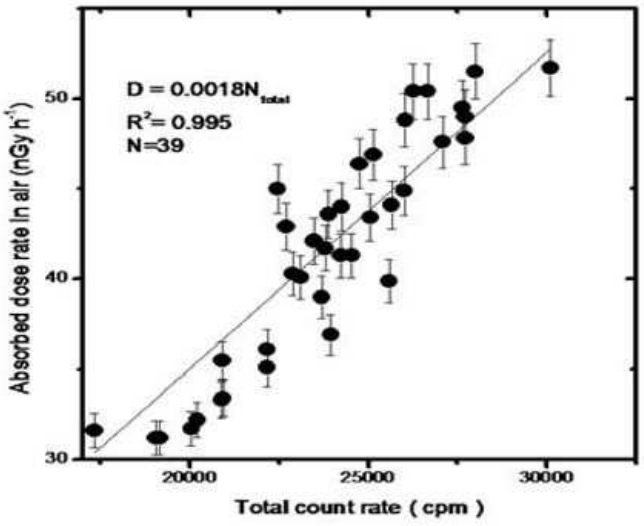

Figure 38: Correlation between absorbed dose rate in air which was calculated by software using the response matrix method and total count rate observed outside the car. This regression formula was used as the dose rate conversion factor.

III.6.3 Air absorbed dose rate distribution in Douala city and effective external dose

Figure 39 show the survey route in Douala. The highest air absorbed dose rates (86 $nGy\ h^{-1}$) were observed at Ndogbong (N4.058778, E9.74635) (see figure 40). The absorbed dose rates in this study range between 28-86 $nGy\ h^{-1}$ with the average value of 50 $nGy\ h^{-1}$ (figure 41a).

According to UNSCEAR [1] at worldwide level, gamma dose rates in air range between 24-160 $nGy\ h^{-1}$ and the average is 59 $nGy\ h^{-1}$, higher than the average value obtained within the framework of this study. However at Ndogbong, Aeroport, Ndogpassi III, Bepanda Omnisports, and Brazzaville, air absorbed dose rates are higher than the worldwide average value. The town of Kerala in India recorded large values of the absorbed dose rate, up to 2100 $nGy\ h^{-1}$, observed near the rare earth mining [82]. In Tokyo, air absorbed dose rates range from 18 to 76 $nGy\ h^{-1}$ with an average value of 49 $nGy\ h^{-1}$ [169], and from 11 to 554 $nGy\ h^{-1}$ with an average value of 50 $nGy\ h^{-1}$ in Turkey [147], which is practically lower than the corresponding worldwide value.

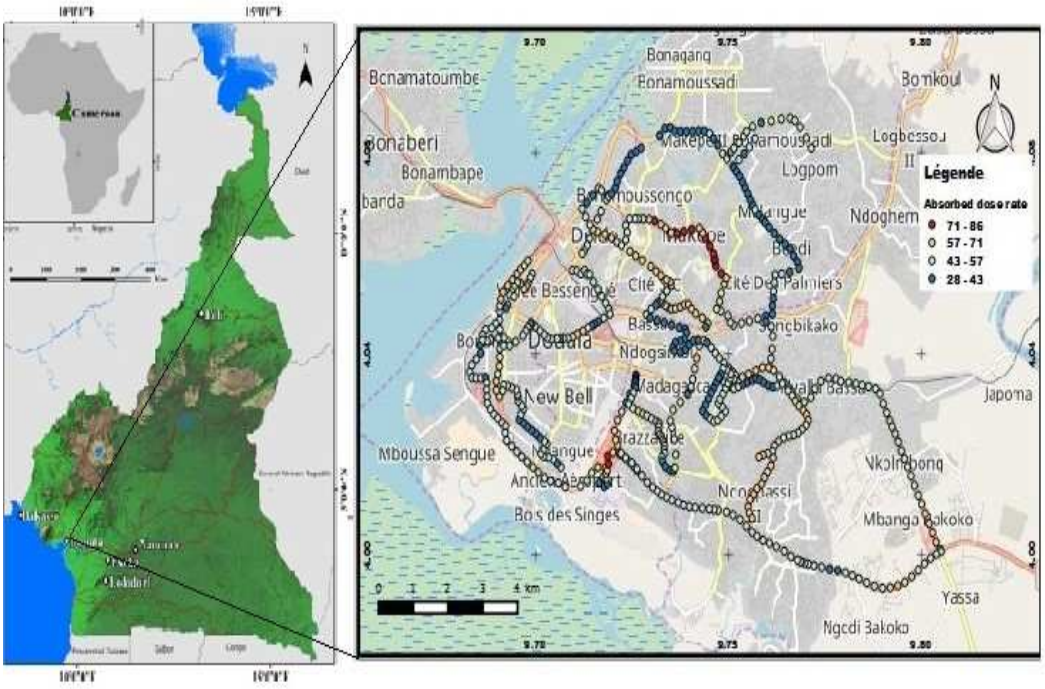

Figure 39: Survey route in Douala. This map was also drawn using QGIS (Background: Openstreet map).

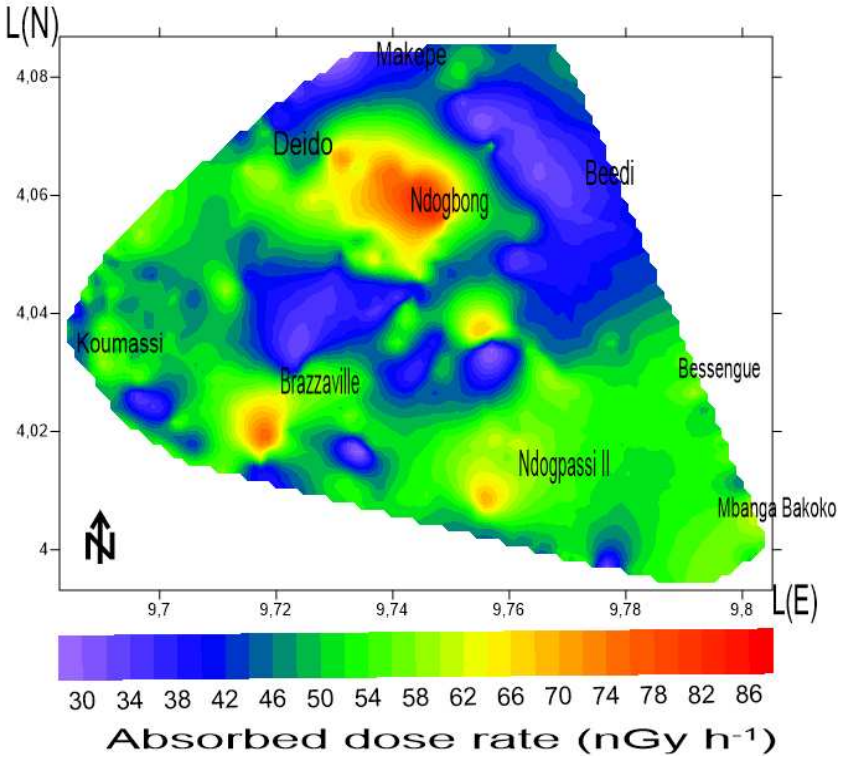

Figure 40: Distribution map of absorbed dose rate ($nGy\ h^{-1}$) in Douala city.

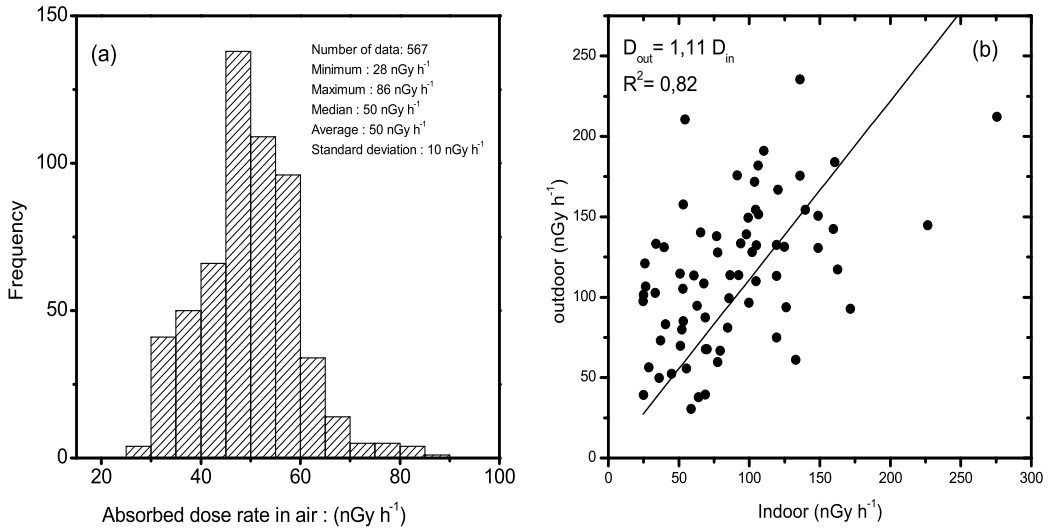

Figure 41: Histogram of absorbed dose rate in air obtained by car-borne survey in Douala (a), correlation between outdoor and indoor dose rate (b).

III.6.4 Absorbed dose rates and Annual effective dose rate in soil samples

The external terrestrial gamma radiation absorbed dose rates range between 34 and 102 $nGy\ h^{-1}$, with an average value of 65 nGy h^{-1}, which is higher than the world average value of 59 $nGy\ h^{-1}$ [1]. According to Table 2, absorbed dose rates at 13 over 20 measurement points were higher than the world average value (59 nGy h^{-1}). External effective dose of 8 over 20 measurement points is higher than the worldwide average value. Table 2 shows that all measurement points have absorbed dose rate lower than the worldwide average value. External effective dose varies from 0.3-0.7 mSv y^{-1} with an average value of 0.42 mSv y^{-1}, which is lower than the worldwide average value (0.5 mSv y^{-1}). The highest effective dose was found at Brazzaville (0.7 mSv y^{-1}) and Oyack (0.6 mSv y^{-1}). The average value of the effective amount obtained in this study compared to other inhabited areas of Cameroun (Poli and Lolordorf) is low, and high in Bakassi [149].

III.7 Inhalation dose

III.7.1 E-perm detector

The total inhalation dose of first survey range between 2 and 163 $mSv\ y^{-1}$ with an average value of 59 $\pm$ 40 $mSv\ y^{-1}$, which is higher than the recommended action level of between 3-10 $mSv\ y^{-1}$ [170]. However for the 2^{nd} survey the total inhalation dose varied from 0.3 to 38 $mSv\ y^{-1}$ with a mean value of 8 $\pm$ 9 $mSv\ y^{-1}$, which is slightly higher than the recommended action level.

Table 14: Range, mean and geometry indoor radon to total inhalation dose received by the general public

Statistics	Inhalation Dose (mSv y^{-1})	
	Rainy season	Dry season
Minimum	2	0.3
Maximum	163	38
Arithmetic Mean (AM)	59	8
Standard deviation (SD)	40	9
Geometric Mean (GM)	45	5
Geometric standard deviation(GSD)	2	3
Median	55	5

III.7.2 Raduet detector

The annual effective dose from exposure to radon and its progeny in the study area has been found to vary from 0.6 to 9 $mSv\ y^{-1}$ with an average of 2.6 $\pm$ 0.1 $mSv\ y^{-1}$. Similarly, the annual effective dose due to thoron and its progeny has been found to vary from 0.3 to 2.9 $mSv\ y^{-1}$ with an average of 1.0 $\pm$ 0.4 $mSv\ y^{-1}$. Figure 42 show the distribution of inhalation dose due to radon, thoron and their progeny.

The mean contribution of radon and its progeny to the total inhalation dose is 75% while that of thoron and its progeny is 26%. The arithmetic mean values of total inhalation dose due to radon, thoron and their progeny in dwellings of the study area was found to be 3.64 $mSv\ y^{-1}$. This inhalation dose received by the general public in

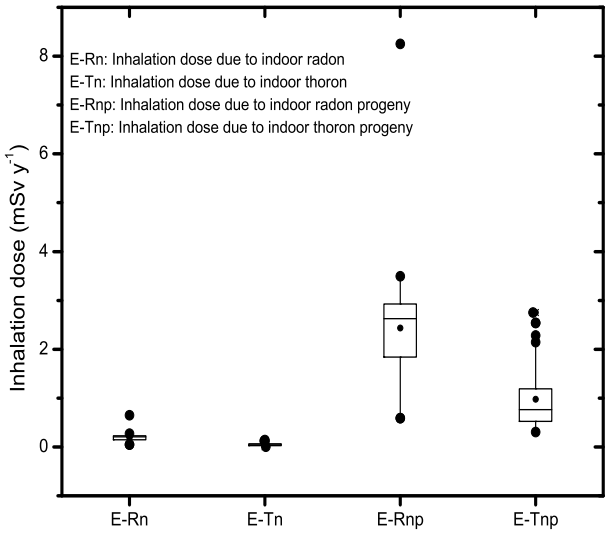

Figure 42: Box plot of inhalation dose of radon, thoron and their progeny.

the study area is lower than the reference level of 10 $mSv\ y^{-1}$ given by the International Commission on Radiological Protection [153]. Table 15 summarizes the contributions of radon, thoron, radon progeny and thoron progeny to the total inhalation dose range between 3-7%, 0.1-4%, 37-93% and 7-59% respectively. We have ascertained that the highest contribution to the inhalation dose of 70% stems from radon progeny and the corresponding least contribution of 1% belongs to thoron. However, thoron and its progeny contribute a significant fraction of 26% to the total inhalation dose. It suggests that thoron and its progeny cannot be neglected when assessing radiation dose as it was belieced in the past.

Indoor radon, thoron and progeny measurements in Douala city are continuing the work done in several regions of Cameroon, namely the uranium and thorium bearing regions of Poli and Lolodorf, and the gold mining areas of Betare-Oya [167]. About 400 RADUET detectors were deployed in dwellings. The results obtained showed a significant contribution of thoron and its progeny to the total inhalation dose. It varies from 12 to 67%, 3 to 80% and from 7 to 70% in the above study areas respectively. The corresponding average values are 49, 53 and 31% respectively.

Table 15: Ranges, mean and contribution of indoor radon, thoron and progeny to total inhalation dose received by the public.

Radionuclides	Range (mSv y^{-1})	Mean inhalation dose (mSv y^{-1})	Total (mSv y^{-1})	Range contribution (%)	Mean contribution (%)
Radon	0.05 - 0.65	0.19		3 - 7	5
Thoron	0.002 - 0.14	0.05	3.64	0.1 - 4	1
Radon Progeny	0.59 - 8.25	2.43		37 - 93	70
Thoron progeny	0.30 - 2.75	0.97		7 - 59	25

III.8 Total Dose

The total dose, as shown in the figure 43, includes the following components: external irradiation and inhalation (^{222}Rn + ^{220}Rn). Total dose was of 4.01 $mSv\ y^{-1}$ for the Douala region and it is about 2 times that of the global average value (2.4 $mSv\ y^{-1}$) defined by UNSCEAR. In the Poli region [97], the total dose received by the population was 5.2 $mSv\ y^{-1}$. The estimated annual effective dose of gamma radiation from the soil and radon inhalation received by the public of Aldama, Chihuahua, Mexico was 3.83 $mSv\ y^{-1}$ [171]. In Kerala (Inde) the average dose received by population is over 15 $mSv\ y^{-1}$ from gamma radiation [172]. Compared to the different doses observed throughout the world, Douala city remains until now acceptable despite the fact that its average total dose is above the global value.

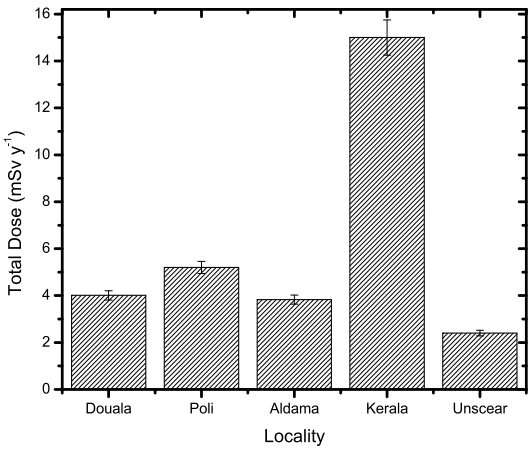

Figure 43: Total Dose of different areas.

III.9 Radiological risk

The appraisal of risk covered the exposure pathway considered in this study. Table (16) shows the average annual effective dose from soils, radon and the estimated risk components. The risk of exposure of low doses and dose rates of radiation was estimated using the 2007 recommended risk coefficients [60].

Table 16: Estimated risk components for the various exposure pathways studied.

Exposure pathway	Average annual effective dose rate (mSv y^{-1})	Fatality cancer risk to population per year (%)	Hereditary effet per year (%)
External irradiation in soil sample	0.42	0.002	0.008
In situ measurement	0.31	0.002	0.006
indoor radon measured with E-perm detector	33.5	0.18	0.67
indoor radon measured with Raduet detector	3.64	0.02	0.073

The average fatality cancer risk of external irradiation in soil samples, *In-situ* measurement, and indoor radon measured with E-perm detector and indoor radon measured with raduet was 0.002%, 0.002%, 0.18% and 0.02% respectively. In addition, hereditary effect of various exposure pathways respectively are 0.008%, 0.006%, 0.67% and 0.073%. The results show that there are no significant health risk due to exposure to natural radiation from external sources, to radon, thoron measured with Raduet detector.

III.10 Conclusion

This chapter shows results and discussion made on the study. ^{238}U, ^{232}Th and ^{40}K concentrations were measured to assess radiation dose to the public due to natural radioactivity. In addition, indoor ^{222}Rn and ^{220}Rn measurements were also made to evaluate radiation dose due to inhalation in Douala City. The total average effective doses due to natural radioactivity and inhalation are 0.37 and 3.64 mSv respectively, and 4.01 mSv in total. In general, radiation doses have shown no significant health risk due to

exposure to natural radioactivity, radon, thoron and their progeny in the study area.

General Conclusion

The present work focused on the study of public exposure to natural radioactivity in Douala city. This study made it possible to quantify natural radioactive elements such as: ^{238}U, ^{232}Th and ^{40}K by two methods, and to measure concentrations of radon, thoron and their progeny, and to assess radiation dose to the public due to natural radioactive elements, and to inhalation of radon and thoron in Douala city, Cameroon. The first called *in-situ* measurement was to determine the concentrations of radionuclides present on the site, the second method was to take soil samples and then analyze them in the laboratory to have the concentrations of natural radionuclides. In addition, the measurement of radon, thoron and their progeny in dwellings was made using E-perm detectors for radon and two types of nuclear track detectors for radon, thoron and their progeny for three months measurements. For *in-situ* measurements the mean values of the specific activities were 29 $Bq\ kg^{-1}$ (18 to 47) for ^{238}U, 38 $Bq\ kg^{-1}$ (21 to 54) for ^{232}Th and 202 $Bq\ kg^{-1}$ (10 to 40) for ^{40}K. However, in soil samples collected and analyzed in the laboratory, the average activity values of ^{238}U, ^{232}Th and ^{40}K were 60 $Bq\ kg^{-1}$ (29 to 98), 57 $Bq\ kg^{-1}$ (29 to 92), and 56 $Bq\ kg^{-1}$ (40 to 79) respectively. The results in this study are related to concentrations [1]. The arithmetic mean radon and thoron concentrations in 71 dwellings are respectively 139 $Bq\ m^{-3}$ and 80 $Bq\ m^{-3}$. Those for EERC and EETC are respectively 51 and 4.6 $Bq\ m^{-3}$. The mean equilibrium factor for thoron is 0.1 $\pm$ 0.1. The radium equivalent activity (Raeq), the external and internal hazard index were calculated to estimate the risk of exposure to natural radioactivity. The mean value of Raeq was 98 $Bq\ kg^{-1}$ and 146 $Bq\ kg^{-1}$ for *in-situ* measurements and soil samples respec-

tively, which are less than the accepted safety limit value of 370 $Bq\ kg^{-1}$. The calculated values of external hazard index and internal hazard index for *in-situ* measurement vary from 0.2 to 0.3 and 0.2 to 0.5 respectively, with the same average value of 0.3. The average value (Hex and Hin) obtained from both methods of measurement was below limit of unity Radiation protection quantities. The absorbed dose rates and annual effective doses were calculated using the formulas given in the UNSCEAR report. The minimum and maximum values obtained for absorbed dose rates in air are 28 $nGy\ h^{-1}$ and 86 $nGy\ h^{-1}$ for *in-situ* measurements respectively. whereas for soil samples analyzed in the laboratory, the absorbed dose rate varies from 34 to 102 $nGy\ h^{-1}$ with an average value of 65 $nGy\ h^{-1}$, which is higher than the world average value of 59 $nGy\ h^{-1}$. The mean total dose (*in-situ* + laboratory) was 0.37 $mSv\ y^{-1}$ for external exposure and this value is below the global mean value (0.5 $mSv\ y^{-1}$), it can be concluded that the population of Douala city is not significantly exposed to natural radiation. The mean effective doses due to inhalation were found to be 2.6 $mSv\ y^{-1}$ for radon and its progeny, 1.0 $mSv\ y^{-1}$ for thoron and its progeny, and 3.6 $mSv\ y^{-1}$ in total (arithmetic mean) which represents 91% of the total dose (4.01$mSv\ y^{-1}$). In general, radiation doses have shown no significant health risk due to exposure to radon, thoron and their progeny in the study area. Moreover, thoron and its progeny have been found to contribute about 26% to the total inhalation dose. This justifies that thoron and its progeny cannot be neglected when assessing radiation doses as it was believed in the past. It will seriously contribute to the radiological protection of the public against harmful effects of natural radiation. In view of the results obtained in this study when compared to other regions of the world, the dosimetry situation of Douala remains until now acceptable. In addition, given an insufficient quantity of dosimeter for a population of about 4 million and the high contribution of radon in the total dose, it is necessary to extend radon measurements throughout the city and others areas of Cameroon for within the framework of the national radon plan under implementation in Cameroon.

Perspectives and recommendations

− Extending the measurement of the concentration of primordial radionuclides (^{238}U, ^{232}Th and ^{40}K) in the soil samples.

− Extending the measurement of the concentration of radon, thoron and their associated progeny in all littoral region.

−Taking into account radon and thoron exposure in the house construction plan.

−Undertake an epidemiological study on lung's cancer due to radon, thoron and associated progeny.

−Putting in place regulations on exposure to radon, thoron and associated progeny.

−Drawing up a radiological map of Cameroon and then define a reference value for radon, thoron and associated progeny at the national level.

Appendix

Gamma spectrum of soil samples measured with NaI detector in laboratory

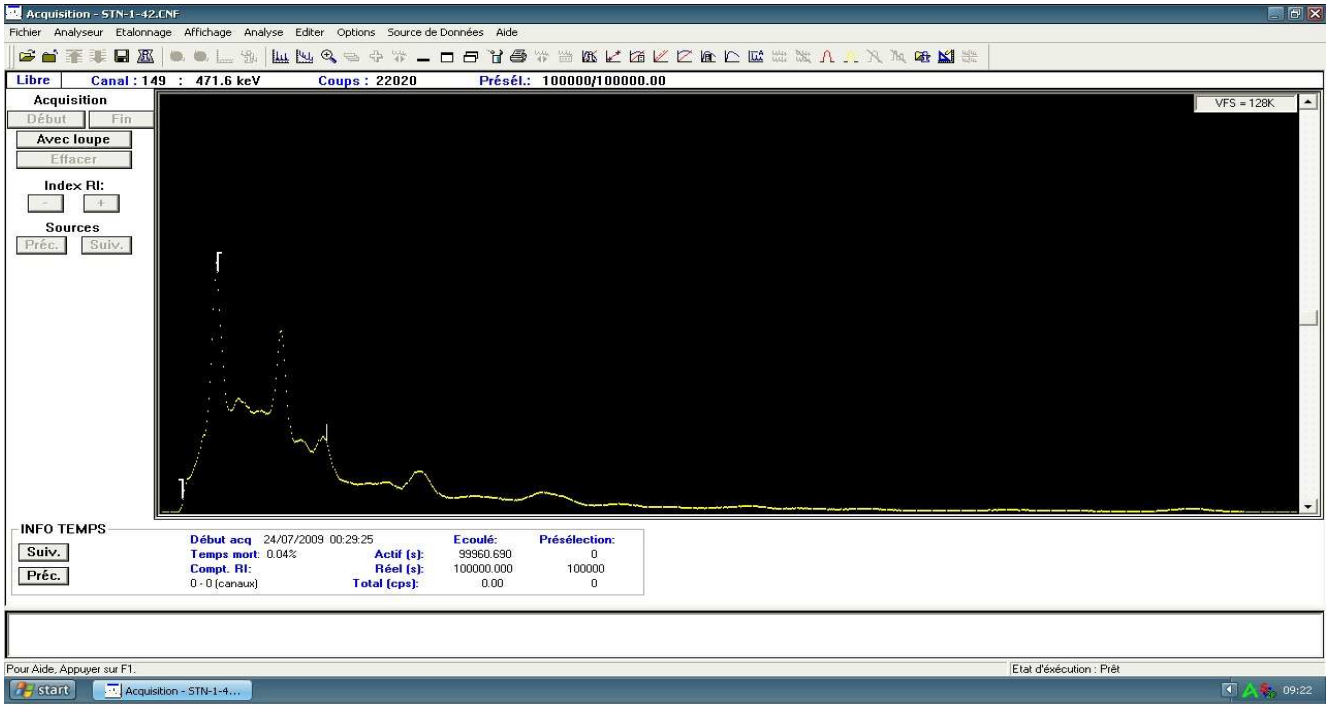

Figure 44: STN-16-39

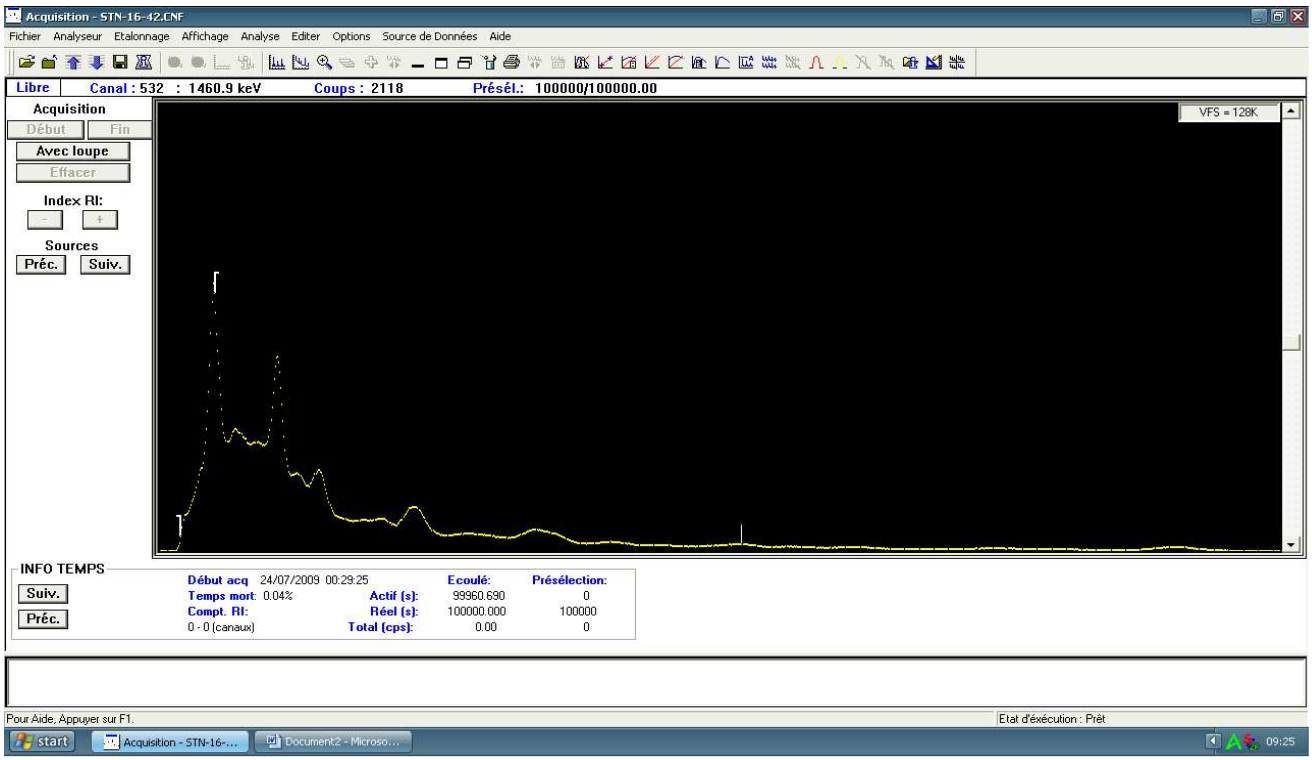

Figure 45: STN-16-42

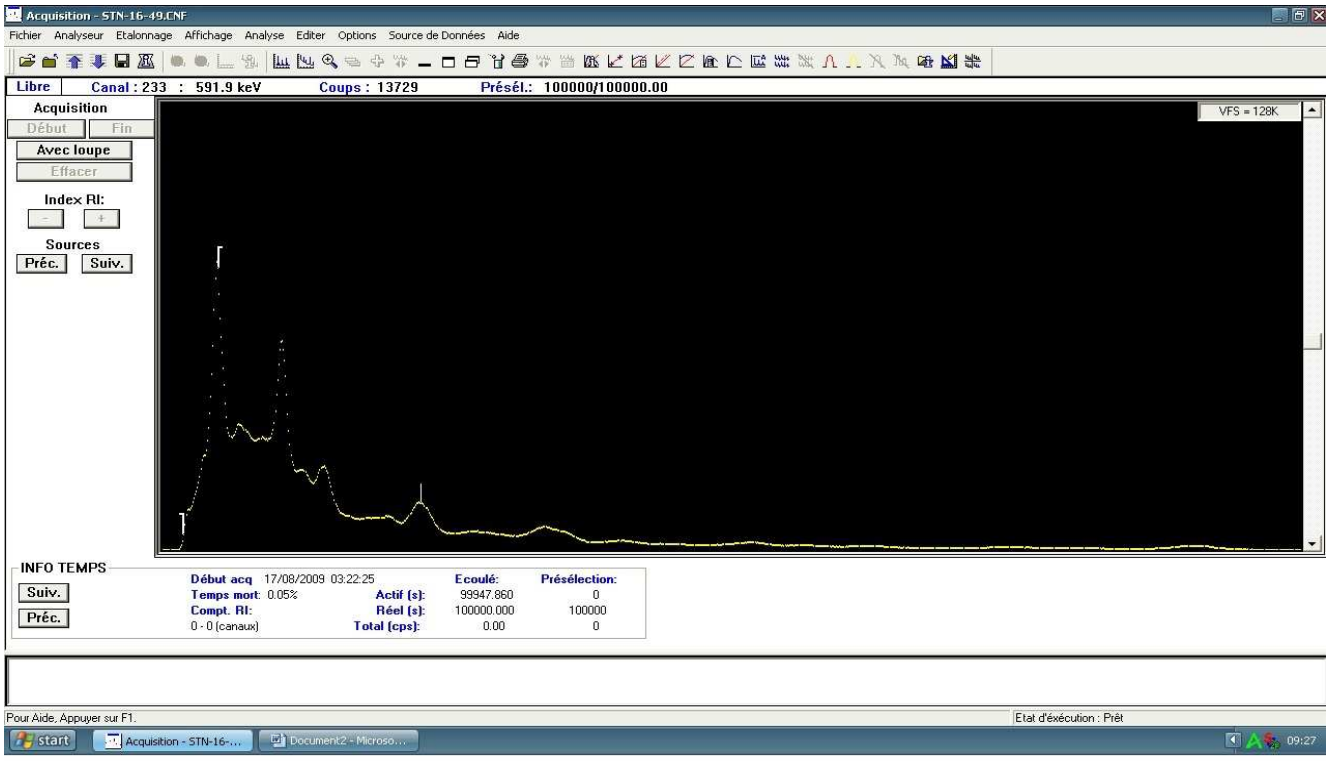

Figure 46: STN-16-49

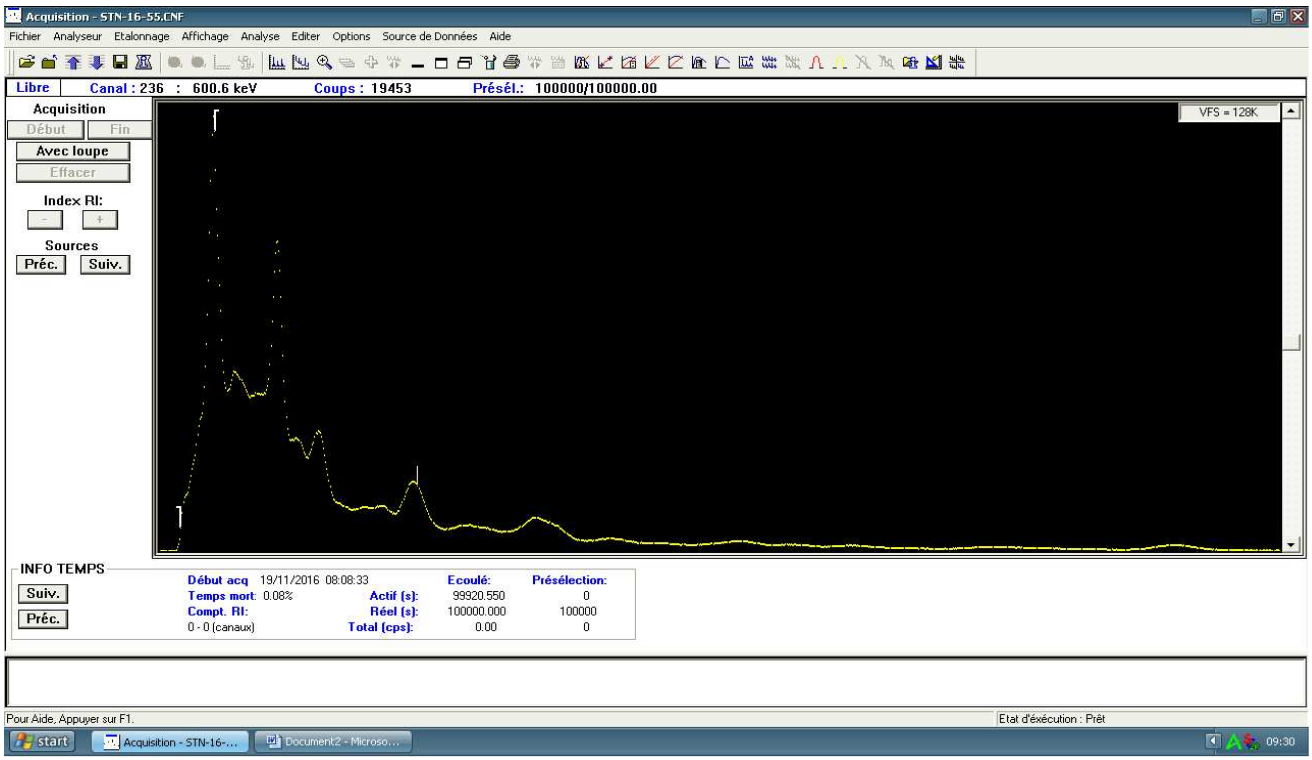

Figure 47: STN-16-55

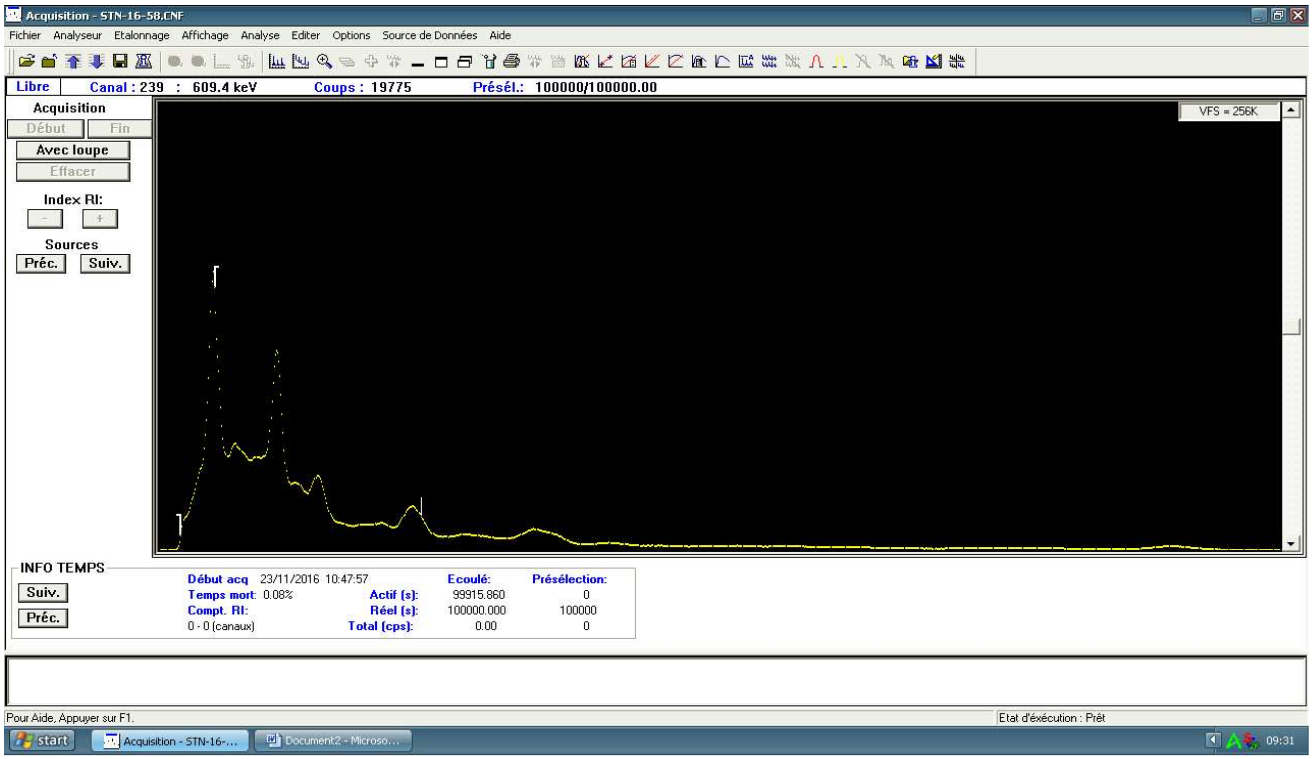

Figure 48: STN-16-58

Bibliography

[1] UNSCEAR (2000) Report to the general assembly, with scientific annexes. Annex B exposures from natural radiation sources. New York Report of the United Nations Scientific.

[2] Faanu, A. (2011) Assessment of Public Exposure to Naturally Occurring Radioactive Materials From Mining and Mineral Processing Activities Of Tarkwa Goldmine in Ghana. Kwame Nkrumah University of Science and Technology. Ph.D Thesis, Kumasi.

[3] Baba, A., Bassari, A., Erees, F., et Cam, S. (2004) Natural radioactivity and metal concentrations in soil samples taken along the Izmir-Ankara E-023 highway, Turkey.

[4] ICRP. (2005) Scope of radiological Protection Control and Measures: ICRP Publication 104: Pentagon Press.Oxford. Ann. ICRP.

[5] UNSCEAR. (2006) Effects of ionizing radiation on immune system. United Nations Scientific Committee on Effects of Atomic Radiation. Report, United Nations, New York.

[6] IAEA. (2014) Perspective, Exposure due to radon in homes, Radiation Protection Unit XXXVI, International Atomic Energy Agency, Hotel Satel, Poprad.

[7] Forkapic S., Bikit I., Conkic L., Veskovic M., Slivka J., Krmar M., Žikic-Todorovic N., Varga E., Mrda D. (2006) Methods of radon measurement, Facta Universitatis, Series: Physics, Chemistry and Technology, 4(1): 1-10.

[8] Yu K.N., Cheung T., Guan Z.J., Mui B.W.N., Ng Y.T. (2000) ^{222}Rn, ^{220}Rn and their progeny concentrations in offices in Hong Kong. Journal of Environmental Radioactivity, 105(48): 211-221.

[9] Saïdou, Abdourahimi, Tchuente Siaka Y. F., Oumarou, B. (2014) Indoor radon Measurements in the uranium regions of Poli and Lolodorf, Cameroon. Journal of Environmental Radioactivity, 136: 36-40.

[10] Saïdou., Shinji Tokonami., Miroslaw Janik., Bineng Guillaume Samuel., Abdourahimi., Ndjana Nkoulou II Joseph Emmanuel. (2014) Radon-thoron discriminative measurements in the high natural radiation areas of southwestern Cameroon. Journal of Environmental Radioactivity, 150: 242-246.

[11] Shoeib M.Y., Thabayneh M.(2014) Assessment of natural radiation exposure and radon exhalation rate in various samples of Egyptian building materials, Journal of Radiation Research and Applied Sciences, 7: 174-181.

[12] Abdellatif NACHAB. (2003) Etudes exprimentales et modélisations Monte Carlo de l'auto-absorption gamma et de la dosimétrie active par capteurs CMOS. Thèse de Doctorat Univ Louis Pasteur Stasbourg I, et Univ Chouaib Doukkali El jadida, Maroc.

[13] Beyzadeoglu M, Ozyigit G, Ebruli C. (2010) Basic Radiation Oncology.Springer Heidelberg Dordrecht London New York: Springer-Verlag Berlin Heidelberg.

[14] Daniel Blanc. (1997) Les rayonnement ionisants, Edition MASSON.

[15] J.RODIER, J.P.CHASSANY. (1974) Manuel de Radioprotection Pratique, Edition MALOINE S.A

[16] Christine Jimonet et Henri Métivier. (2007) Personne compétente en radioprotection principes de radioprotection réglementation.

[17] André Sorriaux, Eléments de physique nucléaire et subnucléaire, Institut national des sciences et technique nucléaires.

[18] Bruno Boyer. (2006) Evolution de radio toxicité résiduelle d'un colis de déchets nucléaire.

[19] Raad Obid Hussain and Hayder Hamza Hussain. (2011) Natural Occurring Radionuclide Materials, Radioisotopes - Applications in Physical Sciences, Prof. Nirmal Singh (Ed.), ISBN: 978-953-307-510-5, InTech, Available from: http://www.intechopen.com/books/radioisotopes-applications-in-physical-sciences/naturaloccurring-radionuclide-materials

[20] Henery S. and John R. A. (1972) Introduction to Atomic and Nuclear Physics, Fifth edition, Holt, Rineart and Winston INC.

[21] Littlefield T.A. and Thorley N. (1974) Atomic and Nuclear Physics, Third edition. Van Nostrand Reinhold company, London, UK.

[22] Benenson W. (2002) Hand book of physics. Fourth Edition. SpringerVelarg, New York, INC.

[23] Harb S. (2004) On the Human Radiation Exposure as Derived From the Analysis of Natural and Man-Made Radionuclides in Soil, Ph.D. Thesis, Hannover University.

[24] Podgorsak E .B. (2005) Radiation Physics for Medical Physicist, Springer Berlin Heidelberg, New York, USA.

[25] Bateman, H. (1910) Solution of a System of Differential Equations Occurring in the Theory of Radioactive Transformations, Proceedings of the Cambridge Philosophical Society, vol. 15,

[26] Abubakar D. Bajoga. (2016) Evaluation of Natural and Anthropogenic Radioactivity in Environmental samples from Kuwait Using High-resolution Gamma-ray Spectrometry. Faculty of Engineering and Physical Sciences University of Surrey Guildford, GU2 7XH UK.

[27] UNSCEAR. (1993) (United Nations Scientific Committee on the Effects of Atomic Radiation). Exposure from Natural Sources of Radiation of Radiation. Report to the General Assembly. 549-552 .

[28] Madelmont, C., A. Rannou, H. Renouard et al. (1984) Sources externes : cosmique, tellurique et domestique. P. 61 in : Congrès sur les données actuelles sur la radioactivité naturelle. Monte Carlo, 1984

[29] UNSCEAR. (1988) Report to the General Assembly with Scientific Annexes, United Nations Sales Publication E.88.IX.7, United Nations, New York.

[30] Robin Corrigan. (2017) Lung Cancer Risks to Canadians from Residential Radon Exposure. Thesis, Faculty of Graduate Studies and Post-Doctoral Studies,University of Ottawa.

[31] NRC. (2009) Health effects of exposure to radon: BEIR VI.

[32] P. K. Hopke, B. Jensen, C.-S. Li, N. Montassier, P. Wasiolek, A. J. Cavallo, K. Gatsby, R. H. Socolow,and A. C. James. (1995) Assessment of the exposure to and dose from radon decay products in normally occupied homes," Environ. Sci. Technol., vol. 29, pp. 1359-1364.

[33] Jun Hua, Guosheng Yang, Miklós Hegedũs, Kazuki Iwaoka, Masahiro Hosoda, Shinji Tokonami. (2018) Numerical modeling of the sources and behaviors of ^{222}Rn, ^{220}Rn and their progenies in the indoor environmentA review. Journal of Environmental Radioactivity, 189 p. 4047.

[34] D. Probert and A. Lugg. (1997) "Indoor radon gas - a potential health hazard resulting from implementing energy-efficiency measures," Applied Energy, vol. 56, no. 2, pp. 93-196.

[35] M. Thoennessen and C. Fry. (2012) "Discovery of the astatine, radon, francium, and radium isotopes," Atomic Data and Nuclear Data Tables, pp. 12-20.

[36] Korea Atomic Energy Research Institute. (2000) http://atom.kaeri.re.kr/

[37] Debertin, K. and Helmer, R.G.(1988) Gamma and X-ray spectrometry with semiconductor detectors. Elsevier Science, Amsterdam.

[38] Todsadol Santawamaitre. (2012) An Evaluation of the Level of Naturally Occurring Radioactive Materials in Soil samples along the Chao Phraya River Basin. Thesis, University of Surrey,Faculty of Engineering and Physical Sciences.

[39] Knoll, G. F. (2000) Radiation Detection and Measurement (3^{rd} edition), USA: John Wiley et Sons Inc.

[40] Lapp, R.E. and Andrews, H.L. (1972) Nuclear Radiation Physics (4^{th} edition) London: Sir Isaac Pitman and Sons Ltd.

[41] Cember, H. and Johnson, T.E. (2009), Introduction to Health Physics (4^{th} edition), New York: McGraw-Hill Companies, Inc.

[42] Das, A. and Ferbel, T. (2003) Introduction to Nuclear and Particle Physics (2^{nd} edition), London: World Scientific.

[43] Kantele, J.(1995) Handbook of Nuclear Spectrometry, London: Academic Press Limited.

[44] Lilley, J. (2001) Nuclear Physics: Principles and Applications, Chichester: John Wiley et Sons, Ltd.

[45] Eisenbud, M. and Gesell, T. (1997) Environmental Radioactivity from Natural, Industrial, and Military Sources (4^{th} edition), London: Academic Press.

[46] L'Annunziata, M. F. (2007) Radioactivity: Introduction and History, Amsterdam: Elsevier B.V.

[47] Kaplan, I. (1962) Nuclear Physics (2^{nd} edition), USA: Addison-Wesley Publishing Company, Inc.

[48] Gilmore, G.R.(2008) Practical Gamma-ray Spectrometry (2^{nd} edition),Chichester: John Wiley et Sons Ltd.

[49] Turner, J.E. (2007) Atoms, Radiation, and Radiation Protection (3^{rd} edition), Weinheim: Wiley-VCH.

[50] TILAHUN TESFAYE. "Physique nucléaire". Université Virtuelle Africaine Addis Ababa, License (Creative Commons), Version 2.5.

[51] PHENOMENES DE FREINAGE. [Online], [cit : Août, (2011)]. http://malek kadri.blogspot.com/2011/08/phenomenes-de-freinage.html

[52] SPECTRO-ALPHA3. "Spectrométrie" http://www.cesr.fr/ jean/SpectroAlpha3.pdf

[53] MEGHELLI. "Interactions entre les rayonnements ionisants et la matère", Biophysique-Médicale. Service Nucléaire, CHU Tlemcen.

[54] AIP. "Interaction des particules ou rayonnements ionisants Avec la matère". http://archiveweb.epfl.ch/ipn.epfl.ch/webdav/site/ipn/shared/.../AIp.pdf

[55] Christine Jimonet et Henri Metivier. (2007) "Personne compétente en radioprotection". Principes de radioprotection-réglementation . EDP Sciences. France. ISBN : 978-2-86883-948-0

[56] Y. ARNOUD. LPSC GRENOBLE.(2009) " Interactions et Détecteurs". [Online]. http://lpsc.in2p3.fr/arnoud/Cours, Master 1 ITDD.

[57] MELLE. BERKOK HOURIA, MR. FARSI ABDELSAMAD.(2009) " Détermination de la qualité des faisceaux de photons de haute énergie utilisés en radiothérapie à l'aide des différents fantômes". Physique médicale. Université de Science et de la Technologie- Mohamed Boudiaf. Oran : s. n. Projet de Fin d'études.

[58] HIGH-DOSE DOSIMETRY, IAEA. (1985) International Atomic Energy Agency, Vienna.

[59] CHRISTOPHE CHAMPION.(2000) " Interaction des ondes et des particules avec la matière biologique". Laboratoire de physique moléculaire et des collisions; Institut de physique de Metz; Université de Metz, Technopôle Doc.

[60] ICRP. (2007) recommendations of the International Commission on Radiological Protection, ICRP Publication 103, Pergamon Press, Oxford.

[61] Noz, M. E. and Maguire Jr., G. Q. (2007) Radiation Protection in the Health Sciences, London: World Scientific Publishing Co. Pte. Ltd.

[62] Martin, A. and Harbison, S. (2006) An Introduction to Radiation Protection (5^{th}edition), London: Hodder Arnold.

[63] International Commission on Radiological Protection.(1991) Radiation Protection, ICRP Publication 60. Elmsford, NY: Pergamon Press, Inc.

[64] DANIEL OKELO ELIJAH (2015). Gamma ray spectrometric analysis of the naturally occurring radionuclides in soils collected along the shores of lake victoria, migori county, KENYA. Ph.D Thesis (Physics). University of Nairobi. Kenya

[65] Tzortzis, M. and Tsertos, H. (2004). Natural radioelemental concentration in the Troodos Ophiolite Complex of Cyprus. Department of Physics, University of Cyprus.

[66] Odunaike,R.K., Ozebo,V.C., Alausa,S.K. andAlausa,I.M. (2008). Radiation exposure to workers and villagers in and around some Quarry sites in Ogun State of Nigeria. Environmental research Journal 2: 348-350

[67] Xinwei, L., Zhang, X. (2006). Measurement of natural radioactivity in sand samples collected from the Baoji Weihe Sands Park, China. Environment Geology 50: 977-982.

[68] Akozcan, S (2012).Distribution of natural radionuclide concentration in sediment samples in Didim and Izmir Bay in Turkey. Journal of Environmental Radioactivity 112:60-63.

[69] Mustapha, A. O., Narayana, D. G. S., Patel, J. p and Otwoma, D. (1997). Natural radioactivity in some building materials in kenya and their contribution to indoor radon external doses.Radiation protection Dosimetry.71(1):65-69.

[70] Hashim, N.O. (2001) The level of Radionuclides and elements in selected Kenyan coastal ecosystem. M.Sc . Thesis (Physics) Kenyatta University. Nairobi, Kenya

[71] M. Ngachin, M. Garavaglia, C. Giovani, M.G. Kwato Njock, A. Nourreddine (2001). Assessment of natural radioactivity and associated radiation hazards in some Cameroonian building materials. Radiat Meas 42, 61-67.

[72] The Organization for Economic Cooperation and Development criterion, OECD (1979).

[73] Saïdou, F.O. Bochud, S. Baechler, M.G. Kwato Njock, M. Ngachin, P. Froidevaux, (2011) Natural radioactivity measurements and dose calculations to the public : case of the uranium-bearing region of Poli in Cameroon, Radiat Meas, 46,254-260.

[74] P. Ele Abiama, P. Owono Ateba, G.H. Ben-Bolie, H.P. Ekobena Fouda, T. El Khou khi (2010) High background radiation investigated by gamma spectrometry of the soil in the southwestern region of Cameroon,J Environ Radioact 101, 739-743.

[75] J.F. Beyala Ateba, P. Owono Ateba, BG.H. Ben-Bolie, H. Ekobena Fouda, P. Ele Abiama, C.R. Abega, S. Mvondo (2011). Determination of uranium in rocks and soil of south Cameroon by gamma spectrometry, Radioisotopes 60, 10.

[76] E.J. Mekongtso Nguelem, M. Moyo Ndontchueng and O. Motapon (2016) Determination of ^{226}Ra, ^{232}Th, ^{40}K, ^{235}U and ^{238}U activity concentration and public dose assessment in soil samples from bauxite ore deposits in western Cameroon, Springerplus. 5, 1, 1253.

[77] Olivry, J.C. (1986) Fleuves et rivières du Cameroun, Meres, ORSTOM. Paris. 733.

[78] Ndontchueng. M, M., Njinga R,L., Nguelem E,J,M., Simo A., Beyala Ateba J,F (2014). ^{238}U, ^{235}U, ^{137}Cs and ^{133}Xe in soils from two campuses in University of Douala-Cameroon. Appl Radiat Isot, 86: 85-89

[79] G.BALEA THEORY OF IN SITU GAMMA-RAY SPECTROMETRY.pdf

[80] Kevin, M., Miller and Peter Shebell. (1993) In situ gamma-ray spectrometry: A tutorial for environmental radiation scientists. Environmental Measurements Laboratory U. S. Department of Energy New York, NY 10014-3621

[81] Beck, HL., DeCampo, J., Gogolak, C. (1972) In-situ Ge(Li) and NaI(T1) gamma-ray spectrometry. Health and Safety Laboratory Report HASL-258, U.S. Atomic Energy Commission. New York. NY 10014.

[82] Hosoda, M., Tokonami, S., Omori, Y., Sahoo, S.K., Akiba, S., Sorimachi, A., Ishikawa, T., Nair, R.R., Jayalekshmi, P.A., Sebastian, P., Iwaoka, K., Akata, N., Kudo, H.(2015) Estimation of External Dose by Car-Borne Survey in Kerala, India. Plos ONE 10(4)e0124433.

[83] Hosoda, M., Inoue, K., Oka, M., Omori, Y., Iwaoka, K., Tokonami, S. (2016) Environmental radiation Monitoring and External Dose Estimation in Aomori prefecture after the Fukushima Daiichi Nuclear Power Plant Accident, jpn.j.Health Phys, 51(1). 41-50

[84] SUSUMU MINATO AND MINORU KAWANO. (1970) On the Constitution of Terrestrial Gamma Radiation. JOURNAL OF GEOPHYSICAL RESEARCH. 75(29)

[85] Minato, S. (2001) Diagonal elements fitting technique to improve response matrixes for environmental gamma ray spectrum unfolding. Radioisotopes, 50(10): 463-471.

[86] Tan, V, L., Inoue, K., Fujisawa, M., Arai, M and Fukushi, M. (2017) Impact on absorbed dose rate in air from Asphalt Pavement Associated with Transport In-

frastructure Developments on Phu Quoc Island, Vietnam. Radiat Environ Med, 2 (6), 88-93.

[87] Inoue, K., Arai, M., Fujisawa, M., Saito, K., Fukushi, M. (2017) Detailed Distribution Map of Absorbed Dose Rate in Air in Tokatsu Area of Chiba Prefecture, Japan, Constructed by Car- Borne Survey 4 Years after the Fukushima Daiichi Nuclear Power Plant Accident. Plos ONE 12(1) e0171100.

[88] Moriuchi, S., Tsutsumi, M., Saito, K. (1990) Examination on conversion factors to estimate effective dose equivalent from absorbed dose in air for natural gamma radiations. Jpn J Health Phys, 25: 121-128 (Japanese with English abstract).

[89] Minato, S. (1978) A response matrix of a 3f $\times$3 NaI(Tl) scintillator for environmental gamma radiation analysis. Rep Governmental Industrial Research Institute. Nagoya, 27(12): 384-397. (in Japanese)

[90] Matsuda, H., Minato, S., Pasquale, V. (2002) Evaluation of accuracy of response matrix method for environmental gamma ray analysis. Radioisotopes, 51 (1): 42-50, (in Japanese).

[91] Minato, S. (2012) Application of a 60$\times$60 response matrix for a NaI(Tl) Scintillator to fallout from the Fukushima reactor accident. Radiat Emerg Med, 1(12): 108-112.

[92] Minato, S. (1971) Terrestrial gamma-radiation field in natural environment. J Nucl Sci Technol, 8: 342-347.

[93] Minato, S. (1977) Analysis of the variation of environmental γ radiation during rainfall. Rep Government Industrial Research Institute. Nagoya, 26(6): 190-202. (in Japanese)

[94] Minato, S. (1980) Monte Carlo calculation of gamma radiation field due to precipitation washout of radon daughters from the atmosphere to the ground surface. Jpn J Health Phys, 15: 19-24.

[95] Beck, HL. (1972) The absolute intensities of gamma rays from the decay of ^{238}U and ^{232}Th. Health and Safety Laboratory Report HASL-262. U.S. Atomic Energy Commission. New York. NY 10014.

[96] Gasser Estelle. (2014) Spectrométrie γ au Laboratoire et in situ: Développement et Application environnementale. Specialité : Physique Subatomique, Université de Strasbourg.

[97] Saïdou. (2007) Mesure de la radioactivite naturelle environnementale par spectrometries α et γ et Calcul de la dose au public : Application à la region uranifere de poli. Thesis, Université de Douala.

[98] Garcia-Talavera, M., (2003). Evaluation of the suitability of various γ lines for the γ spectrometric determination of ^{238}U in environmental samples. Appl. Radiat. and Isot, 59: 165-173

[99] Ycel, H., Cetiner, M.A., Demirel, H., (1998). Use of the 1001 keV peak of ^{234m}Pa daughter of ^{238}U in measurement of uranium concentration by HPGe gamma-ray spectrometry. Nucl.Instr. and Meth. A 413: 74-82.

[100] Huy, N.Q., Luyen, T.V., (2004) A method to determine ^{238}U activity in environmental soil samples by using 63.3 keV photopeak-gamma HPGe spectrometer. Appl. Radiat. and Isot, 61: 1419-1424.

[101] Wong, C.T., Liu, Y.-G., Perera, S.K.(2001) Quantification of ^{226}Ra in soil using 186-keV gamma-ray peak. Radioact. Radiochem, 12(1): 11-20.

[102] Dowdall, M., Selnaes., O.G., Gwynn, J.P., Davids, C.(2004) Simultaneous determination of ^{226}Ra and ^{238}U in soil and environmental materials by gamma-spectrometry in the absence of radium progeny equilibrium. J. Radioanal. Nucl. Chem, 261(3): 513-521.

[103] Karangelos, D.J., Anagnostakis, M.J., Hinis, E.P.(2004) Determination of depleted uranium in environmental samples by gamma-spectroscopic techniques. J. of Environ. Radioactivity, 76: 295-310.

[104] Wissam Chehade. (2007) True Coincidence Summing Correction in Gamma Spectroscopy. Thesis, Universität Bremen Faculty of Environmental Physics.

[105] Thomas Vigineix. (2012), Exploitation des spectres gamma par méthode non paramétrique et indépendante d'a priori formulés par l'opérateur. Rapport CEA-R-6288

[106] Saïdou, Bochud F, Laedermann JP, Kwato Njock MG, Froidevaux P.A (2008) Comparison of alpha and gamma spectrometry for environmental natural radioactivity surveys. Appl Radiat Isot, 66(2): 215-22

[107] Debertin, K., Helmer, R.G.(1998) Gamma- and X-ray spectrometry with semiconductor detectors. Elsevier, Amsterdam.

[108] Klement, A.W. (1982), CRC Handbook of Environmental Radiation, Florida: CRC Press, Inc.

[109] Curie, L.A. (1968), Limits for Qualitative Detection and Quantitative Determination. Application to Radiochemistry, Analytical Chemistry, 40(3): 586-593.

[110] Hurtgen, C., Jerome, S. and Woods, M. (2000), Revisiting Currie-How Low Can You Go?, Applied Radiation and Isotopes, 53: 45-50.

[111] NF ISO 11929,(2010) ≪Détermination des limites caractéristiques (seuil de décision, limite de detection et extrémités de l' intervalle de confiance) pour mesurages de rayonnements ≫ AFNOR.

[112] M. Lépy, J. Plangnard, J. Moune, E. Verdeau et F. Damoy. (2008) ≪la spectrométrie de photons au LNHB : Principes et applications≫

[113] Cember H. and E. Johnson. (2009) Introduction to health physics. 4^{th}, McGraw-Hill companies.

[114] NF ISO 18589-3,(2007) Mesurage de la radioactivité dans l' environement-Sol, partie 3 : Mesurage des radionucléides émetteurs gamma AFNOR.

[115] F. Khan,(2010) ≪ The physics of radiation therapy (4^{th} ed.)≫, Lippincott Williams et Wikins.

[116] E. Krisiuk, S. Tarasov, V. Shamov, N.shalk, E. Lisachenkov et L.G. Gomelsky.(1971) ≪ A study of radioactivity in building materials≫ Research institute for Radiation Hygiene.

[117] J. Beretka et P.J. Matthew.(1985) ≪ Natural radioactivity of Australian building materials, industrial wastes and by-products≫ Health Physics, vol. 48, n11, pp. 87.

[118] D. Amrani et M. Tahtat. (2001) ≪Natural radioactivity in Algerian building materials≫ Applied Radiation and Isotopes, vol. 54 n14, pp. 687-689.

[119] F. Otoo, O. Adukpo, E. Darko, G. Emi-Reynolds, A. Awudu, H. Ahiamadjie, J. Tandoh, F. Hasford, S. Adu et O. Gyampo. (2011) ≪ Assessment of natural radioactive materials in building materials used along the coast of central region of Ghana≫ Research Journal of Environmental and Earth Sciences, vol. 3, n13, pp. 261-268.

[120] M. Tufail, Nasim-Akhta et M. Waqaq (2006) ≪Measurement of terrestrial radiation for assessment of gamma dose from cultivated and barren saline soils of Faisalabad in Pakistan≫ Radiation Measurements, vol. 41, pp. 443-451.

[121] A. El-Taher, S. Makluf, A. Nossair et A. Halim. (2010) ≪ Assessment of natural radioactivity levels and radiation hazards due to cement industry≫Applied Radiation and Isotopes vol. 68, pp. 169-174, 2010

[122] K. Wesche (1991) ≪Fly Ash in Concrete: Properties and performance ≫, E and FN Spon.

[123] R. Krieger. (1981) ≪ Radioactivity of construction materials ≫ Betonwerk und Fertigteil-Technik, vol. 47, pp. 468-473.

[124] OECD, (1979) ≪ Exposure to radiation from the natural radioactivity in building materials≫, Organization of Economic Cooperation and Development.

[125] E. Straden. (1976) ≪ Some aspects on radioactivity of building materials≫ Physicy norvegica, vol. 8, n3.

[126] R. Hewamanna, C. S. Sumithrarachch, P. Mahawatte, H. L. Nanayakkara et H. C. Ratnayake. (2001) ≪ Natuaral radioactivity and gamma dose Sri Lankan clay bricks used in building construction≫ Applied radiation and Isotopes, vol. 54, n12, pp. 365-369.

[127] Kuma, A., et al.(2003) Natural activities of ^{238}U, ^{232}Th and ^{40}K in some Indian building materials. Radiation Measurements, 36 1-6: p. 465-469.

[128] Kocher, D.C., Sjoreen, A.L. (1985) Dose-rate conversion factors for external exposure to photon emitters in soil. Health Phys, 48: 193-205.

[129] Jacob, P., Paretzke, H.G., Rosenbaum, H., Zankl, M. (1986) Effective dose equivalents for photon exposure from plane sources on the ground. Radiat. Prot. Dosim. 14: 299-310.

[130] Leung, K.C., Lau, S.Y., Poon, C.B. (1990) Gamma radiation dose from radionuclides in Hong Kong soil. J. Environ. Radioact, 11: 279-290.

[131] Saïdou., Ele, A.P., Tokonami, S. (2015) Comparative study of natural radiation exposure to the public in three uranium and oil regions of Cameroon. Radioprotection. 1-7

[132] Tokonami S, Takahashi H, Kobayashi Y, Zhuo W and Hulber E. (2005) Up-to-date radon-thoron discriminative detector for a large scale survey. Rev Sci Instrum. 76 113505.

[133] Masahiro H, Hiromi K, Kazuki I, Ryohei Y, Takahito S, Yuki T, Tokonami S. (2017) Characteristic of thoron (^{220}Rn) in environment Applied Radiation and Isotopes, 120: 7-10

[134] Tokonami S.(2010) Why is ^{220}Rn (thoron) measurement important? Radiat Prot Dosim. 141: 3359.

[135] Sorimachi A, Tokonami S, Kranrod C, Ishikawa T.(2015) Preliminary experiments using a passive detector for measuring indoor ^{220}Rn progeny concentrations with an aerosol chamber Health Phys. 108: 597-606.

[136] Zhuo W, Iida T.(2000) Estimation of thoron progeny concentrations in dwellings with their deposition rate measurements. Jpn J Health Phys, 35: 365-370.

[137] Janik M, Tokonami S, Kranrod C, Sorimachi A, Ishikawa T, Hosoda M, Mclaughlin J and Kim YJ. (2013) Comparative analysis of radon, thoron and thoron progeny concentration measurements. J. Radiat. Res, 54: 597610.

[138] Kudo H, Tokonami S, Omori Y, Ishikawa T, Iwaoka K, Sahoo SK, Akata N, Anabongse P, Pornnumpa C, Sun Q, Li X, Akiba S, and Hosoda M.(2015) Comparative dosimetry for radon and thoron in high background radiation areas in china. Radiat Prot Dosim pp. 1-5.

[139] KOTRAPPA, P., AND STE3FF, L.R.(1993) "Recent Advances In Electret Ion Chamber Technology For Radiation Measurements" Radiation Protection Dosimetry, 47: 461-464.

[140] EPA, United States Environmental Protection Agency. (1992) Indoor Radon and Radon Decay Product Measurement Device Protocols. EPA-402-R-92-004.Washington, DC, USA

[141] International Standard, Measurement of radioactivity in the environment-Air-Radon 220:(2014) Integrated measurement methods for the determination of the average activity concentration using passive solid-state nuclear track detectors. ISO 16641(E)

[142] ICRU. (2012) International Commission on Radiation Units and Measurements. Measurement and reporting of radon exposures. ICRU Report 88, J.ICRU 12(2).

[143] Prasad M, Rawat M, Dangwal A, Kandari T, Gusian GS, Mishra R, Ramola RC (2016) Variability of radon and thoron equilibrium factors in indoor environment of Garhwal Himalaya. J Environ Radioact 151:238243. https://doi.org/10.1016/j.jenvrad.2015.10.017.

[144] UNSCEAR (United Nations Scientic Committee on the Effect of Atomic Radiation) (2008) Sources and effects of ionizing radiation. United Nations, New York.

[145] Ojo, T.J., Gbadegesin, K.A.J. (2015) Terrestrial Radiation Doses from Selected Towns of Southwestern Nigeria International Journal of Physics Vol. 3, No. 6, 244-247.

[146] Ademola, K.A., Bello, K.A., Adejumobi, C.A. (2014) Determination of natural radioactivity and hazard in soil samples in and around gold mining area in Itagunmodi. south-western, Nigeria, journal of radiation research and applied sciences 7. 249-255.

[147] S. Turhan, Í. H. Arkan, F. Oǧuz, T. Özdemir, B. Yücel, A. Varinlioǧlu and A. Köse. (2012) CAR-BORNE SURVEY OF NATURAL BACKGROUND GAMMA DOSE RATE IN ANAKKALE REGION, TURKEY Radiation Protection Dosimetry. Vol. 148, No. 1, pp. 45-50

[148] Hosoda, M., Tokonami, S., Omori, Y., Sahoo, S.K., Akiba, S., Sorimachi, A., Ishikawa, T., Nair, R.R., Jayalekshmi, P.A., Sebastian, P., Iwaoka, K., Akata, N.,

Kudo, H. (2015) Estimation of External Dose by Car-Borne Survey in Kerala, India. Plos ONE 10(4)e0124433.

[149] Saïdou., Abdourahimi., Tchuente, Siaka, Y.F., Kwato, Njock M.G. (2015) Natural Radiation Exposure to the public in the oil bearing Bakassi peninsula. Cameroon Radioprotection 50 (1): 35-41.

[150] Guembou, Shouop, S.J., Ndontchueng, Moyo, M., Chene, Gregoire., Nguelem, Mekontso, E.J., Motapon, Ousmanou., Kayo, Arnold, S., Strivay, David. (2017) Assessment of natural radioactivity and associated radiation hazards in sand building material used in Douala Littoral Region of Cameroon using gamma spectrometry.

[151] Sorimachi, A., Takahashi, H., Tokonami, S. (2009) Influence of the presence of humidity, ambient aerosols and thoron on the detection responses of electret radon monitors. Radiat. Meas. 44, 111e115.

[152] Ćurguz Z, Stojanovska Z, Žunić ZS, Kolarž P, Ischikawa T, Omori Y, Mishra R, Sapra BK, Vaupotič J, Ujić P, Bossew P. (2015) Long-term measurements of radon, thoron and their airborne progeny in 25 schools in Republic of Srpska. J. Environ. Radioact, 148: 163169.

[153] ICRP (2009). Adult reference computational phantoms, ICRP Publication 110, Ann, ICRP 39 (2).

[154] WHO Handbook on Indoor Radon ISBN 978-92-4-154767-3 Available on http://whqlibdocwhoint/publications/2009/9789241547673engpdf. 2009.

[155] USEPA. National primary drinking water regulations; radio nuclides; proposed rules. Federal register, vol 56. U.S. Environmental Protection Agency. 1991 p 33050.

[156] European Union. Commission recommendation on the protection of the public against indoor exposure to radon (90/143/Euroatom). Brussels, Commission of the European Communities, 1990

(http://ec.europa.eu/energy/nuclear/radioprotection/doc/legislation/90143en.pdf, accessed 4 April 2007).

[157] Prasad M, Rawat M, Dangwal A, Prasad G, Mishra R, Ramola RC.(2016) STUDY OF RADIATION EXPOSURE DUE TO RADON, THORON AND PROGENY IN THE INDOOR ENVIRONMENT OF YAMUNA AND TONS VALLEYS OF GARHWAL HIMALAYA.Radiat Prot Dosimetry, 171(2): 187-191.

[158] Chen J, Tokonami S, Sorimachi A, Takahashi H, Falcomer R.(2008) preliminary results of simultaneous radon and thoron tests in Ottawa Radiat. Prot. Dosim, 130: 253-256

[159] Visnuprasad AK, Jaikrishnan G, Sahoo BK, Pereira CE, Jojo PJ.(2017) Contribution of thoron and progeny towards inhalation dose in a thorium abundant beach environment. Radiat Prot Dosim pp 1-9.

[160] Gierl S, Meisenberg O, Feistenauer P, Tschiersch J.(2014) Thoron and thoron progeny measurements in German clay houses. Radiat. Prot. Dosim, 160: 160-163.

[161] Shang B, Chen B, Gao Y, Wang Y, Cui H, and Li Z. (2005) Thoron levels in traditional Chinese residential dwellings. Radiat. Environ. Biophys, 44: 193-199.

[162] Harley N, Chittaporn P, Medora R, Merrill R. (2010) Measurement of the indoor and outdoor ^{220}Rn (thoron) equilibrium factor: application to lung dose. Radiat. Prot. Dosim, 141: 357-362.

[163] Hosoda M, Kudo H, Iwaoka K , Yamada R , Suzuki T, Tamakuma Y , Tokonami S. (2017) Characteristic of thoron (^{220}Rn) in environment. Appl. Radiat. Isot, 120: 710.

[164] Prasad M, Rawat M, Dangwal A, Kandari T, Gusian GS, Mishra R, Ramola RC. (2015) Variability of radon and thoron equilibrium factors in indoor environment of Garhwal Himalaya. J Environ Radioact. 151: 238-243. https://doi.org/10.1016/j.jenvrad.2015.10.017.

[165] Ramola RC, Negi MS, Choubey VM. (2003) Measurements of equilibrium factor F between radon and its progeny and thoron and its progeny in the indoor atmosphere using nuclear track detectors. Indoor. Built. Environs. 12: 351-355. https://doi.org/10. 1177/142032603035368.

[166] Lindsay R, Newman RT, Speelman WJ.(2008) A study of airborne radon levels in Paarl houses (South Africa) and associated source terms, using electret ion chambers and gamma-ray spectrometry. Appl. Radiat. Isot, 66: 1611-1614.

[167] Saïdou, Tokonami S, Hosoda M, Ndjana NIIJE, Akata N, Tchuente SYF, Oumar BM, Bineng GS, Takoukam SSD. Natural Radiation Exposure to the Public in Mining and Ore bearing Regions of Cameroon. Radiat. Prot. Dosim. Doi: 10.1093/rpd/nc0000.

[168] Joint Committee for Guides in Metrology. Evaluation of measurement data-guide to the expression of uncertainty in measurement. JCGM 100:(2008). http://www.bipm.org/utils/common/documents/jcgm/JCGM-100-2008-E.pdf. Accessed 19 August 2016.

[169] Inoue, K., Hosoda, M., Fukushi, M., Furukawa, M., Tokonami, S. (2015) Absorbed Dose rate in air in Metropolitain Tokyo Before The Fukushima Daiichi Nuclear Power Plant Accident. Radiat. Prot. Dosim. 1-4

[170] International Commission on Radiological Protection (ICRP).(1993) Protection against radon-222 at home and at work. ICRP Publication 65. Pergamon Press.

[171] Colmenero SL, Montero Cabrera ME, Villalba L, Renter VM, Torres ME, M. García León, García-Tenorio R, F. Mireles García, Herrera PEF, Sánchez AD (2004) Uranium-238 and thorium-232 series concentrations in soil, radon-222 indoor and drinking water concentrations and dose assessment in the city of Aldama, Chihuahua, Mexico Journal of Environmental Radioactivity, 77: 205-219

[172] Mary Thomas Derin, Perumal Vijayagopal, Balasubramaniam Venkatraman, Ramesh Chandra Chaubey , Anilkumar Gopinathan. (2012) Radionuclides and Radiation Indices of High Background Radiation Area in Chavara-Neendakara Placer Deposits (Kerala, India) PLOS ONE vol, 7(11) e50468

List of Publications

List of publications included as part of the thesis

1- **Takoukam Soh Serge Didier**, Saïdou, Masahiro Hosoda, Ndjana Nkoulou II Joseph Emmanuel, Naofumi Akata, Oumarou Bouba and Shinji Tokonami. *Natural radioactivity measurements and external dose estimation by car-borne survey in Douala city, Cameroon*. Radioprotection **53**(4),255-263 (2018).

2- **Takoukam Soh Serge Didier**, Saïdou, Shinji Tokonami, Masahiro Hosoda,Takahito SUZUKI, Hiromi Kudo and Oumarou Bouba. *Simultaneous measurements of indoor radon and thoron and inhalation dose assessment in Douala City, Cameroon* . Isotopes in Environmental and Health Studies. (2019). DOI: 10.1080/10256016.2019.1649258.

Radioprotection 2018, 53(4), 255–263

https://doi.org/10.1051/radiopro/2018032

Available online at:
www.radioprotection.org

ARTICLE

Natural radioactivity measurements and external dose estimation by car-borne survey in Douala city, Cameroon

S.D. Takoukam Soh[1,2], Saïdou[1,2,*], M. Hosoda[3], J.E. Ndjana Nkoulou II[2], N. Akata[4], O. Bouba[1] and S. Tokonami[5]

[1] Nuclear Physics Laboratory, Faculty of Science, University of Yaoundé I, P.O. Box 812 Yaoundé, Cameroon.
[2] Nuclear Technology Section, Institute of Geological and Mining Research, P.O. Box 4110 Yaoundé, Cameroon.
[3] Hirosaki University Graduate School of Health Sciences, Hirosaki City, Aoromi, Japan.
[4] National Institute for Fusion Science, 322-6 Oroshi, Toki, Gifu 509-5292, Japan.
[5] Department of Radiation Physics, Institute of Radiation Emergency Medicine, Hirosaki University, Hirosaki City, Aomori 036-8564, Japan.

Received: 23 January 2018 / Accepted: 27 July 2018

Abstract – A car-borne survey was carried out in Douala, the largest city in Cameroon to make a detailed distribution map of the absorbed dose rate in the city, to locate the high natural radiation areas useful later to carry out indoor radon, thoron, and thoron progeny measurements. Gamma-ray dose rates were measured using 3-in × 3-in NaI(Tl) detector. Activity concentrations of ^{238}U, ^{232}Th and ^{40}K in soil from Douala city were determined by two methods: the first, using *in situ* gamma spectrometry and the second, at the laboratory using a NaI(Tl) detector. A heterogeneous distribution of absorbed dose rates in air was observed on the dose rate distribution map, and varies from 29 to 86 nGy h^{-1} with an average of 50 nGy h^{-1}, lower than the world average value of 59 nGy h^{-1}. The activity concentrations with NaI(Tl) detector varied from 18 to 47 Bq kg^{-1} for ^{238}U, 21 to 54 Bq kg^{-1} for ^{232}Th, and 10 to 410 Bq kg^{-1} for ^{40}K with averages of 29, 38, and 202 Bq kg^{-1} respectively, for *in situ* measurements. They vary between 29–98 Bq kg^{-1} for ^{238}U, 29–92 Bq kg^{-1} for ^{232}Th, and 40 to 79 Bq kg^{-1} for ^{40}K, with averages of 60, 57, and 56 Bq kg^{-1} respectively for soil samples collected at Douala III subdivision. The highest value of the annual effective dose for *in situ* measurements by car was observed at Ndogbong and was found to be 0.7 mSv y^{-1}, higher than the world average value of 0.5 mSv y^{-1}.

Keywords: car-borne survey / NaI(Tl) detector / natural radioactivity / air absorbed dose rate / external effective dose

1 Introduction

Exposure to natural radiation sources varies substantially from one area to another and even locally (UNSCEAR, 1982). Gamma radiation from natural radionuclides such as ^{238}U, ^{232}Th and ^{40}K is the main source of external exposure. There are three sources of environmental radioactivity: terrestrial, manmade and cosmic. The most significant terrestrial radionuclides include the uranium and thorium decay series, potassium and rubidium (EPA, 2009). The terrestrial component is due to the radioactive nuclides that are present in air, soil, rocks, water and building materials whose amounts vary significantly depending on the geological and geographical features of the regions. Cosmic radiation from space contributes to the background changes chiefly through elevation and latitude (UNSCEAR, 2000). Although background radiation is present everywhere, radionuclide concentrations and distributions are not constant (EPA, 2009). For ages, humans have been exposed to radionuclides that occur naturally in the environment. It is therefore important to measure the activity concentrations of radionuclides in the living environment.

There have been many surveys to measure natural radioactivity and to estimate corresponding radiation dose to the public in Cameroon. According to Guembou *et al.* (2017), absorbed dose rates and annual effective dose due to radioactivity in sand used as building material in Douala, were normal and within the recommended limits. Also, Saïdou *et al.* (2015a, 2015b) reported no significant radiological risk to population living in the oil-bearing Bakassi peninsula, in the uranium-bearing regions of Poli and Lolodorf. The average total radiation dose and external radiation dose were respectively 5.9 and 0.6 mSv y^{-1} for Poli, 7.6 and 0.7 mSv y^{-1} for Lolodorf, and 22.3 and 0.3 mSv y^{-1} for Bakassi.

*Corresponding author: saidous2002@yahoo.fr

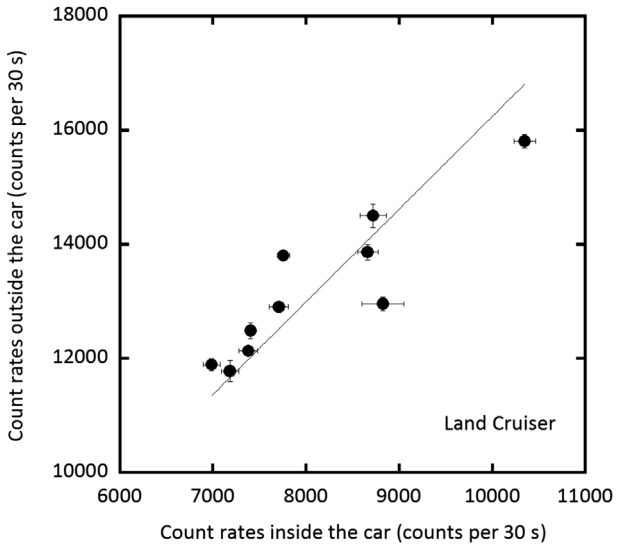

Fig. 1. Correlation between count rates outside and inside the car. This regression formula was used as the shielding factor of the car body.

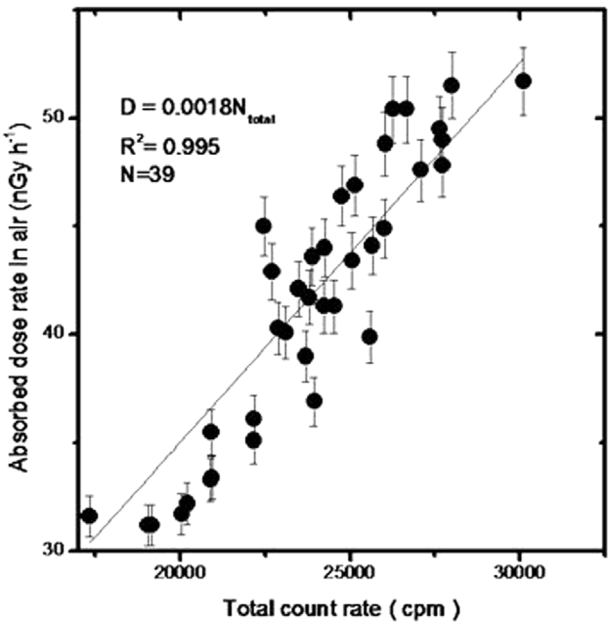

Fig. 2. Correlation between absorbed dose rate in air which was calculated by software using the response matrix method and total count rate observed outside the car. This regression formula was used as the dose rate conversion factor.

In this study, a car-borne survey was carried out to establish the dose rate distribution map, to assess the annual external dose and to perform natural radioactivity measurements in soil from Douala, the largest city in Cameroon. Gamma ray spectrometry based on NaI(Tl) detector was also used in the laboratory to determine activity concentrations of ^{238}U, ^{232}Th and ^{40}K in soil.

2 Material and methods

2.1 Survey area

Douala is a coastal city, the economic capital of Cameroon, the main business center and the largest city of the country; with approximately 4 million inhabitants. It is the chief town of the Littoral Region and the Wouri Division. Located on the edge of the Atlantic Ocean, at the bottom of the Gulf of Guinea, at the mouth of the Wouri River, Douala has the largest port in the Cameroon and one of the most important in Central Africa. The annual rainfall ranges between 3000 and 5000 mm, and the annual average temperature is 26°C (Olivry, 1986). The geology of the region consists of sedimentary rocks, mainly, tertiary and quaternary sediments (Ndontchueng *et al.*, 2014).

2.2 Car-borne survey

A car-borne survey was carried out using a mobile vehicle moving at a speed of approximatively 40 km h^{-1}, in which was positioned a measuring system consisting of a sodium iodide detector 3-in × 3-in NaI(Tl), a global positioning system (GPS) to record coordinates at each measuring point, and a computer to analyze gamma-ray spectra (EMF-211, EMF Japan Co, Japan). Absorbed dose rate measurements inside the vehicle were performed every 30 seconds along the way and corrected by multiplying with a shielding factor with the aim of representing the unshielded external dose rate. The shielding factor (Fig. 1) was evaluated in order to be able to convert the values measured inside the vehicle to ambient dose rate outside of the car, and was estimated by making measurements inside and outside the vehicle at 10 measurement points and correcting them with count rates inside. The absorbed dose rates in air were calculated using a dose rate conversion factor based on the correlation of dose rate (nGy h^{-1}) and total count rate (cpm) from 0 to 1023 channels in the gamma-ray pulse height distribution (Hosoda *et al.*, 2015, 2016). Commonly, the gamma-ray pulse height distribution is obtained by 15 min measurements at each point. Measurements of gamma-ray pulse height distributions were carried out at 1 m above the ground surface at 39 measurement points in Douala City. The gamma-ray pulse height distributions were unfolded using a 22×22 response matrix for the estimation of absorbed dose rate in air (Minato and Kawano, 1970; Minato, 2001). The dose rate conversion factor of the scintillation spectrometer used in the present survey was determined to be 1.75×10^{-3} nGy h^{-1}.cpm^{-1}. Figure 2 gives the relationship between absorbed dose rate (nGy h^{-1}) which was calculated by software using the response matrix method and total count rates outside the vehicle. Absorbed dose rate in air (D_{out}) 1 m above the ground surface at each measurement point can be estimated by the following equation (Tan *et al.*, 2017):

$$D_{out} = 2D_{in} \times (1.62) \times 0.00175, \quad (1)$$

where (D_{in}) is the count rate inside the car (cps) obtained by the measurements for 30 seconds. Since the dose rate conversion factor was given as a dose rate (nGy h^{-1}) for counts per minute (cpm), it is necessary to double D_{in} in order to convert into the counts per minute.

Following *in situ* measurements, external effective dose in Douala was assessed using the following equation (Inoue *et al.*, 2017):

$$E = D_{out} \times DCF \times T \times (Q_{in} \times R + Q_{out}) \times 10^{-6}, \quad (2)$$

where E is the external effective dose (mSv y^{-1}), D_{out} is the absorbed dose rate in air (nGy h^{-1}), DCF is the dose conversion factor from the dose rate to the external effective dose for adults (0.748 ± 0.007 Sv Gy^{-1}) (Moriuchi *et al.*, 1990), T is 8766 h, and Q_{in} and Q_{out} are indoor (0.6) and outdoor (0.4) occupancy factor respectively. R (1.11) is the ratio of indoor and outdoor dose rate.

2.3 Activity concentrations of ^{238}U, ^{232}Th and ^{40}K and their contribution to the air absorbed dose rate

The evaluation of activity concentrations and the contribution of ^{238}U, ^{232}Th and ^{40}K to the absorbed dose rate in air were obtained by measuring the spectra of gamma-ray pulse height distributions and using a 22×22 response matrix conceived by Minato (1978, 2001). The gamma-ray pulse height distribution obtained by measurements was converted to the energy bin spectrum of incident gamma-ray which is a distribution of gamma-ray flux density to each energy bin. The energy ranges from 0 to 3.2 MeV, energies above 3.2 MeV were not included for evaluation because the maximum value of the gamma-ray energy from natural radionuclides is 2.615 Mev emitted by ^{208}Tl (^{232}Th-series). The gamma-ray lines utilized for natural radionuclides are: 1.464 MeV for ^{40}K, 1.768 MeV and 2.205 MeV for ^{214}Bi (^{238}U-series), and also 2.615 MeV for ^{208}Tl (^{232}Th-series). The 22×22 matrix for the 3-in $\times$ 3-in NaI(Tl) scintillator for an isotropic field was calculated using the Monte Carlo code, SPHERIX (Matsuda *et al.*, 1982; Minato, 2012). The gamma-ray flux density and dose rate per unit solid angle are considered almost isotropic in the natural environment (Minato, 1971). The calculation of gamma-ray flux densities per unit activity concentrations of ^{238}U-series, ^{232}Th-series and ^{40}K are necessary, in order to evaluate each activity concentrations of natural radionuclides from an energy bin spectrum. This calculation assumed that a semi-infinite volume source was formed in the ground (Minato, 2001). The primary and scattered gamma-ray flux density per unit activity concentrations could be calculated using one-dimensional Monte Carlo gamma transport code, MONARIZA/G2 (Minato, 1977, 1980). A total of a million histories were traced for each natural radionuclide. The nuclear data of gamma-ray energies and disintegration rates used the reported values by Beck (1972) and Beck *et al.* (1972) for this Monte Carlo simulation. The activity concentration of each natural radionuclide was evaluated by a successive approximation which used a 3×3 matrix, determined by Minato (2001), to the values of energy bins for ^{238}U-series, ^{232}Th-series and ^{40}K. The statistical errors for absorbed dose rates in air and activity concentrations for ^{40}K, ^{238}U-series and ^{232}Th-series obtained using this software depend on the integral air kerma (nGy h^{-1}) at each measurement point (Matsuda *et al.*, 2002), and these were evaluated in this study as 2%, 2%, 6–8% and 4–5%, respectively.

2.4 Sampling and sample preparation

For radioactivity measurements in soil, twenty soil samples from a depth of 0–5 cm, weighing about 1 kg each were collected at Douala III, pulverized and then dried at a temperature of 70 °C for 48 hours to remove moisture. Samples were then transferred to Marinelli containers of 500 cm^3, each hermetically sealed and stored for more than 40 days to bring ^{222}Rn and its short-lived daughter products into equilibrium with ^{226}Ra (Ravisankar *et al.*, 2011).

2.5 Radioactivity measurements in laboratory

^{238}U, ^{232}Th and ^{40}K activity concentrations in soil samples were measured using a gamma ray spectrometer. The samples were placed in a shielded gamma ray spectrometry unit for a counting time of 10^5 seconds. Radioactivity measurements were carried out using a NaI(Tl) detector of 7.6 cm $\times$ 7.6 cm size and a resolution of 7.5% at 661.6 keV with a 1024 channels multichannel analyzer. The detector was calibrated using the standard gamma ray source of ^{137}Cs with known peak at 661.6 keV, ^{152}Eu with known peaks at 1089.7 keV, and 1408.1 keV and ^{60}Co with known peaks at 1173.2 keV and 1332.5 keV. The efficiency calibration curve for NaI(Tl) detector was obtained using standards containing ^{40}K (1460.8 keV), ^{137}Cs (661.6 keV), ^{208}Tl (2614.4 keV) and ^{228}Ac (940.1 keV). Gamma-ray lines of ^{214}Bi were used to determine ^{238}U activity concentrations after reaching secular equilibrium between ^{222}Rn and its daughter products ^{214}Bi and ^{214}Pb. Gamma-ray lines of ^{228}Ac were considered to determine activity concentrations of ^{232}Th.

The spectral analysis was performed using Genie-2000. Activity concentrations of natural radionuclides in samples were computed using the following equation (IAEA, 1989):

$$A = \frac{N_p}{t_c I_\gamma(E_\gamma)\varepsilon(E_\gamma)M}, \quad (3)$$

where N_P is the number of counts in a given peak area corrected for background peaks of a peak at energy E, $\epsilon(E_\gamma)$ the detection efficiency at energy E, t_c is the counting lifetime, $I_\gamma(E_\gamma)$ is the number of gamma rays per disintegration of this nuclide at energy E, and M the mass in kg of the sample.

2.6 Estimation of absorbed dose rate in air and external effective dose

The external terrestrial gamma-radiation absorbed dose rates in air at a height of about 1 m above the ground are calculated by using the conversion factor 0.0417 (nGy h^{-1}) (Bq kg^{-1})$^{-1}$ for ^{40}K, 0.462 (nGy h^{-1})(Bq kg^{-1})$^{-1}$ for ^{238}U and 0.604 (nGy h^{-1})(Bq kg^{-1})$^{-1}$ for ^{232}Th (UNSCEAR, 2000). Assuming that, ^{137}Cs, ^{90}Sr and the ^{235}U decay series can be neglected as they contribute very little to the total dose from the environmental background (Kocher and Sjoreen, 1985; Jacob *et al.*, 1986; Leung *et al.*, 1990):

$$D(\text{nGy h}^{-1}) = 0.462A_U + 0.604A_{Th} + 0.0417A_K, \quad (4)$$

where A_U, A_{TH} and A_K are the mean activity concentrations of ^{238}U, ^{232}Th and ^{40}K, respectively in (Bq kg^{-1}).

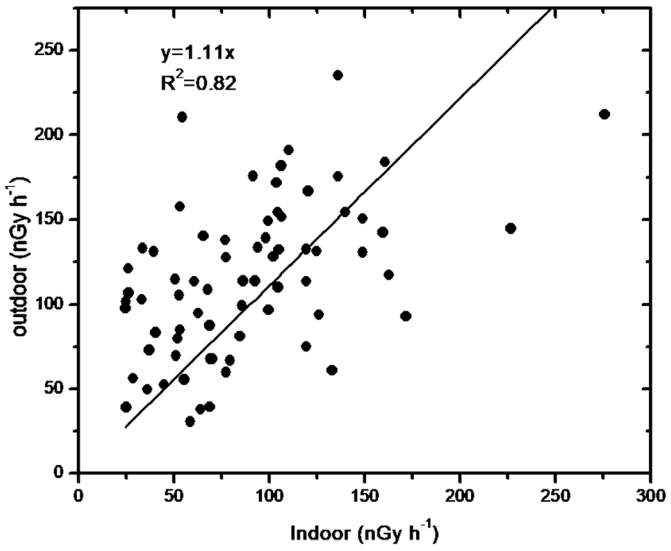

Fig. 3. Correlation between outdoor and indoor dose obtained by car-borne survey in Douala rate.

In the estimation of external effective dose, the conversion coefficient and occupancy factor must be taken into account. In the present work, a conversion factor of 0.7 Sv Gy^{-1} and occupancy factors Q have been used to convert the absorbed rate to human effective dose equivalent with an outdoor and indoor occupancy of 40% and 60% respectively. However, since the materials used in the construction of most these buildings also contain radionuclides, R (1.11) is the ratio of indoor and outdoor dose rate (Fig. 3). It should be noted that the dwellings were built mainly using locally made soil bricks. A_i are average activity concentrations of ^{238}U, ^{232}Th and ^{40}K. $(KCF)_i$ are corresponding air kerma conversion factors given previously. The external effective dose is determined as follows (Saïdou *et al.*, 2015b):

$$E_{ext}(\text{mSv y}^{-1}) = F_C \times [Q_{in} \times R + Q_{out}] \sum_{i=1}^{3} A_i (KCF)_i \times t. \quad (5)$$

3 Results and discussion

3.1 Shielding factor and dose rate conversion factor

The relationship between count rates inside and outside the car is shown in Figure 1, and the shielding factor and standard uncertainty (JCGM 100, 2008) were found to be 1.62 and 0.03, respectively. However, the shielding factor is influenced by the type of car, number of passengers and detector position inside the car.

Figure 2 shows the correlation between absorbed dose rates in air (nGy h^{-1}) calculated using the 22 × 22 response matrix method and count rate outside the car (cps) (that is corrected count rate inside the car). The dose conversion factor and uncertainty were found to be 0.00175 nGy h^{-1} cps^{-1} and 0.01, respectively (Fig. 2). Thus, the absorbed dose rate in air (D_{out}) outside the car 1 m above the ground surface at each measuring point can be estimated using the following equation (Tan *et al.*, 2017):

$$D_{out} = 2D_{in} \times 1.62 \times 0.00175, \quad (6)$$

where (D_{in}) is count rate inside the car (cps) obtained by measurements for 30 seconds.

3.2 Air absorbed dose rate distribution in Douala city and effective external dose

Figure 4 shows the survey route and Figures 5 and 6 show the measurement points of gamma-ray pulse height distribution of Douala. The highest air absorbed dose rates (86 nGy h^{-1}) were observed at Ndogbong (N4.058778, E9.74635). The absorbed dose rates in this study range between 28–86 nGy h^{-1} with the average value of 50 nGy h^{-1} (Fig. 7). According to UNSCEAR (2000) at worldwide level, gamma dose rates in air range between 24–160 nGy h^{-1} and the average is 59 nGy h^{-1}, higher than the average value obtained within the framework of this study. However at Ndogbong, Aeroport, Ndogpassi III, Bepanda Omnisports, and Brazzaville, air absorbed dose rates are higher than the worldwide average value. The town of Kerala in India recorded large values of the absorbed dose rate, up to 2100 nGy h^{-1}, observed near the rare earth mining (Hosoda *et al.*, 2015). In Tokyo, air absorbed dose rates range from 18 to 76 nGy h^{-1} with an average value of 49 nGy h^{-1} (Inoue *et al.*, 2015), and from 9 to 554 nGy h^{-1} with an average value of 50 nGy h^{-1} in Turkey (Turhan *et al.*, 2012), which is practically lower than the corresponding worldwide value.

3.3 Effective dose assessment

The external annual effective dose ranged from 0.21 to 0.41 mSv y^{-1} with a mean value of 0.31 mSv y^{-1}, less than the worldwide average value of 0.5 mSv y^{-1} (UNSCEAR, 2000). In the Gold Mining Areas of Betare-Oya, Eastern-Cameroon, the mean value of effective dose is 0.33 mSv y^{-1} (0.17–0.60 mSv y^{-1}) (Ngoa *et al.*, 2017) and in Tokyo, before the Fukushima Daiichi Nuclear Power plant Accident, the arithmetic annual effective dose was 0.32 mSv y^{-1} (0.26–0.40 mSv y^{-1}) (Inoue *et al.*, 2015), which are practically lower than the corresponding worldwide value.

3.4 *In situ* activity concentrations of ^{238}U, ^{232}Th and ^{40}K and their contribution to air absorbed dose rate

According to Table 1, activity concentrations for primordial radionuclides range between 18–47 Bq kg^{-1}, 21–54 Bq kg^{-1} and 110–410 Bq kg^{-1} for the ^{238}U series, ^{232}Th series and ^{40}K respectively, with corresponding average values of 29 Bq kg^{-1}, 38 Bq kg^{-1} and 202 Bq kg^{-1}. For ^{238}U and ^{232}Th, 7/39 and 32/39 measurement points have respectively activity concentrations higher than the world average value (UNSCEAR, 2000). For ^{40}K, 1/39 measurement point has activity concentrations higher than the world average. By comparing the average *in situ* activity concentrations of ^{238}U, ^{232}Th and ^{40}K in Douala with the average values in other areas of Cameroon and other countries as shown in Table 3, it should be noted that the

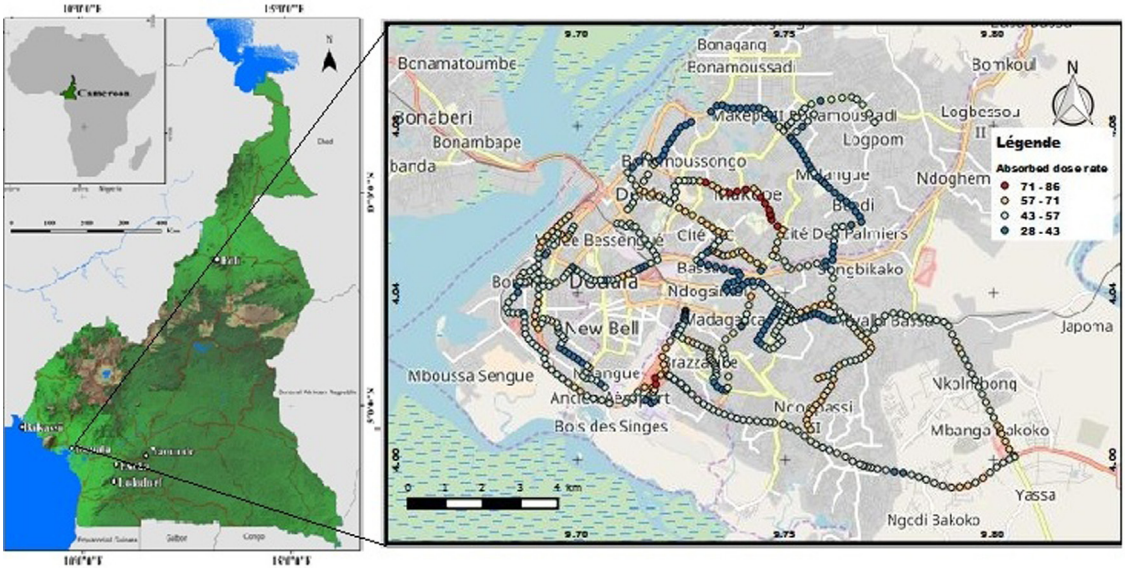

Fig. 4. Survey route in Douala. This map was also drawn using QGIS (Background: Openstreet map).

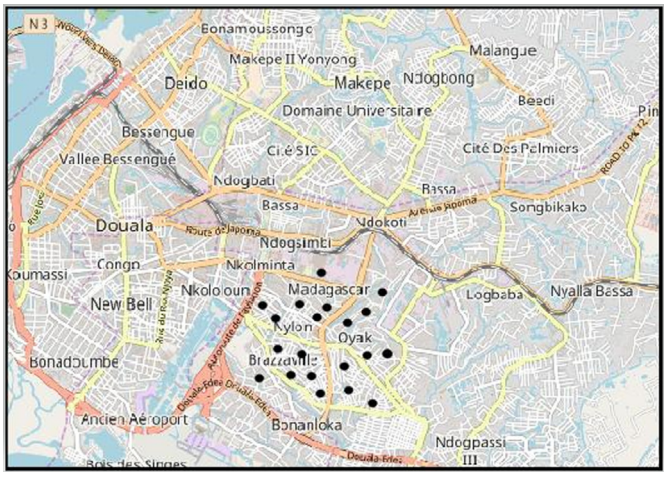

Fig. 5. Location of sampling point (20) pulse.

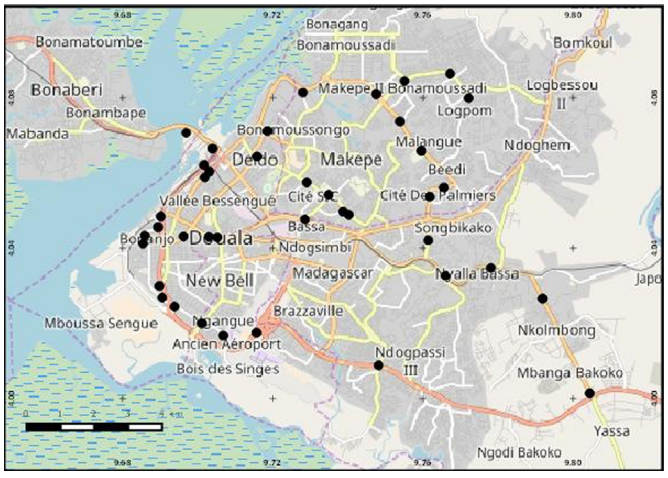

Fig. 6. *In situ* measurement points (39) of gamma-ray pulse height distribution using a NaI(Tl) scintillation spectrometer.

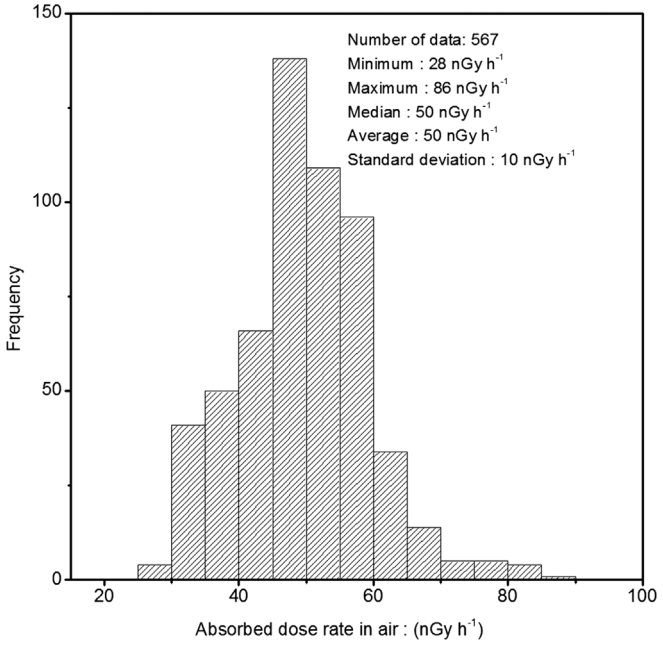

Fig. 7. Histogram of absorbed dose rate in air.

mean activity concentration of ^{238}U is higher than the average value measured in other areas of Cameroon such as Bakassi and Poli, and lower than those measured in Lolodorf and Douala quarries. The same comparison can be made with those measured in Lagos state in Nigeria, in Itagunmodi and Canakkale in Turkey, and in Kerala in India. For ^{232}Th, the average activity concentration found out in the present study is higher than those of Bakassi and Poli, and lower than those measured at Douala-quarriers and Lolodorf. This value is also higher than those of Itagunmodi and Lagos State and lower than that of Kerala. The average value of ^{40}K

Table 1. *In situ* activity concentrations and the contributions of ^{40}K, ^{238}U and ^{232}Th to air absorbed dose rates in Douala using the car-borne survey method.

Point	Latitude	Longitude	Absorbed dose rate in air	Contribution to the dose rate (%)			Activity concentrations (Bq kg^{-1})		
	N	E	(nGy h^{-1})	^{40}K	^{238}U	^{232}Th	^{40}K	^{238}U	^{232}Th
Douala	N4.05883	E9.701882	50 ± 1	12	28	60	146 ± 3	33 ± 2	48 ± 2
Douala	N4.060352	E9.703057	50 ± 1	23	25	53	292 ± 6	31 ± 2	44 ± 2
Douala	N4.062082	E9.701685	59 ± 1	27	33	40	386 ± 8	45 ± 3	36 ± 2
Douala	N4.06649	E9.703935	32 ± 1	34	24	40	290 ± 6	18 ± 1	21 ± 1
Douala	N4.070663	E9.696892	45 ± 1	36	23	41	410 ± 8	25 ± 3	30 ± 2
Douala	N4.048405	E9.690173	32 ± 1	23	23	53	185 ± 4	18 ± 1	27 ± 1
Douala	N4.045582	E9.689423	41 ± 1	17	28	54	187 ± 4	29 ± 2	37 ± 2
Douala	N4.043308	E9.685862	29 ± 1	15	28	57	110 ± 2	20 ± 1	28 ± 1
Douala	N4.041148	E9.685378	39 ± 1	12	30	58	129 ± 3	30 ± 2	39 ± 2
Douala	N4.029897	E9.68979	45 ± 1	16	26	59	184 ± 4	28 ± 2	44 ± 2
Douala	N4.026803	E9.690527	36 ± 1	14	26	60	130 ± 3	24 ± 2	36 ± 2
Douala	N4.024398	E9.693795	52 ± 1	13	30	58	177 ± 4	39 ± 3	51 ± 3
Douala	N4.019988	E9.701103	40 ± 1	20	26	55	210 ± 4	26 ± 2	37 ± 2
Douala	N4.016748	E9.706783	33 ± 1	16	29	55	146 ± 3	25 ± 2	32 ± 2
Douala	N4.05417	E9.734857	48 ± 1	16	25	58	208 ± 4	31 ± 2	47 ± 2
Douala	N4.057508	E9.729035	41 ± 1	23	26	51	246 ± 5	27 ± 2	35 ± 2
Douala	N4.064372	E9.715773	49 ± 1	15	29	56	200 ± 4	36 ± 3	47 ± 2
Douala	N4.071107	E9.718553	36 ± 1	23	26	52	208 ± 4	22 ± 2	31 ± 2
Douala	N4.081412	E9.728038	31 ± 1	16	29	56	131 ± 3	23 ± 2	30 ± 2
Douala	N4.080985	E9.747512	37 ± 1	13	27	60	124 ± 2	26 ± 2	38 ± 2
Douala	N4.084458	E9.755105	44 ± 1	13	29	59	143 ± 3	30 ± 2	42 ± 2
Douala	N4.086427	E9.767235	46 ± 1	23	21	56	286 ± 6	25 ± 2	44 ± 2
Douala	N4.079912	E9.772208	32 ± 1	15	28	57	130 ± 3	18 ± 1	32 ± 2
Douala	N4.073662	E9.753895	35 ± 1	13	28	59	125 ± 3	25 ± 2	36 ± 2
Douala	N4.065873	E9.759602	33 ± 1	16	27	57	139 ± 3	23 ± 2	32 ± 2
Douala	N4.056127	E9.765598	43 ± 1	15	25	61	167 ± 3	27 ± 2	44 ± 2
Douala	N4.053658	E9.761817	52 ± 1	15	25	61	201 ± 4	33 ± 2	54 ± 3
Douala	N4.042078	E9.761412	42 ± 1	16	24	59	176 ± 4	25 ± 2	42 ± 2
Douala	N4.032633	E9.766025	42 ± 1	22	25	53	237 ± 5	26 ± 2	37 ± 2
Douala	N4.03475	E9.778138	49 ± 1	15	25	60	194 ± 4	31 ± 2	50 ± 3
Douala	N4.026533	E9.791902	44 ± 1	16	25	60	184 ± 4	28 ± 2	45 ± 2
Douala	N4.00135	E9.804472	40 ± 1	22	24	54	223 ± 4	24 ± 2	36 ± 2
Douala	N4.049702	E9.738715	50 ± 1	24	25	51	312 ± 6	31 ± 2	43 ± 2
Douala	N4.048875	E9.740258	48 ± 1	16	25	59	200 ± 4	30 ± 2	47 ± 2
Douala	N4.047623	E9.728583	31 ± 1	20	27	54	155 ± 3	20 ± 1	28 ± 1
Douala	N4.04285	E9.705237	43 ± 1	20	44	36	231 ± 5	47 ± 3	26 ± 1
Douala	N4.043018	E9.702948	47 ± 1	29	33	39	359 ± 7	39 ± 3	31 ± 2
Douala	N4.043115	E9.696225	44 ± 1	17	35	48	197 ± 4	39 ± 3	36 ± 2
Douala	N4.017505	E9.715673	40 ± 1	12	36	52	127 ± 3	37 ± 3	36 ± 2

is higher than that is obtained in Bakassi and less than the average values found at Douala-quarriers, Lolodorf and Poli. Compared to other studies in the world, this value is higher than that of Canakkale, lower than those of Lagos state, Itagunmodi and Kerala. Figure 8 shows a weak correlation between thorium and uranium (correlation coefficient = 0.09).

The contributions of ^{238}U, ^{232}Th and ^{40}K to the absorbed dose rates in air range respectively between 21–44%, 36–61% and 12–36% with the average values of 27%, 54% and 19% respectively. The highest contributions of ^{238}U, ^{232}Th and ^{40}K to the absorbed dose rate were respectively found at Akwa (44%) (N4.04285, E9.705237), Beedi (61%) (N4.053658, E9.761817) and SCDP (36%) (N4.06649, E9.703935) while

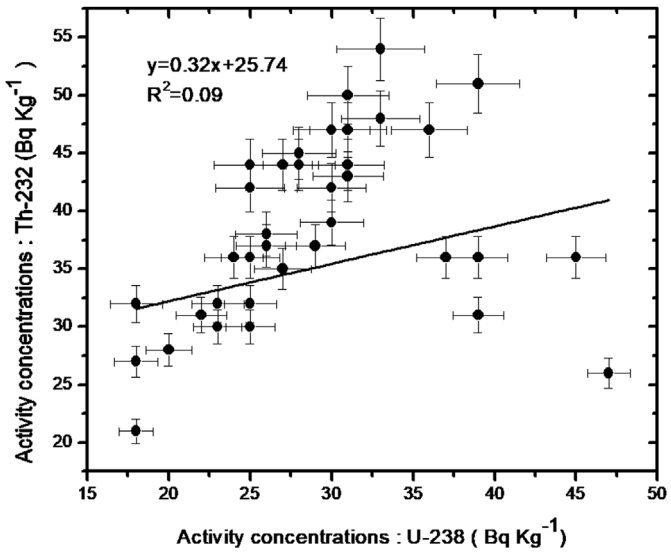

Fig. 8. Correlation between ^{232}Th and ^{238}U activity concentrations.

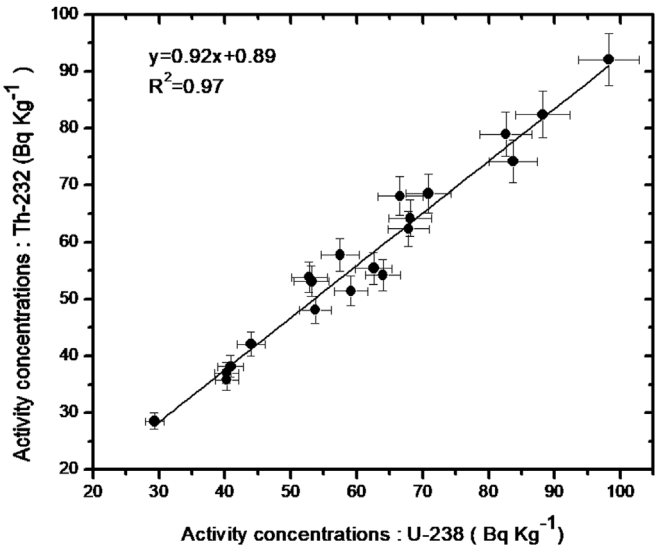

Fig. 9. Correlation between ^{232}Th and ^{238}U activity concentrations.

Table 2. Activity concentrations of ^{238}U, ^{232}Th and ^{40}K in soil, air absorbed dose rates and annual effective dose following radioactivity measurements at the laboratory.

	Location		Activity concentration (Bq kg^{-1})			Absorbed dose rate	Annual effective dose
Sample code	Latitude	Longitude	^{40}K	^{238}U	^{232}Th	(nGy h^{-1})	(mSv y^{-1})
STN-16-39	04°01'640"	09°44'424"	40 ± 8	88 ± 17	82 ± 18	92 ± 13	0.6 ± 0.1
STN-16-40	04°01'625"	09°44'510"	41 ± 9	52 ± 10	53 ± 12	58 ± 9	0.4 ± 0.1
STN-16-41	04°01'642"	09°44'345"	43 ± 9	66 ± 13	64 ± 14	72 ± 10	0.5 ± 0.1
STN-16-42	04°01'395"	09°44'284"	53 ± 11	39 ± 08	37 ± 8	43 ± 6	0.3 ± 0 (<0.1)
STN-16-43	04°01'342"	09°44'240"	42 ± 9	52 ± 10	48 ± 11	55 ± 8	0.4 ± 0.1
STN-16-44	04°01'136"	09°44'239"	77 ± 16	29 ± 06	29 ± 6	34 ± 5	0.2 ± 0 (<0.1)
STN-16-45	04°00'995"	09°44'766"	44 ± 9	65 ± 13	68 ± 15	73 ± 11	0.5 ± 0.1
STN-16-46	04°00'907"	09°44'810"	47 ± 10	69 ± 14	69 ± 15	76 ± 11	0.5 ± 0.1
STN-16-47	04°00'835"	09°44'746"	60 ± 13	39 ± 08	36 ± 8	43 ± 6	0.3 ± 0 (<0.1)
STN-16-48	04°00'769"	09°44'619"	59 ± 13	52 ± 10	54 ± 12	59 ± 9	0.4 ± 0.1
STN-16-49	04°00'822"	09°44'595"	62 ± 13	43 ± 08	42 ± 9	48 ± 7	0.3 ± 0 (<0.1)
STN-16-50	04°00'861"	09°44'702"	43 ± 9	56 ± 11	58 ± 13	63 ± 9	0.4 ± 0.1
STN-16-51	04°01'047"	09°44'320"	51 ± 11	58 ± 11	51 ± 11	60 ± 8	0.4 ± 0.1
STN-16-52	04°01'016"	09°44'089"	64 ± 13	62 ± 12	54 ± 12	65 ± 9	0.4 ± 0.1
STN-16-53	04°01'258"	09°44'046"	74 ± 16	61 ± 12	55 ± 12	65 ± 9	0.4 ± 0.1
STN-16-54	04°01'302"	09°44'055"	67 ± 14	40 ± 08	38 ± 8	45 ± 6	0.3 ± 0 (<0.1)
STN-16-55	04°01'433"	09°44'016"	79 ± 17	66 ± 13	62 ± 14	72 ± 10	0.5 ± 0.1
STN-16-56	04°01'421"	09°43'763"	68 ± 14	82 ± 16	74 ± 16	86 ± 12	0.6 ± 0.1
STN-16-57	04°01'371"	09°43'740"	52 ± 11	81 ± 16	79 ± 17	88 ± 13	0.6 ± 0.1
STN-16-58	04°01'188"	09°43'941"	46 ± 10	96 ± 19	92 ± 20	102 ± 15	0.7 ± 0.1

the lowest contributions were found at Makepe (36%) (N4.04285, E9.705237) and Akwa (12%) (N4.017505, E9.715673) for ^{232}Th and ^{40}K respectively.

3.5 Activity concentrations of ^{238}U, ^{232}Th and ^{40}K in soil following laboratory measurements

Activity concentrations of natural radionuclides ^{238}U, ^{232}Th and ^{40}K in 20 soil samples using gamma spectrometry in laboratory are listed in Table 2. They range respectively between 29–96 Bq kg^{-1}, 29–92 Bq kg^{-1}, and 40–79 Bq kg^{-1} with respective average values of 60 Bq kg^{-1}, 57 Bq kg^{-1} and 56 Bq kg^{-1}. The world average values of ^{238}U, ^{232}Th and ^{40}K in the earth's crust are 35, 30 and 400 Bq kg^{-1}, respectively (UNSCEAR, 2000). It appears that average values of ^{238}U and ^{232}Th are higher than the corresponding world average activity concentrations. Figure 9 shows a good correlation between thorium and uranium in soil samples (correlation coefficient = 0.97). The highest ^{238}U and ^{232}Th activity concentrations were found at Brazzaville (96 Bq kg^{-1}), and

Table 3. Comparison of activity concentrations of ^{238}U, ^{232}Th and ^{40}K in soil samples from Douala littoral region following laboratory and *in situ* measurements with values from other areas around the world.

Country			Activity concentration (Bq kg^{-1})			References
			^{238}U	^{232}Th	^{40}K	
Nigeria	Lagos state		1.20–55.30(23)	2.18–60.33(23)	44.74–489.96(204)	Ojo and Gbadegesin (2015)
	Itagunmodi		18.5–90.3(55)	12.5–52.4(26)	200.5–901.2(501)	Ademola *et al.* (2014)
Turkey	Canakkale		14.9–118(42)	18.7–146(53)	197.1–1033.4(54)	Turhan *et al.* (2012)
India	Kerala		25–1269	42–2374	22–964	Hosoda *et al.* (2015)
Cameroon	Poli		12–57(24)	15–58(28)	112–1124(506)	Saïdou *et al.* (2015b)
	Bakassi		17–23(19)	27–38(32)	93–138(110)	Saïdou *et al.* (2015b)
	Lolodorf		60–270(130)	100–700(390)	370–1530(850)	Saïdou *et al.* (2015b)
	Douala (quarries)		11.8–146.7(40)	8–102.9(43)	54–928(342)	Guembou *et al.* (2017)
	Douala	*In situ*	18–47(29)	21–54(38)	110–410(202)	Present work
		Labo	29–96(60)	29–92(57)	40–79(56)	

( ): mean values.

Dakar for ^{40}K (79 Bq kg^{-1}) and the lowest activity concentrations of ^{238}U and ^{232}Th were found at Bilongue (29 Bq kg^{-1}) and Oyack for ^{40}K (40 Bq kg^{-1}). The results of activity concentrations of natural radionuclides in soil samples taken from Douala III at different locations and in other parts of the world are displayed in Table 3. It clearly appears that activity concentrations of ^{238}U and ^{232}Th were higher than those of other areas in Cameroon (Bakassi, Poli and Douala-quarries), except Lolodorf and other countries (Lagos state, Itagunmodi, Canakkale).

The external terrestrial gamma radiation absorbed dose rates range between 34 and 102 nGy h^{-1}, with an average value of 65 nGy h^{-1}, which is higher than the world average value of 59 nGy h^{-1} (UNSCEAR, 2000). According to Table 2, absorbed dose rates at 13 over 20 measurement points were higher than the world average value (59 nGy h^{-1}). External effective dose of 8 over 20 measurement points is higher than the worldwide average value. The highest effective dose was found at Brazzaville (0.7 mSv y^{-1}) and Oyack (0.6 mSv y^{-1}). However, for *in situ* measurements, Table 1 shows that all measurement points have absorbed dose rate lower than the worldwide average value. External effective dose varies from 0.3–0.7 mSv y^{-1} with an average value of 0.42 mSv y^{-1}, which is lower than the worldwide average value (0.5 mSv y^{-1}). The average value of the effective amount obtained in this study compared to other inhabited areas of Cameroun (Poli and Lolordorf) is low, and high in Bakassi (Saïdou *et al.*, 2015b).

4 Conclusion

The car-borne survey using NaI(Tl) scintillation spectrometer was carried out in Douala, the largest city of Cameroon to make the detailed distribution map of absorbed dose rate in air. Activity concentrations of ^{238}U, ^{232}Th and ^{40}K were also determined using *in situ* gamma spectrometry. They range respectively between 18–47 Bq kg^{-1}, 21–54 Bq kg^{-1} and 110–410 Bq kg^{-1} with respective average values of 29 Bq kg^{-1}, 38 Bq kg^{-1} and 202 Bq kg^{-1}. Mean activity concentrations of ^{238}U and ^{40}K are lower than the world average values (UNSCEAR, 2000) while the mean activity concentration of ^{232}Th is higher than the corresponding world average value. The contributions of ^{238}U, ^{232}Th and ^{40}K to the absorbed dose rates in air range respectively between 21–44%, 36–61% and 12–36% with the average values of 27%, 54% and 19%. The average activity concentrations of natural radionuclides ^{238}U, ^{232}Th and ^{40}K in the soil were found to be 60 Bq kg^{-1}, 57 Bq kg^{-1} and 56 Bq kg^{-1} respectively. The total average effective dose is 0.37 mSv y^{-1} which is lower than the worldwide average value (0.5 mSv y^{-1}). Finally, it can be concluded that the population of Douala city is not significantly exposed to natural radiation.

References

Ademola KA, Bello KA, Adejumobi CA. 2014. Determination of natural radioactivity and hazard in soil samples in and around gold mining area in Itagunmodi, south-western, Nigeria. *J. Radiat. Res. Appl. Sci*. 7: 249–255.

Beck HL. 1972. *The absolute intensities of gamma rays from the decay of ^{238}U and ^{232}Th. Health and Safety Laboratory Report HASL-262.* New York: U.S. Atomic Energy Commission.

Beck HL, DeCampo J, Gogolak C. 1972. *In-situ Ge(Li) and NaI(T1) gamma-ray spectrometry. Health and Safety Laboratory Report HASL-258.* New York: U.S. Atomic Energy Commission.

EPA. 2009. Sources of background radioactivity. http://www.epa.gov/radiation/marssim/docs/marsame/appendix.B.pdf. Accessed 9 August 2011.

Guembou Shouop SJ, Ndontchueng Moyo M, Chene G, Nguelem Mekontso EJ, Motapon Ousmanou, Kayo AS, Strivay D. 2017. Assessment of natural radioactivity and associated radiation hazards in sand building material used in Douala Littoral Region of Cameroon using gamma spectrometry. *Environ. Earth Sci.* 76: 1–12.

Hosoda M, Tokonami S, Omori Y, Sahoo SK, Akiba S, Sorimachi A, Ishikawa T, Nair RR, Jayalekshmi PA, Sebastian P, Iwaoka K, Akata N, Kudo H. 2015. Estimation of external dose by car-borne survey in Kerala, India. *Plos ONE* 10: e0124433.

Hosoda M, Inoue K, Oka M, Omori Y, Iwaoka K, Tokonami S. 2016. Environmental radiation monitoring and external dose estimation

in Aomori prefecture after the Fukushima Daiichi Nuclear Power Plant accident. *Jpn. J. Health Phys.* 51: 41–50.

IAEA. 1989. Measurement of radionuclides in food and the environment, a guidebook. International Atomic Energy Agency Technical Reports Series No. 229, Vienna.

Inoue K, Hosoda M, Fukushi M, Furukawa M, Tokonami S. 2015. Absorbed dose rate in air in metropolitan Tokyo before the Fukushima Daiichi Nuclear Power Plant accident. *Radiat. Prot. Dosim.*167: 231–234.

Inoue K, Arai M, Fujisawa M, Saito K, Fukushi M. 2017. Detailed distribution map of absorbed dose rate in air in Tokatsu area of Chiba prefecture, Japan, constructed by car-borne survey 4 years after the Fukushima Daiichi Nuclear Power Plant accident. *Plos ONE* 12: e0171100.

Jacob P, Paretzke HG, Rosenbaum H, Zankl M. 1986. Effective dose equivalents for photon exposure from plane sources on the ground. *Radiat. Prot. Dosim.* 14: 299–310.

JCGM 100. 2008. Joint Committee for Guides in Metrology. Evaluation of measurement data-guide to the expression of uncertainty in measurement, September 2008. http://www.bipm.org/utils/common/documents/jcgm/JCGM_100_2008_E.pdf. Accessed 19 August 2016.

Kocher DC, Sjoreen AL. 1985. Dose-rate conversion factors for external exposure to photon emitters in soil. *Health Phys.* 48: 193–205.

Leung KC, Lau SY, Poon CB. 1990. Gamma radiation dose from radionuclides in Hong Kong soil. *J. Environ. Radioact.* 11: 279–290.

Matsuda H, Furukawa S, Kaminishi T, Minato S. 1982. A new method for evaluating weak leakage gamma-ray dose using a 3"$\varphi \times 3$" NaI (Tl) scintillation spectrometer (I) Principle of background estimation method. Rep Government Industrial Research Institute. *Nagoya* 31: 132–146. In Japanese.

Matsuda H, Minato S, Pasquale V. 2002. Evaluation of accuracy of response matrix method for environmental gamma ray analysis. *Radioisotopes* 51: 42–50. In Japanese.

Minato S. 1971. Terrestrial gamma-radiation field in natural environment. *J. Nucl. Sci. Technol.* 8: 342–347.

Minato S. 1977. Analysis of the variation of environmental γ radiation during rainfall. Rep Government Industrial Research Institute. *Nagoya* 26: 190–202. In Japanese.

Minato S. 1978. A response matrix of a 3"$\varphi \times 3$" NaI(Tl) scintillator for environmental gamma radiation analysis. Rep Governmental Industrial Research Institute. *Nagoya* 27: 384–397. In Japanese.

Minato S. 1980. Monte Carlo calculation of gamma radiation field due to precipitation washout of radon daughters from the atmosphere to the ground surface. *Jpn. J. Health Phys.* 15: 19–24.

Minato S. 2001. Diagonal elements fitting technique to improve response matrixes for environmental gamma ray spectrum unfolding. *Radioisotopes* 50: 463–471.

Minato S. 2012. Application of a 60×60 response matrix for a NaI (Tl) Scintillator to fallout from the Fukushima reactor accident. *Radiat. Emerg. Med.* 1: 108–112.

Minato S, Kawano M. 1970. Evaluation of exposure due to terrestrial gamma-radiation by response matrix method. *J. Nucl. Sci. Technol.* 7: 401–406.

Moriuchi S, Tsutsumi M, Saito K. 1990. Examination on conversion factors to estimate effective dose equivalent from absorbed dose in air for natural gamma radiations. *Jpn. J. Health Phys*. 25: 121–128. Japanese with English abstract.

Ndontchueng MM, Njinga RL, Nguelem EJM, Simo A, Beyala Ateba JF. 2014. ^{238}U, ^{235}U, ^{137}Cs and ^{133}Xe in soils from two campuses in University of Douala-Cameroon. *Appl. Radiat. Isot.* 86: 85–89.

Ngoa EL, Ndjana NJE, Hosoda M, Bongue D, Saïdou, Akata N, Koukong HR, Kwato NMG, Tokonami S. 2017. Air absorbed dose rate measurements and external dose assessment by car-borne survey in the gold mining areas of Betare-Oya, Eastern-Cameroon. *Jpn. J. Health Phys.* 53: 5–11.

Ojo TJ, Gbadegesin KAJ. 2015. Terrestrial radiation doses from selected towns of Southwestern Nigeria. *Int. J. Phys.* 3: 244–247.

Olivry CJ. 1986. Fleuves et rivières du Cameroun. Collection Monographies Hydrologiques. Paris : ORSTOM, n° 9.

Ravisankar R, Vanasundari K, Chandrasekaran A, Suganya M, Eswaran P, Vijayagopal P, Meenakshisundaram V. 2011. Measurement of natural radioactivity in brick samples of Namakkal, Tamilnadu, India using gamma ray spectrometry. *Arch. Phys. Res.* 2: 95–99.

Saïdou, Abdourahimi, Tchuente Siaka YF, Kwato Njock MG. 2015a. Natural radiation exposure to the public in the oil bearing Bakassi Peninsula, Cameroon. *Radioprotection* 50(1): 35–41.

Saïdou, Ele Abiama P, Tokonami S. 2015b. Comparative study of natural radiation exposure to the public in three uranium and oil regions of Cameroon. *Radioprotection* 50(4): 265–271.

Tan VL, Inoue K, Fujisawa M, Arai M, Fukushi M. 2017. Impact on absorbed dose rate in air from Asphalt Pavement Associated with Transport Infrastructure Developments on Phu Quoc Island, Vietnam. *Radiat. Environ. Med.* 2: 88–93.

Turhan S, Arıkan IH, Oguz F, Özdemir T, Yücel B, Varinlioglu A, Köse A. 2012. Car-borne survey of natural background gamma dose rate in Çanakkale region, Turkey. *Radiat. Prot. Dosim.* 148: 45–50.

UNSCEAR. 1982. Ionizing radiation sources and biological effects. United Nations, New York.

UNSCEAR. 2000. Report to the general assembly, with scientific annexes. Annex B exposures from natural radiation sources. New York Report of the United Nations Scientific.

Cite this article as: Takoukam Soh SD, Saïdou, Hosoda M, Ndjana Nkoulou II JE, Akata N, Bouba O, Tokonami S. 2018. Natural radioactivity measurements and external dose estimation by car-borne survey in Douala city, Cameroon. *Radioprotection* 53(4): 255–263

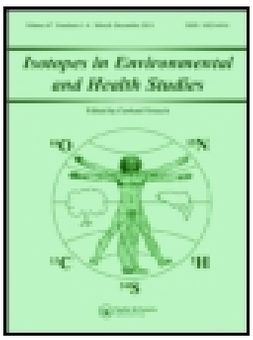

Isotopes in Environmental and Health Studies

ISSN: 1025-6016 (Print) 1477-2639 (Online) Journal homepage: https://www.tandfonline.com/loi/gieh20

Simultaneous measurements of indoor radon and thoron and inhalation dose assessment in Douala City, Cameroon

Takoukam Soh Serge Didier, Saïdou, Shinji Tokonami, Masahiro Hosoda, Takahito Suzuki, Hiromi Kudo & Oumarou Bouba

To cite this article: Takoukam Soh Serge Didier, Saïdou, Shinji Tokonami, Masahiro Hosoda, Takahito Suzuki, Hiromi Kudo & Oumarou Bouba (2019): Simultaneous measurements of indoor radon and thoron and inhalation dose assessment in Douala City, Cameroon, Isotopes in Environmental and Health Studies, DOI: 10.1080/10256016.2019.1649258

To link to this article: https://doi.org/10.1080/10256016.2019.1649258

Published online: 09 Aug 2019.

ISOTOPES IN ENVIRONMENTAL AND HEALTH STUDIES
https://doi.org/10.1080/10256016.2019.1649258

Taylor & Francis
Taylor & Francis Group

Simultaneous measurements of indoor radon and thoron and inhalation dose assessment in Douala City, Cameroon

Takoukam Soh Serge Didier[a,b], Saïdou [a,b], Shinji Tokonami[c] , Masahiro Hosoda[d], Takahito Suzuki[d], Hiromi Kudo[d] and Oumarou Bouba[a]

[a]Nuclear Physics Laboratory, Faculty of Science, University of Yaoundé I, Yaoundé, Cameroon; [b]Nuclear Technology Section, Institute of Geological and Mining Research, Yaoundé, Cameroon; [c]Department of Radiation Physics, Institute of Radiation Emergency Medicine, Hirosaki University, Hirosaki City, Japan; [d]Department of Radiation Science, Graduate School of Health Sciences, Hirosaki University, Hirosaki City, Aomori, Japan

ABSTRACT

Radon, thoron and associated progeny measurements have been carried out in 71 dwellings of Douala city, Cameroon. The radon–thoron discriminative detectors (RADUET) were used to estimate the radon and thoron concentration, while thoron progeny monitors measured equilibrium equivalent thoron concentration (EETC). Radon, thoron and thoron progeny concentrations vary from 31 ± 1 to 436 ± 12 Bq m^{-3}, 4 ± 7 to 246 ± 5 Bq m^{-3}, and 1.5 ± 0.9 to 13.1 ± 9.4 Bq m^{-3}. The mean value of the equilibrium factor for thoron is estimated at 0.11 ± 0.16. The annual effective dose due to exposure to indoor radon and progeny ranges from 0.6 to 9 mSv a^{-1} with an average value of 2.6 ± 0.1 mSv a^{-1}. The effective dose due to the exposure to thoron and progeny vary from 0.3 to 2.9 mSv a^{-1} with an average value of 1.0 ± 0.4 mSv a^{-1}. The contribution of thoron and its progeny to the total inhalation dose ranges from 7 to 60 % with an average value of 26 %; thus their contributions should not be neglected in the inhalation dose assessment.

ARTICLE HISTORY
Received 31 December 2018
Accepted 13 July 2019

KEYWORDS
Equilibrium factor; inhalation dose; ionogenic radiation exposure; radio ecology; radon; thoron; Rn–Tn discriminative detector

1. Introduction

It is well known that about 50 % of the total dose received by the public comes from airbone radon and its short-lived daughter products [1]. Radon has been identified as the second leading cause of lung cancer after tobacco smoking [2,3]. Radon and thoron are produced in the ground by the decay of ^{238}U and ^{232}Th, respectively. Radon (^{222}Rn) with a half-life of 3825 days tends to be concentrated in enclosed spaces such as caves, underground mines and dwellings [4]. Many studies have shown that radon and thoron are present in dwellings almost everywhere [1,5–14]. Nevertheless, the contribution of indoor ^{220}Rn and its progeny is generally negligible, compared to those of ^{222}Rn and its progeny, because of the short half-life of ^{220}Rn ($T_{1/2} = 56$ s). The ventilation condition of the residential dwellings is one of the factors which decide the indoor ^{222}Rn and ^{220}Rn concentrations [15]. Being an inert gas, the radon can easily diffuse out of the soil surface into

CONTACT Saïdou saidous2002@yahoo.fr, ous.saidou@gmail.com

the air in an indoor environment, it can be trapped in poorly ventilated houses, and so its concentration can build up to higher levels. The type of house, wind speed, building materials, humidity, pressure and temperature [16] also decide the radon concentration in an environment. In Karunagappallly Taluk, India, the exposure to thoron may contribute significantly to the inhalation dose, due to the presence of thorium-rich monazite sand [17]. Saïdou et al. [18] reported indoor radon measurements in the uranium regions of Poli and Lolodorf, Cameroon. Radon concentrations in Poli and Lolodorf range between 29 and 2240 Bq m^{-3}, and 24 and 4390 Bq m^{-3}, respectively. Their arithmetic and geometric means are 294 Bq m^{-3} and 200 Bq m^{-3} for the uranium region of Poli, 687 Bq m^{-3} and 318 Bq m^{-3} for the uranium region of Lolodorf, respectively.

The study [18] showed that high indoor residential radon distributions observed in the uranium regions of Poli and Lolodorf could stem from the combined effect of ground and floor type and building material. Saïdou et al. [19] reported radon–thoron discriminative measurements in the high natural radiation areas of southwestern Cameroon. It resulted that 30 % of houses have thoron concentrations above 300 Bq m^{-3}, and the mean contribution of indoor thoron to the total inhalation was of 47 %. Takoukam et al. [20] studied natural radioactivity measurements and external dose estimation by car-borne survey in Douala city, Cameroon. They found that the population of Douala city is not significantly exposed to natural radiation from external sources.

The aim of this work is to measure simultaneously the activity concentrations of indoor radon, thoron and thoron progeny, and then to estimate the radiation doses due to inhalation of radon, thoron and their progeny. Thus indoor radon and thoron concentrations were measured in 71 dwellings in Douala city using passive type radon–thoron detectors for long-term measurements. Thoron progeny concentrations were also measured with deposition detectors placed with the radon–thoron detectors.

2. Material and methods

2.1. Study area

Douala basin is one of the coastal sedimentary basins with basement made up of granite and gneiss in Cameroon, and covers an area of 19,000 km^2 of which 7000 km^2 are emerging (Figure 1). Geological regions containing surface granite and gneiss formations are prone to exhibit elevated radon concentrations [21]. Douala is the main business centre and the largest city of the country; with approximately 4 million inhabitants. The Douala basin extends under the waters of the Gulf of Guinea by a 25 km wide continental platform and is made up of two sub-basins. The Douala sub-basin is limited on the north by the volcanic line of Cameroon and on the south by the Nyong River, and the Kribi-Campo sub-basin is located between the Nyong River in the north and the Ntem River in the south [22]. Douala city lies between the northern latitude of 4°02′ and the eastern longitude of 9°40′; the average altitude is 13 m. The annual rainfall ranges between 3000 and 5000 mm, and the annual average air temperature is 26 °C [23].

2.2. Methodology

To determine radon and thoron concentrations, passive integrated radon–thoron discriminative detector developed at the National Institute of Radiological Sciences (NIRS) in Japan

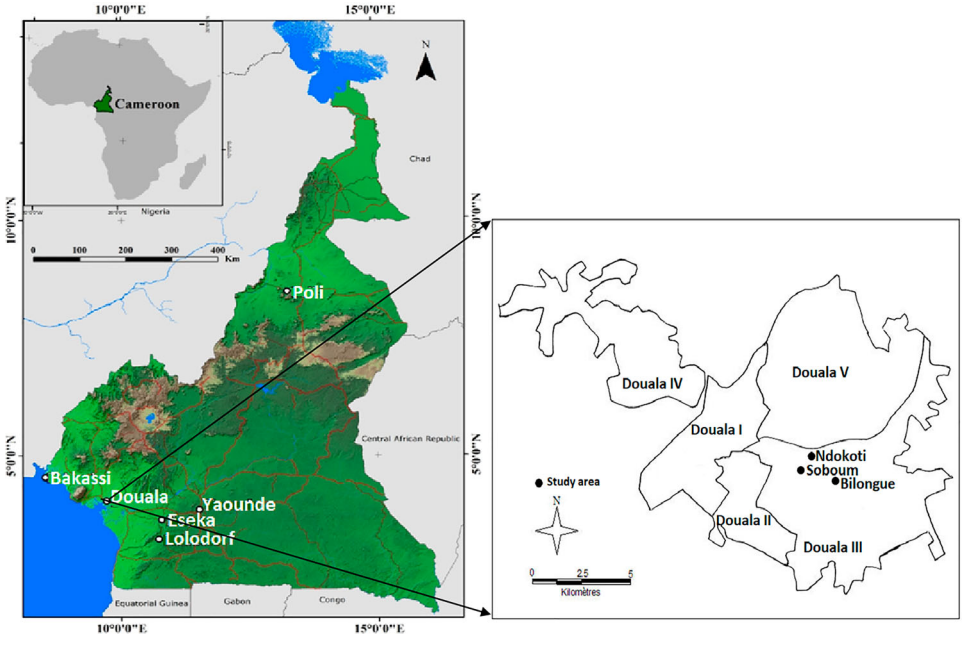

Figure 1. Location of the study area.

(commercially RADUET) were used. These detectors have two diffusion chambers with different ventilation rates and each chamber contains a CR-39 chip 10×10 mm^2 in size (RADUET, Radosys Ltd., Hungary, Figure 2) [24] for detecting the alpha particles emitted from radon and thoron as well as their progeny. The low diffusion rate chamber is made of electron conductive plastic with an inner volume of 30 cm^3. The high diffusion rate chamber made of the same material has six holes in the wall, electro-conductive sponges covering the holes to prevent radon and thoron progeny, and aerosols from infiltrating inside. While one chamber measures radon only, the other chamber combines radon and thoron detection. Thoron concentration is then determined by substracting the result of one detector from the other. The difference in track density between the two CR-39 chips makes it possible to estimate radon and thoron concentrations separately. After the exposure, the CR-39 plates were chemically etched for 24 h in a 6 M NaOH solution at 60 °C, and alpha tracks were counted with an optical microscope [26].

The average radon ($\overline{C_{Rn}}$) and thoron ($\overline{C_{Tn}}$) concentrations are calculated using the following formulaes [27]:

$$\overline{C_{Rn}} = (d_L - \bar{b})\frac{f_{Tn2}}{t \times (f_{Rn1} \times f_{Tn2} - f_{Rn2} \times f_{Tn1})} - (d_H - \bar{b})\frac{f_{Tn1}}{t \times (f_{Rn1} \times f_{Tn2} - f_{Rn2} \times f_{Tn1})} \quad (1)$$

$$\overline{C_{Tn}} = (d_H - \bar{b})\frac{f_{Rn1}}{t \times (f_{Rn1} \times f_{Tn2} - f_{Rn2} \times f_{Tn1})} - (d_L - \bar{b})\frac{f_{Rn2}}{t \times (f_{Rn1} \times f_{Tn2} - f_{Rn2} \times f_{Tn1})}, \quad (2)$$

where d_L and d_H are alpha track densities for low and high air-exchange rate chamber in tracks per square centimetre (track cm^{-2}), respectively. $\bar{b}$ is track density due to background in (track cm^{-2}), t is sampling duration (h), f_{Rn1} and f_{Tn1} are calibration factors for ^{222}Rn, ^{220}Rn in a low air-exchange rate chamber in (tracks cm^{-2} h^{-1})/(Bq m^{-3}),

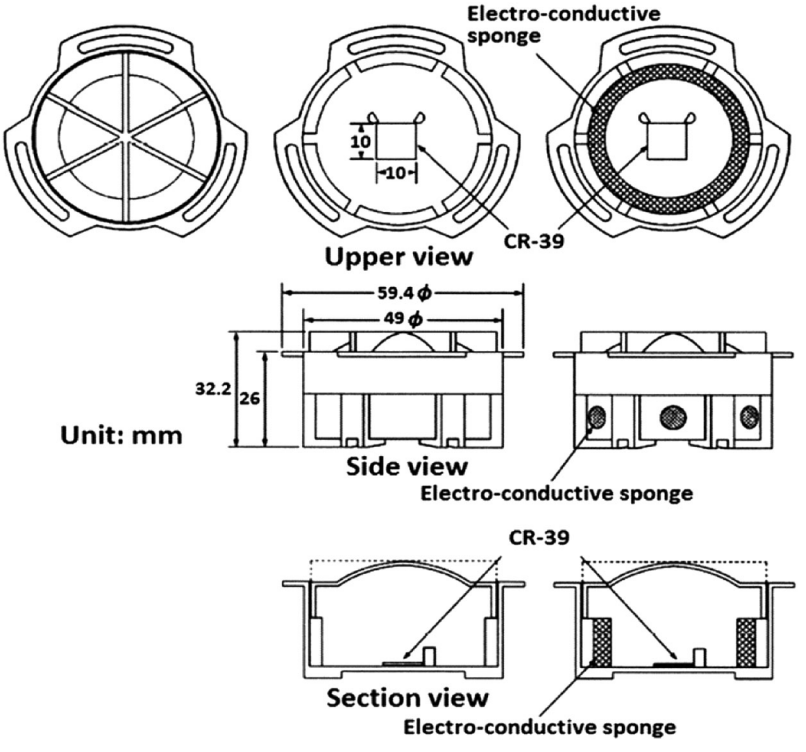

Figure 2. Overview of the radon-thoron discrimination detector (RADUET) [24].

respectively. f_{Rn2} and f_{Tn2} are calibration factors for ^{222}Rn, ^{220}Rn in a high air-exchange rate chamber in (tracks cm^{-2} h^{-1})/(Bq m^{-3}).

The thoron progeny monitors also use CR-39 chips mounted on a stainless steel plate and covered with a thin absorption sheet [28,29]. Zhuo and Iida [30] developed the prototype of a thoron progeny monitor (Figure 3). The CR-39 pieces are covered with an aluminium-vaporised Mylar film of 71 mm of air equivalent thickness. The thickness of the Mylar film allows the detection of only the 8.8 MeV alpha particles emitted from ^{212}Po (thoron progeny). According to Janik et al. [31], the lower limit of detection (LLD) calculated based on an ISO Guideline depends on the concentration of both gases and on the exposure period. For example, when a radon concentration of 15 Bq m^{-3} and a thoron concentration of 15 Bq m^{-3} are given with a measurement period of 90 days, the detection limits are estimated to be 5 and 7 Bq m^{-3}, respectively. While detection limit of thoron progeny concentration is 5 mBq m^{-3}.

With simultaneous measurements of thoron and its progeny concentrations, the equilibrium factor for thoron F_{Tn} can be determined as

$$F_{Tn} = \frac{\mathrm{EETC}}{C_{Tn}}, \tag{3}$$

where C_{Tn} is the thoron gas concentration and EETC refers to equilibrium equivalent thoron concentration.

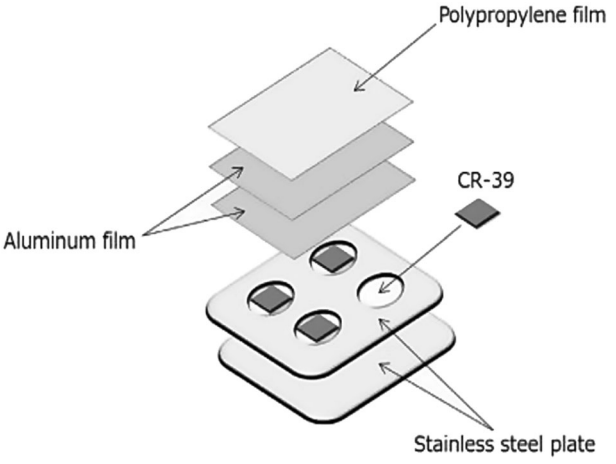

Figure 3. Schematic drawings of the passive type thoron progeny monitor [25].

In this study, each RADUET detector was paired with a thoron progeny monitor for a minimum of 3 months. All detectors were hung at a height of 1–2 m above the ground level using hard wire and at least 20 cm away from any of the wall surfaces in bed- or living rooms of the dwellings. Main building materials of houses in Douala city are either wood or sand and cement. Most of houses consist of bricks made with sand and cement, and cemented floors. RADUET detector and thoron progeny monitor were placed only in cemented houses with no storey and no basement. The equilibrium equivalent progeny concentrations for radon were calculated using equation:

$$\mathrm{EERC} = F_R \times C_{Rn}, \tag{4}$$

where C_{Rn} and F_R are the concentration and the equilibrium factor of radon ($F_R = 0.4$) [1], respectively. However, F_R depends on the environmental conditions [32].

2.3. Total inhalation dose assessment

The total inhalation dose due to exposure to indoor radon, thoron and their progeny has been calculated using the relation given by UNSCEAR [1]:

$$E_{Rn}(\mathrm{mSv}\,a^{-1}) = (0.17 + 9F_R) \times C_{Rn} \times T \times F_{occ} \times 10^{-6} \tag{5}$$

$$E_{Tn}(\mathrm{mSv}\,a^{-1}) = (0.11 \times C_{Tn} + 40 \times \mathrm{EETC}) \times T \times F_{occ} \times 10^{-6}, \tag{6}$$

where F_R is the equilibrium factor for radon, C_{Rn} and C_{Tn} are measured radon and thoron concentrations in Bq m^{-3}, respectively, EETC is the equilibrium equivalent thoron concentration. The quantities 0.17 and 9 are dose conversion factors for radon and its progeny concentrations, while 0.11 and 40 are the dose conversion factors for thoron and its progeny concentrations in nSv, respectively [1]. The exposure time T was 8760 h, and the indoor occupancy factor (F_{occ}) was assumed to be 0.6. The multiplication factor 10^{-6} is used to convert nSv into mSv.

3. Results and discussion

Table 1 summaries the results obtained for radon and thoron in 71 dwellings of Douala. The measured values of radon and thoron concentrations vary from 31 ± 1 to 436 ± 12 Bq m^{-3} with an AM of 139 ± 47 Bq m^{-3}, and from 4 ± 7 to 246 ± 5 Bq m^{-3} with an AM of 80 ± 52 Bq m^{-3}, respectively. The geometric means of C_{Rn} and C_{Tn} result to 118 and 62 Bq m^{-3}, respectively, which are lower than the international indoor geometric mean of 45 Bq m^{-3} [1]. According to Ćurguz et al. [32], the geometric mean of radon depends on building materials. In our study, the indoor geometric mean of radon is different from other parts of the world because the building material of dwellings in Douala is hardly comparable.

Less than 2 % of dwellings among those surveyed had radon concentration higher than the permissible level of 300 Bq m^{-3} [33]. 32 % and 34 % of dwellings have respectively radon concentrations below 100 Bq m^{-3} [3] and 148 Bq m^{-3} [34]. Only 32 % of dwellings have radon concentrations below 200 Bq m^{-3} as recommended by EU countries [35]. In the uranium-bearing region of Lolodorf and Poli, Saidou et al. [18] measured radon concentrations using electrical ionization chambers in a range between 24 and 4390 Bq m^{-3} for Lolodorf, and 29 and 2240 Bq m^{-3} for Poli with AMs of 687 and 294 Bq m^{-3}, respectively. These values are higher than the corresponding values reported in the present study. Figure 4 shows the radon concentrations plotted against thoron concentrations, but they do not correlate each other. In Cameroon, there are not yet reference levels for radon indoors. However, the national radon action plan is being elaborated.

Similar studies were carried out worldwide. Results of the radon and thoron activity concentrations, the EERC and the EETC in several countries are summarized in Table 2. Prasad et al. [36] reported a study of radiation exposure due to radon, thoron and progeny in the indoor environment of Yamuna and Tons valleys of Garhwal Himalaya. Simultaneous measurements of radon and thoron using a passive integrating radon–thoron discriminative detector were performed in 93 houses of Ottawa in Canada [12]. Visnuprasad et al. [37] reported the contribution of thoron and progeny towards inhalation dose in a thorium abundant beach environment in Kerala, India. Gierl et al. [38] performed a similar study on thoron and thoron progeny measurements in German clay houses. The results show that gas concentrations range between 20 and 160 Bq m^{-3} for radon and between 10 and 90 Bq m^{-3} for thoron 20 cm from the wall. This study showed that increased thoron gas concentrations as well as thoron progeny concentrations can occur in houses built of unfired clay. The traditional Chinese residential dwelling is constructed with loam bricks or mud walls (so-called raw-soil building) for which Shang et al. [9] determined the radon and thoron concentrations (Table 2). The value of the

Table 1. The ranges, arithmetic mean, geometric mean and median of the indoor radon, thoron and progeny: levels and the equilibrium factor of thoron.

	Min	Max	AM ± SD[a]	GM(GSD)[a]	Median
Rn concentration (Bq m^{-3})	31 ± 1	436 ± 12	139 ± 47	118(1.3)	139
Tn concentration (Bq m^{-3})	4 ± 7	246 ± 5	80 ± 52	62(2.1)	71
FTn	0.01 ± 0.01	0.83 ± 1.55	0.11 ± 0.16	0.07(9.90)	0.07
TnP (EETC) (Bq m^{-3})	1.5 ± 0.9	13.1 ± 9.4	4.6 ± 2.9	3.9(1.8)	3.6
RnP (EERC) (Bq m^{-3})	12 ± 1	174 ± 5	51 ± 21	47(1.6)	55

[a]AM: arithmetic mean; SD: standard deviation; GM: geometric mean; GSD: geometric standard deviation.

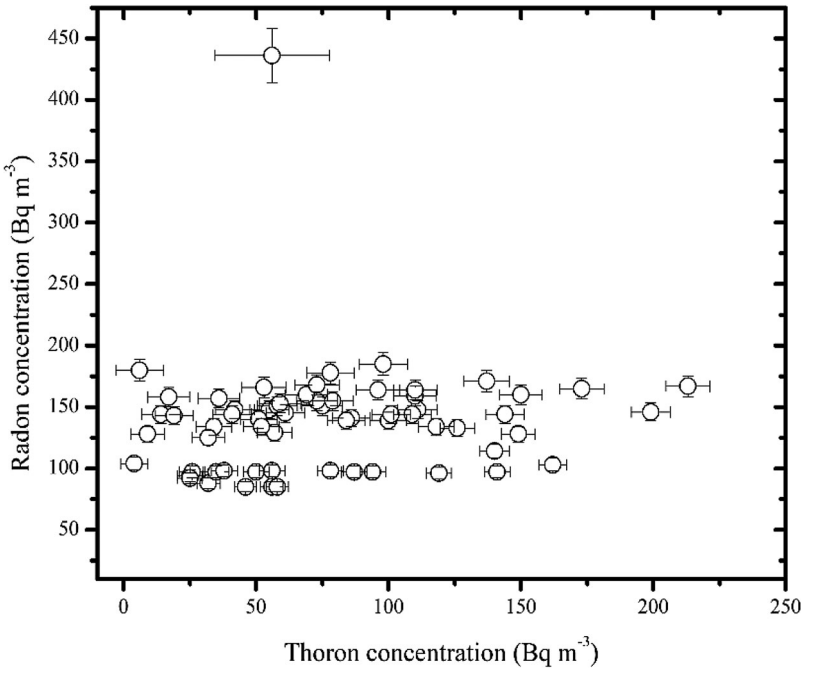

Figure 4. Scatter plots of radon-thoron concentration.

Table 2. Results of measurements of the radon, thoron activity concentration, the EERC and the EETC.

Country/area		C_{Rn} (Bq m^{-3})		C_{Tn} (Bq m^{-3})		EERC (Bq m^{-3})		EETC (Bq m^{-3})		Reference
		Range (AM)	GM	Range (AM)	GM	Range (AM)	GM	Range (AM)	GM	
South Africa	West	28–465(132)	–	–	–	–	–	–	–	[21]
	East	8–98(37)								
India	Himalaya	4–174(38)	24	1–108(25)	18	1.6–76.1(17.4)	13.2	0.1–3.6(0.9)	0.7	[36]
Canada	Ottawa	8–1525(110)	74	5–924(56)	19	–	–	–	–	[12]
India	Kerala	8–89(24)	22	4–129(37)	28	1.9–31.5(10.9)	9.50	0.1–11.4(1.6)	1.1	[37]
German		20–160	–	10–90	–	–	–	2–10	–	[38]
Chinese		12–427(72)	58	LLD–1,860(318)	162	–	–	LLD–15.8(3.8)	–	[9]
Cameroon	Poli	46–143(82)	–	24–238(94)	–	–	–	4–9(6.4)	–	[39]
	Lolodorf	27–937(97)		6–700(160)				0.4–36(10.3)		
	Betare-Oya	88–282(133)		4–383(92)				0.6–19(6)		

equilibrium factor of indoor thoron for concrete and brick houses is higher (0.020–0.038) than in soil-structure houses (0.004–0.007). These results point to high thoron concentrations in Chinese traditional residential dwellings constructed with loam bricks or soil wall. Indoor thoron contributes 13–57 % to the total inhalation dose. The radon and thoron concentrations in Douala investigated within our study appear in comparable ranges to the worldwide results. General radon concentrations are greater than the associated thoron levels based upon the numerous studies (Table 2).

From Figure 5(a) we can notice that the highest frequencies of the C_{Rn} results are in intervals lower than 150 Bq m^{-3}. Only one of the surveyed dwellings has C_{Rn} higher than 400 Bq m^{-3}. In all dwellings, C_{Tn} was lower than 300 Bq m^{-3} (Figure 5(b)). The equilibrium equivalent radon concentration (EERC) and equilibrium equivalent thoron

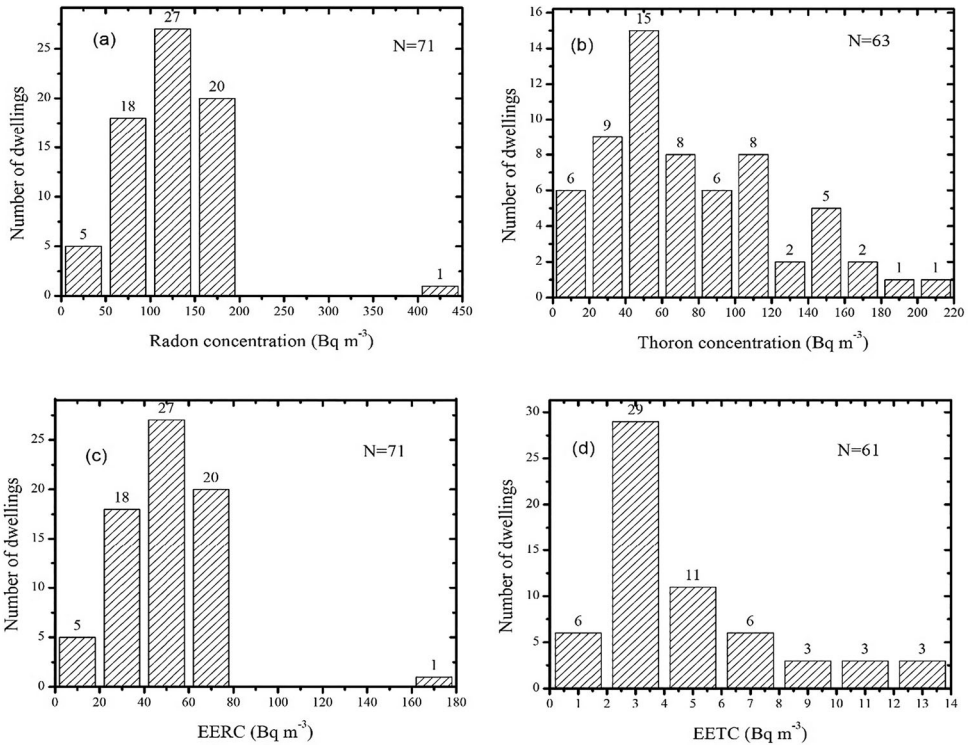

Figure 5. Frequency distribution of radon and its progeny (a,c), thoron and its progeny (b,d) in the dwellings of Douala.

concentration (EETC) vary from 12 to 174 Bq m^{-3} and from 1.5 ± 0.9 to 13.1 ± 9.4 Bq m^{-3} with the respective arithmetic and geometric means (Table 1). Figure 5(b,d) presents the frequency distributions of the radon, thoron and progeny concentrations from the 71 dwellings of the investigated area in Douala.

The average equilibrium factor for thoron was calculated from the measurements to the AM of 0.1 ± 0.1 (Table 1). This mean value is higher than the value (0.02) given by UNSCEAR [1]. The distribution of equilibrium factor for thoron is shown in Figure 6. About 20 % of the dwellings have F_{Tn} values less than or equal to 0.02. Harley et al. [40] reported an EETC of 0.04 ± 0.01 for indoor thoron using a large database obtained by a long-term measurement of thoron and its progeny. However, Hosoda et al. [26] presented widely ranged EETCs from 0.008 to 0.07 obtained by the recent measurements in several countries. These results vary because the equilibrium factor depends largely on the environment conditions such as hours, humidity, time, place and modes of ventilation, etc. [8,41].

The annual effective dose due to exposure to radon and its progeny in the study area vary from 0.6 to 9 mSv a^{-1} with an average value of 2.6 ± 0.1 mSv a^{-1}. Similarly, the annual effective dose due to thoron and its progeny range from 0.3 to 2.9 mSv a^{-1} with an average of 1.0 ± 0.4 mSv a^{-1}. Figure 7 shows the distribution of inhalation dose due to radon, thoron and their progeny. The mean contribution of radon and its progeny to the total inhalation dose is 75 % while that of thoron and its progeny is 26 %. The AM values of total inhalation dose due to radon, thoron and their progeny in dwellings of

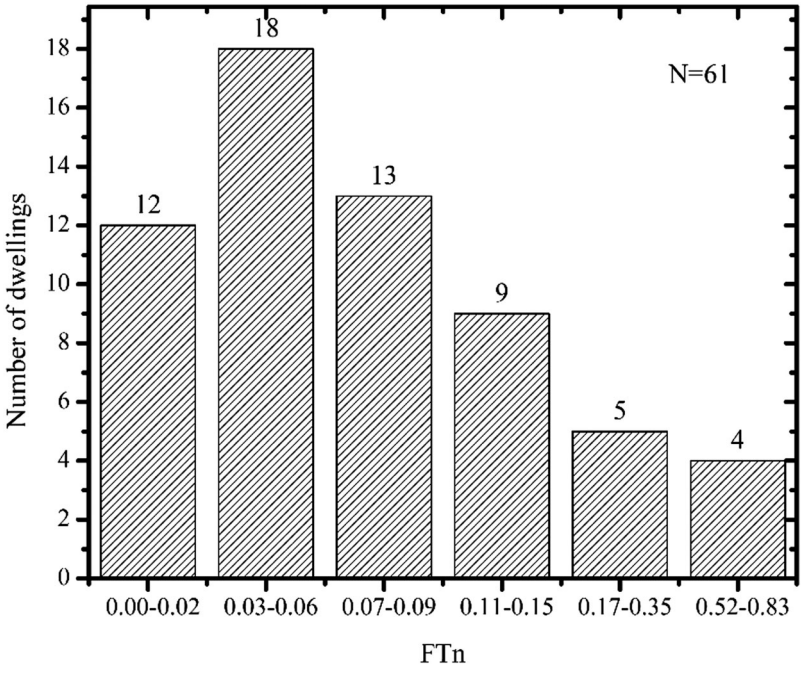

Figure 6. Frequency distribution of the equilibrium factor between thoron and its progeny.

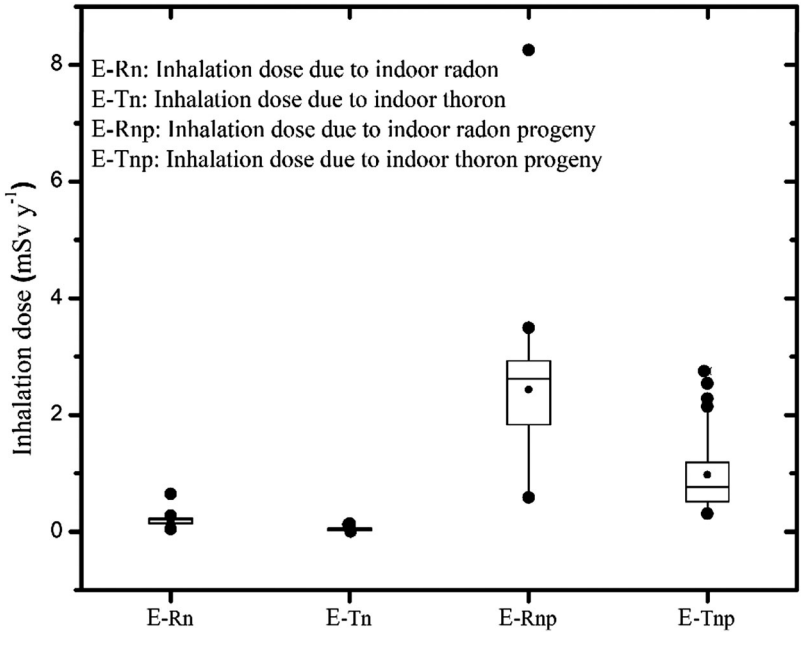

Figure 7. Box plot of inhalation dose of radon, thoron and their progeny.

the study area was found to be 3.64 mSv a^{-1}. This inhalation dose received by the public in the study area is lower than the reference level of 10 mSv a^{-1} given by the International Commission on Radiological Protection (ICRP) [33]. Table 3 summarizes the contributions

Table 3. Ranges, mean and contribution of indoor radon, thoron and progeny to total inhalation dose received by the public.

Radionuclide	Range (mSv a^{-1})	Mean inhalation dose (mSv a^{-1})	Total (mSv a^{-1})	Range contribution (%)	Mean contribution (%)
Radon	0.05–0.65	0.19	3.64	3–7	5
Thoron	0.002–0.14	0.05		0.1–4	1
Radon progeny	0.59–8.25	2.43		37–93	70
Thoron progeny	0.30–2.75	0.97		7–59	25

of radon, thoron, radon progeny and thoron progeny to the total inhalation dose range between 3 and 7 %, 0.1 and 4 %, 37 and 93 %, and 7 and 59 %, respectively. We have ascertained that the highest contribution to the inhalation dose of 70 % stems from radon progeny, and the corresponding least contribution of 1 % belongs to thoron. However, thoron and its progeny contribute a significant fraction of 26 % to the total inhalation dose. It suggests that thoron and its progeny cannot be neglected when assessing radiation dose as it was believed in the past.

Indoor radon, thoron and progeny measurements in Douala city are continuing the work done in several regions of Cameroon, namely the uranium and thorium bearing regions of Poli and Lolodorf and the gold mining areas of Betare-Oya [39]. About 400 RADUET detectors were deployed in dwellings. The results obtained showed a significant contribution of thoron and its progeny to the total inhalation dose. It varies from 12 to 67 %, 3 to 80 % and from 7 to 70 %, respectively, in the above study areas. The corresponding average values are 49, 53 and 31 %, respectively.

4. Conclusion

In this study, we analysed the radon, thoron and progeny concentrations to assess radiation dose to the public due to inhalation of radon and thoron in Douala city, Cameroon. Two types of nuclear track detectors were used for three-month measurements. From these, AM radon and thoron concentrations in 71 dwellings were estimated to be 139 and 80 Bq m^{-3}, respectively. The AMs for EERC and EETC are 51 and 4.6 Bq m^{-3}, respectively. The mean equilibrium factor for thoron is 0.1 ± 0.1. The mean effective doses due to inhalation were found to be 2.6 mSv a^{-1} for radon and its progeny, 1.0 mSv a^{-1} for thoron and its progeny, and 3.6 mSv a^{-1} in total (AM). Generally, radiation doses have shown no increased health risk due to exposure to radon, thoron and their progeny in the study area compared to the reference level. Moreover, we obtained that thoron and its progeny contribute about 26 % to the total inhalation dose. This justifies that thoron and its progeny has to be considered when assessing radiation doses. There is a technical cooperation project between Cameroon and the International Atomic Energy Agency (IAEA) running from 2018 to 2019 on 'Establishing a national radon plan for controlling public exposure due to radon indoors'. Reference levels for radon will be defined and the national radon action plan adopted by 2019. Radon and radon-risk mapping will be extended in the whole country.

Disclosure statement

No potential conflict of interest was reported by the authors.

Funding

This work was supported by JSPS KAKENHI Grant Number 26305021 and by the Ministry of Scientific Research and Innovation of Cameroon through the Public Investment Budget 2016.

References

[1] UNSCEAR. Sources and effects of ionizing radiation. New York (NY): United Nations Scientific Committee on the Effects of Atomic Radiation; 2008.
[2] WHO. Fact Sheet No 291 [Internet]: Radon and cancer. World Health Organization; 2005. Available from: http://wwwwhoint/mediacentre/factsheets/fs291/en/indexhtml
[3] WHO [Internet]. Handbook on indoor radon. World Health Organization; 2009. Available from: http://whqlibdocwhoint/publications/2009/9789241547673_engpdf. 2009
[4] Ramola RC, Prasad M, Kandari T, et al. Dose estimation derived from the exposure to radon, thoron and their progeny in the indoor environment. Sci Rep. 2016;6:31061.
[5] IAEA. Radiation protection and safety of radiation sources: international basic safety standards. Vienna: International Atomic Energy Agency; 2014; (IAEA Safety Standards Series No. GSR Part 3).
[6] Zhuo W, Iida T, Yang X. Environmental radon and thoron progeny concentrations in Fujian province of China. Radiat Prot Dosim. 2000;87:137–140.
[7] Zhou W, Iida T, Moriizumi J, et al. Simulation of the concentrations and distributions of indoor radon and thoron. Radiat Prot Dosim. 2001;93:357–368.
[8] Ramola RC, Negi MS, Choubey VM. Measurements of equilibrium factor "F" between radon and its progeny and thoron and its progeny in the indoor atmosphere using nuclear track detectors. Indoor Built Environ. 2003;12:351–355.
[9] Shang B, Chen B, Gao Y, et al. Thoron levels in traditional Chinese residential dwellings. Radiat Environ Biophys. 2005;44:193–199.
[10] Stewart H, Steck DJ. Radon, thoron and their progeny in Lancaster PA homes. In: Proceedings of the American Association of Radon Scientists and Technologists 2008 International Symposium, Las Vegas NV, September 14–17. AARST; 2008.
[11] Zhang L, Liu C, Guo Q. Measurements of thoron and radon progeny concentrations in Beijing China. J Radiol Prot. 2008;28:603–607.
[12] Chen J, Tokonami S, Sorimachi A, et al. Preliminary results of simultaneous radon and thoron tests in Ottawa. Radiat Prot Dosim. 2007;130:253–256.
[13] Chen J, Schroth E, Fife I, et al. Simultaneous ^{222}Rn and ^{220}Rn measurements in Winnipeg Canada. Radiat Prot Dosim. 2009;134:75–78.
[14] Mishra R, Mayya YS, Kushwaha HS. Measurement of ^{220}Rn/^{222}Rn progeny deposition velocities on surfaces and their comparison with theoretical models. J Aerosol Sci. 2009;40:1–15.
[15] Mishra R, Prajith R, Sapra BK, et al. Response of direct thoron progeny sensors (DTPS) to various aerosol concentrations and ventilation rates. Nucl Inst Meth Phys Res B. 2010;268:671–675.
[16] Nazaroff WW, Doyle SM. Radon entry in the houses having crawl space. Health Phys. 1985;48:265–281.
[17] Omori Y, Tokonami S, Sahoo SK, et al. Radiation dose to radon and thoron progeny inhalation in high-level natural radiation areas of Kerala, India. J Radiol Prot. 2017;37:111–126.
[18] Saïdou, Abdourahimi, Tchuente SYF, et al. Indoor radon measurements in the uranium regions of Poli and Lolodorf Cameroon. J Environ Radioact. 2014;136:36–40.
[19] Saïdou, Tokonami S, Miroslaw J, et al. Radon-thoron discriminative measurements in the high natural radiation areas of southwestern Cameroon. J Environ Radioact. 2015;150:242–246.
[20] Takoukam SSD, Saïdou, Hosoda M, et al. Natural radioactivity measurements and external dose estimation by car-borne survey in Douala city, Cameroon. Radioprotection. 2018;53:255–263.
[21] Lindsay R, Newman RT, Speelman WJ. A study of airborne radon levels in Paarl houses (South Africa) and associated source terms, using electret ion chambers and gamma-ray spectrometry. Appl Radiat Isot. 2008;66:1611–1614.
[22] Nguene FR, Tamfu S, Loule JP, et al. Paleoevironments of the Douala and Kribi-Campo Subbasins in Cameroon, West Africa. In: Curnelle R, editor. Géologie Africaine: Recueil des

communications. Boussens: Elf Aquitaine; 1992. p. 129–139 (Bulletin de Centres de Recherche Exploration–Production Elf-Aquitaine, Mémoire 13).
[23] Olivry CJ. Fleuves et rivières du Cameroun. Paris: MESRES-ORSTOM; 1986; (Collection Monographies Hydrologiques ORSTOM; No. 9).
[24] Tokonami S, Takahashi H, Kobayashi Y, et al. Up-to-date radon–thoron discriminative detector for a large scale survey. Rev Sci Instrum. 2005;76:113505.
[25] Kudo H, Tokonami S, Omori Y, et al. Comparative dosimetry for radon and thoron in high background radiation areas in China. Radiat Prot Dosim. 2015;167:155–159.
[26] Hosoda M, Kudo H, Iwaoka K, et al. Characteristic of thoron (^{220}Rn) in environment. Appl Radiat Isot. 2017;120:7–10.
[27] ISO/TC 85/SC 2. Measurement of radioactivity in the environment – Air – Radon 220: Integrated measurement methods for the determination of the average activity concentration using passive solid-state nuclear track detectors (ISO 16641:2014). Geneva (Switzerland): International Organization for Standardization; 2014.
[28] Tokonami S. Why is ^{220}Rn (thoron) measurement important? Radiat Prot Dosim. 2010;141:335–339.
[29] Sorimachi A, Tokonami S, Kranrod C, et al. Preliminary experiments using a passive detector for measuring indoor ^{220}Rn progeny concentrations with an aerosol chamber. Health Phys. 2015;108:597–606.
[30] Zhuo W, Iida T. Estimation of thoron progeny concentrations in dwellings with their deposition rate measurements. Jpn J Health Phys. 2000;35:365–370.
[31] Janik M, Tokonami S, Kranrod C, et al. Comparative analysis of radon, thoron and thoron progeny concentration measurements. J Radiat Res. 2013;54:597–610.
[32] Ćurguz Z, Stojanovska Z, Žunić ZS, et al. Long-term measurements of radon, thoron and their airborne progeny in 25 schools in Republic of Srpska. J Environ Radioact. 2015;148:163–169.
[33] ICRP. Radiological protection against radon exposure. ICRP Publication 126. Ottawa: International Commission on Radiological Protection; 2014 (Annals of the ICRP 43, No. 3).
[34] USEPA. National primary drinking water regulations; radio nuclides; proposed rules. Federal register, vol 56. U.S. Environmental Protection Agency; 1991. p. 33050.
[35] European Union [Internet]. Commission recommendation on the protection of the public against indoor exposure to radon (90/143/Euroatom) [cited 2007 Apr 4]. Brussels: Commission of the European Communities; 1990; Available from: http://ec.europa.eu/energy/nuclear/radioprotection/doc/legislation/90143_en.pdf
[36] Prasad M, Rawat M, Dangwal A, et al. Study of radiation exposure due to radon, thoron and progeny in the indoor environment of Yamuna and Tons valleys of Garhwal Himalaya. Radiat Prot Dosim. 2016;171:187–191.
[37] Visnuprasad AK, Jaikrishnan G, Sahoo BK, et al. Contribution of thoron and progeny towards inhalation dose in a thorium abundant beach environment. Radiat Prot Dosim. 2018;178(4):405–413.
[38] Gierl S, Meisenberg O, Feistenauer P, et al. Thoron and thoron progeny measurements in German clay houses. Radiat Prot Dosim. 2014;160:160–163.
[39] Saïdou, Tokonami S, Hosoda M, et al. Natural radiation exposure to the public in mining and ore bearing regions of Cameroon. Radiat Prot Dosim. Forthcoming 2019. doi:10.1093/rpd/nc0000.
[40] Harley N, Chittaporn P, Medora R, et al. Measurement of the indoor and outdoor ^{220}Rn (thoron) equilibrium factor: application to lung dose. Radiat Prot Dosim. 2010;141:357–362.
[41] Prasad M, Rawat M, Dangwal A, et al. Variability of radon and thoron equilibrium factors in indoor environment of Garhwal Himalaya. J Environ Radioact. 2016;151:238–243.